https://doi.org/10.1070/RCR5033

Phase change memory materials and their applications

Sergey A. Kozyukhin,[a] Petr I. Lazarenko,[b] Anatoliy I. Popov,[c] Igor L. Eremenko [a]

[a] *N.S.Kurnakov Institute of General and Inorganic Chemistry, Russian Academy of Sciences, Leninsky prosp. 31, 11991 Moscow, Russian Federation*
[b] *National Research University of Electronic Technology, pl. Shokina 1, Zelenograd, 124498 Moscow, Russian Federation*
[c] *National Research University 'Moscow Power Engineering Institute', Krasnokazarmennaya ul. 14, 111250 Moscow, Russian Federation*

Over the past 30 years, phase change memory materials based on chalcogenide semiconductors have rapidly developed from laboratory prototypes to materials extensively used as functional layers in various devices. First of all, this concerns compounds of the Ge–Sb–Te system, which can be reasonably considered as full-fledged functional materials. The review presents a current view of the control of properties of phase change memory materials by their chemical and structural modification. Both the existing and prospective applications of these materials are highlighted. The discussion of chemical modification focuses on popular dopants such as bismuth, tin, oxygen and nitrogen and also refractory metals. In the discussion of structural modification, the use of laser radiation is considered in detail. Currently, this is a key trend in increasing the operation speed of devices based on phase change memory materials. Data on the formation of periodic surface structures in these materials are highlighted and it is emphasized that this effect could find application in nanophotonics and optoelectronics in the near future.
The bibliography includes 336 references.

Contents

1. Introduction 1
2. Phase change memory materials: properties and applications 2
2.1. Phase change memory effect in materials based on chalcogenide compounds 2
2.2. Advanced compositions of phase change memory materials 5
2.3. Functional properties of phase change memory materials 7
2.4. Application areas 10
2.4.1. Optical data storage systems 10
2.4.2. Electrical data storage systems 11
2.4.3. Prospects for application in nanophotonic and optoelectronic devices 12
3. Chemical modification 15
3.1. Methods of dopant introduction for chemical modification of thin films 15
3.2. Modifying dopants 16
3.2.1. Isomorphous impurities 17
3.2.2. Light elements 19
3.2.3. Refractory metals 22
4. Structural modification 24
4.1. Control of the properties of semiconductor materials by changing their structure 24
4.2. Levels of structural modification 24
4.2.1. First level: change in the short-range order parameters 24
4.2.2. Second level: change in the medium-range order parameters 24
4.2.3. Third level: change in the morphology and/or heterogeneity 25
4.2.4. Fourth level: changes in the subsystem of defects 25
4.3. Structural modification induced by laser radiation 25
4.3.1. Thermal and athermal aspects of phase transformations under pulsed laser irradiation 26
4.3.2. Periodic surface structures in phase change memory materials 27
4.3.3. Photostructural transformation effects under laser irradiation 29
5. Conclusion 30
6. List of abbreviations and symbols 30
7. References 31

1. Introduction

The foundations of band theory of semiconductors were laid in 1931 in publications of A.Wilson.[1,2] The design of semiconductor devices on the basis of this theory predetermined the vigorous development of electronics using single crystal semiconductors, transition from discrete devices to integrated circuits, increase in the degree of integration of semiconductor elements, the number of which increases according to Moore's law as their size decreases. Meanwhile, non-crystalline materials with < 1 nm regions of ordered atomic structure (short-range order in the positions of atoms) possess semiconductor properties, which makes them applicable for the design of various devices. This was confirmed by the discovery of chalcogenide glassy semiconductors by Kolomiets and Gorunova in 1955[3,4] and by the preparation of hydrogenized amorphous silicon in 1975.[5]

Received 15 July 2021

© 2022 Uspekhi Khimii, ZIOC RAS, Russian Academy of Sciences

The changes in the electronic structure upon transition from single crystal semiconductors to disordered semiconductors affect not only the properties of the material, but also the efficiency of controlling these properties.[6] The electrophysical parameters of semiconductors in the crystalline state are known to be strongly dependent on the presence of substitutional impurities. Doping of a single crystal semiconductor with donor or acceptor impurities changes not only the magnitude, but also the type of electrical conductivity. The development of effective method for targeted modification of the properties of single crystal semiconductor materials by introducing substitutional impurities is one of the main achievements in micro- and nanoelectronics.

However, soon after the discovery of non-crystalline chalcogenide glassy semiconductors, it was shown[7] that impurity conduction is normally absent in these materials. In other words, the introduction of substitutional impurities into a material slightly changes its electrophysical properties. This is a distinctive feature of such materials.[6] The nature of this phenomenon lies in the fact that the absence of a translational symmetry in combination with elasticity of the atomic structure inherent in glassy materials leads to structural relaxation, and the impurity atoms become electrically inactive. Moreover, even though doping of a melt gives electrically active impurity atoms (donors or acceptors), atomic structure relaxation is accompanied by a change in the ratio of charged intrinsic defects (Fig. 1 *a*), the concentration of which is fairly high: approximately $10^{17}-10^{18}$ cm^{-1} (Refs 8, 9). For example, when charged donor levels appear, the concentration of negatively charged intrinsic defects (C_1^-) becomes equal to the sum of concentrations of positively charged intrinsic defects (C_3^+) and electrically active impurity atoms (D^+) (Fig. 1 *b*).[10] As a consequence, the position of the Fermi level and electrophysical properties of a semiconductor do not depend on the degree of doping.

When the properties of non-crystalline semiconductor materials cannot be efficiently modified by doping, this hampers the design of instruments and devices based on these materials. The necessity to optimize the properties of chalcogenide semiconductors that are currently used as phase change memory (PCM) materials has been repeatedly mentioned in reviews devoted to such materials[11–15] and also to electrical[16–18] and optical[19–22] devices based on them.

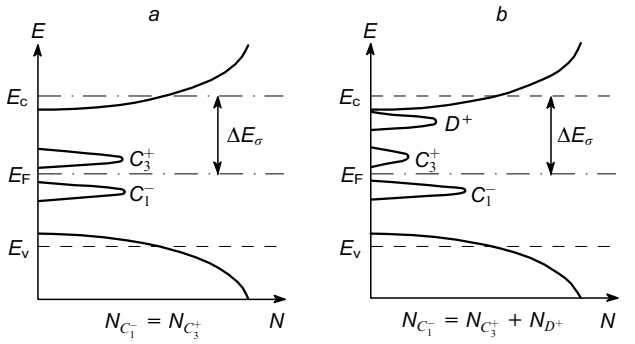


Figure 1. Distribution of charge centres in the band gap of undoped (*a*) and doped (*b*) chalcogenide glassy semiconductor. Designations: E_c is conduction band bottom, E_F is Fermi level, E_v is valence band top, ΔE_σ is activation energy for conduction, N is the density of distribution of charge centres.[10] Published with permission from Jenny Stanford Publishing.

This challenge was addressed by development of methods for the chemical and structural modification of properties of amorphous semiconductors, which are the subject of the present review. Earlier, this subject matter has also attracted research attention. Among the series of publications, note paper by Kang and Chen[23] discussing methods for optimization of properties of phase change memory materials.

In this review, we present our views on the problem of chemical and structural modification based on the model of intrinsic defects considering the results of a few recent years. The application of this approach to control the properties of disordered semiconductors is discussed in relation to PCM materials, which have been intensively studied in the last decades and are used in many data storage systems. It should also be emphasized that we discuss only chalcogenide semiconductors, although the term phase change memory materials is often used to describe effects in compounds of other classes, *e.g.*, organic polymers,[24,25] liquids,[26,27] *etc.*, usually related to processes of energy accumulation, storage or release upon phase transitions.

2. Phase change memory materials: properties and applications

2.1. Phase change memory effect in materials based on chalcogenide compounds

The dependence of the fundamental properties on the degree of atomic structure ordering forms the grounds for a new class of semiconductors — PCM materials and devices based on them. The principle of functioning of such devices is based on the change in the degree of ordering of the material structure in the working region under a low-energy external impact.[28–30] Currently, such materials are widely used to design optical data storage systems (optical discs) and non-volatile memory integrated circuits; also, they start to be used as active and passive components in nanophotonic and optoelectronic devices (see, *e.g.*, a review[19]). The application areas of PCM materials are considered below.

S.A.Kozyukhin. Doctor of Chemical Sciences, Professor, Chief Researcher at IGIC RAS.
E-mail: sergkoz@igic.ras.ru
Current research interests: physical chemistry of non-crystalline semiconductors and chalcogenide glasses, structural studies, optical spectroscopy, chemistry of nanomaterials, phase transitions in chalcogenide semiconductors, thin films.
P.I.Lazarenko. Candidate of Engineering Sciences, Associate Professor at the Institute of Advanced Materials and Technologies of the National Research University of Electronic Technology (MIET).
E-mail: lpi@org.miet.ru, aka.jum@gmail.com
Current research interests: chalcogenide semiconductors, disordered structures, phase change materials, thin films, phase transitions, non-volatile memory devices, integrated optical elements, thermoelectricity
A.I.Popov. Doctor of Engineering Sciences, Professor at the Electronics and Nanoelectronics Department of the National Research University 'Moscow Power Engineering Institute'.
E-mail: popovai2009@gmail.com
Current research interests: disordered and nano-ordered semiconductors, thin films, structure–property relationships, property control, non-volatile memory, phase transition memory.
I.L.Eremenko. Academician, Doctor of Chemical Sciences, Professor, Head of Laboratory of IGIC RAS.
E-mail: ilerem@igic.ras.ru
Current research interests: coordination chemistry, structural chemistry, chemistry of nanomaterials.

Translation: Z.P.Svitanko

The beginning of the studies of phase change memory materials dates back to the first half of the 1960s when electronic switching in thin amorphous chalcogenide films of complex composition upon application of an electrical pulse was observed almost simultaneously by researchers in the USA [31] and in the USSR.[32] The effect consisted in switching of the amorphous high-resistance phase to a low-resistance state at voltages above a threshold value, but, which is of key importance, the material remained amorphous. Later, a reversible transformation of memory materials caused, in this case, by phase transition (crystallization) was discovered.[33,34] This served as an impetus for the design in the 1970s of integrated circuits for the first-generation non-volatile memory in which the cell was a solid-state metal/CGS film/metal sandwich structure (CGS is a chalcogenide glassy semiconductor).[35] The parameters of these integrated circuits were not very impressive when viewed from today s standpoint, since chalcogenide alloys of the Ge–As–Te–Si–P system used at that time were characterized by a low switching rate, high threshold switching currents and, correspondingly, high power consumption. A 16×16 size matrix had a 256 bit capacity, and the data writing voltage was 25 V (SET mode characterizing transition to the low-resistance crystalline state) at a 5 mA current; erasing (or zeroing) was induced by 5 μs long pulses at a voltage of <25 V (RESET mode characterizing transition to the high-resistance amorphous state) and 200 mA current; reading (READ mode) was performed with 2.5 mA pulses at 5 V. These parameters made the phase change technology not very attractive for commercial use in comparison with the types of memory that existed at that time, although it is noteworthy that the works on the design and commercialization of effective devices based on PCM materials were continued in the USA and USSR throughout the 1970s.

Apart from electric pulses, attempts were made to use laser radiation to induce the reversible phase transition. One of the first publications on this subject was the paper by Feinleib *et al.*,[36] who used a pulse laser and thus accomplished fast crystallization of the amorphous semiconductor $Te_{81}Ge_{15}Sb_2S_2$ and back reamorphization. The phase transition was accompanied by a sharp change in the optical transmittance and reflectance. This provided a fairly important conclusion that the optical switching is similar in nature to electrical switching and that the phase transition is accompanied by a change in both electrical and optical characteristics.

The temperature–time profile of the switching pulses, demonstrating the formation of an amorphous region (left-hand part) and a crystalline spot (right-hand part) in the initially polycrystalline film is shown in Fig. 2.[11–15] A specific feature of the process, associated with the nature of transitions, is the necessity to apply a high-intensity pulse with a short trailing edge (decline) in the case of phase transition from the crystalline to amorphous state *via* melting; in the reverse transition, the pulse amplitude is much smaller, but the pulse duration is longer.

A new stage in the development of phase change memory materials and devices based on them dates back to the late-1980s–early-1990s; it is associated with appearance of a number of publications of Professor Yamada's research group,[37–39] dealing with high-performance compositions in the Ge–Sb–Te (GST) ternary system. Compounds of this system showed a high optical contrast over a wide range of wavelengths, good cyclability and short crystallization time. The appearance of these materials was

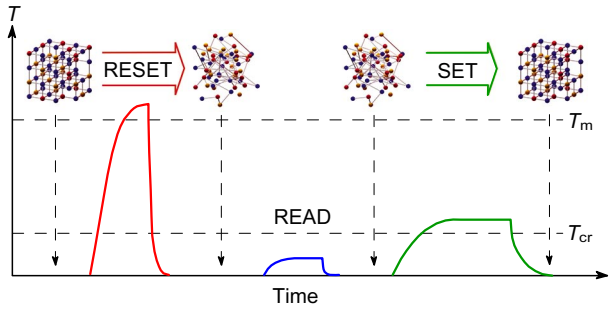


Figure 2. Temperature–time profile of switching pulses. T_m is melting point, T_{cr} is crystallization temperature. The Figure was created by the authors using data of Refs 11–15.

a powerful impetus for the development of optical data recording systems. In 1998, Matsushita Electric (Panasonic Corporation) released rewritable digital versatile discs (DVDs) based on GST system materials, while in 2003, they manufactured Blu-ray disks (BDs). As one of the most recent achievements in the development of electrical phase change memory devices (phase change random access memory, PCRAM), mention should be made of the technology that was first presented in 2015 as the Intel Optane memory (3D-XPoint technology), which is currently utilized to manufacture non-volatile memory with a 16–64 GB capacity and a short time lag.[40] The manufactured devices of electrical phase change memory are 1000 times faster than the NAND (NOT–AND) flash memory [41] and are characterized by 4.5 times higher data storage density than the DRAM (dynamic random access memory) devices manufactured by a similar 20-nanometre technology, which ensures their commercially successful application as a storage-class memory (SCM).[42]

As can be seen from the diagrams shown in Fig. 3,[13,15] phase change memory has the optimal relationship between cost and efficiency for SCM applications and has obvious prospects to find its niche in the quite competitive market of data storage devices.

An advantage of devices based on chalcogenide glassy semiconductors is their radiation tolerance, which is higher than that of devices with crystalline semiconductor-based hardware components and which has been actively studied for more than 50 years.[43] PCM materials of the GST system and, hence, devices based on them also robustly operate under ionizing radiation, which implies the possibility of specific applications.[44] Since the operation of these devices is based, first of all, on the stability of phase states and the possibility of reliable switching between them, the attention is focused on particularly these aspects. For example, it was shown [45] that germanium-rich compositions do not undergo repeated crystallization of the amorphous phase (RESET) even at high fluences (approximately 5×10^{10} ions per cm^2) of gold heavy ions with an energy of 1.635 GeV. High radiation tolerance of GST materials was confirmed by Konstantinou *et al.*,[46] who carried out molecular dynamics simulation and found out that the radiation tolerance of both amorphous and crystalline phases of these materials is determined, first of all, by specific features of their structure, particularly, lability caused by the presence of defects.

Currently, compounds of the $GeTe–Sb_2Te_3$ quasi-binary section are used most often as functional materials

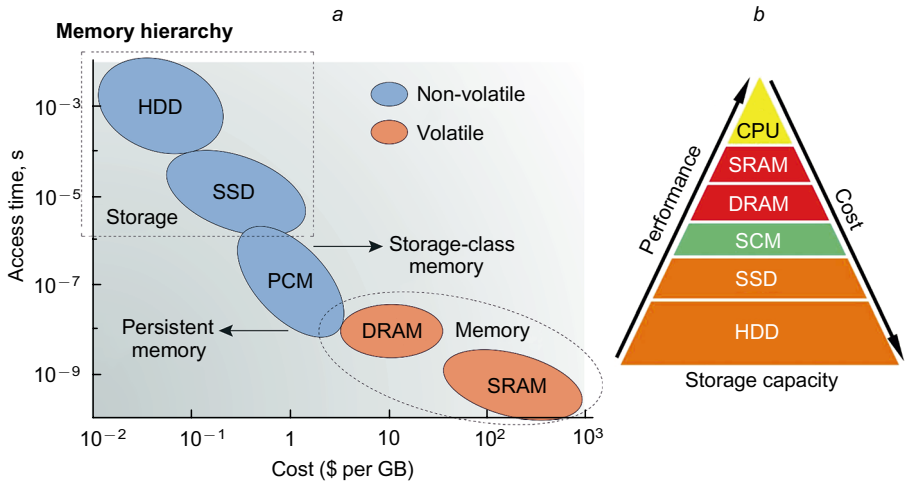


Figure 3. Diagrams illustrating the correlation between the memory device access time during a write operation and the approximate cost of 1 GB of memory (*a*),[13] and hierarchy of memory devices including their cost and performance (*b*).[15] HDD is hard disk drive, SSD is solid-state drive, SRAM is static random access memory, CPU is central processing unit. Figure 3 *a* is published with permission from Springer Nature; Fig. 3 *b* is published in accordance with the Creative Commons Attribution 3.0 license.

in phase change memory devices. Other chalcogenide semiconductors such as compounds of In–Sb–Te, Ag–Sb–Te, Sn–Sb–Te and other ternary systems were also studied as PCM materials. The choice of these systems is due to the materials science approach to optimizing performance characteristics by replacement of one of the major elements of the GST system by another element; for example, germanium atoms were replaced by tin or indium atoms, while antimony atoms were replaced by arsenic or bismuth. The Gibbs triangle for PCM materials that are used most widely for the manufacture of optical discs is shown in Fig. 4. One of actively studied classes of PCM materials of this type is doped Sb_2Te_3 (indium and silver are often used as dopants).[47]

Characteristics of thin films of GST compounds† such as high rate of phase transitions (< 50 ns), high electrical[48] and optical[11,49] contrasts (Fig. 5), and the possibility of

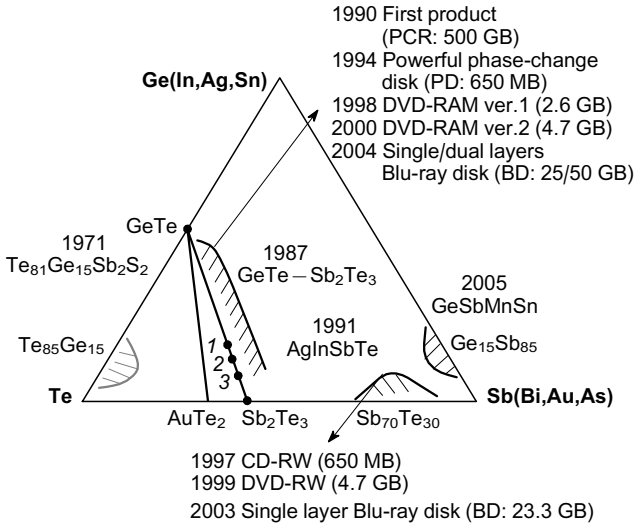


Figure 4. Most popular PCM materials for electrical and optical memory devices; for some compositions, the discovery dates are indicated.[47] (*1*) $Ge_2Sb_2Te_5$, (*2*) $GeSb_2Te_4$, (*3*) $GeSb_4Te_7$. Published with permission from Springer Nature.

† The following designations are used below for frequently mentioned GST compounds:

Compound	Designation
$Ge_2Sb_2Te_5$	GST225
$GeSb_2Te_4$	GST124
$GeSb_4Te_7$	GST147

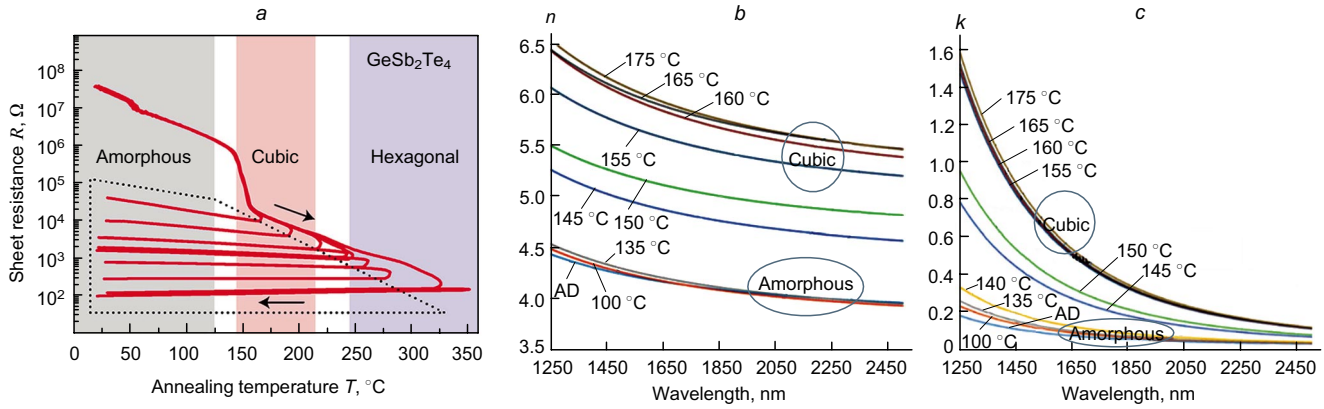


Figure 5. Temperature dependences of the sheet resistance of $GeSb_2Te_4$ thin films (*a*)[48] and optical characteristics: refractive index *n* (*b*) and absorption coefficient *k* (*c*) of $Ge_2Sb_2Te_5$ in the amorphous and crystalline states. The arrows in Fig. *a* show the temperature change following the resistivity change; the red lines outside the dashed line were obtained during heating; the lines encompassed by the dashed line were measured during cooling. AD is the as-deposited film. Published in accordance with the Creative Commons Attribution license.

formation of numerous states with different degrees of crystallization account for the pronounced interest in the search for their new applications, in particular, for the design of electro-optical and all-optical elements. First of all, of interest is the design of multilevel non-volatile elements.

In conclusion, it should be noted that materials of the GST system have obvious application prospects in various data storage, nanophotonic and optoelectronic devices; however, optimization of their physicochemical characteristics is required.

2.2. Advanced compositions of phase change memory materials

The advances in the use of PCM materials based on GST system (see above) are associated with the fact that the search for appropriate compounds was based on the fast crystallization concept. Initially, Yamada *et al.*[37–39] studied chalcogenide compositions that demonstrated fast and reproducible crystallization upon cyclic external stimuli. This strategy fundamentally differed from the approaches in which the primary attention was paid to the search for compositions with a minimum crystallizability and, correspondingly, a high glass-forming ability. Most synthetic chemists and materials scientists who work with chalcogenide glasses or amorphous films used these approaches. In the general case, amorphization of any material is not a purely scientific problem, since at sufficiently high rate of melt cooling, any composition is expected to remain amorphous. The problem is how to implement this practically. Compounds of the GST system possessing low glass-forming ability cannot be obtained as bulk glassy materials even at the highest accessible cooling rates; nevertheless, they can be obtained in the amorphous states as thin films, which meets the requirements of the manufacturers of data storage devices. However, crystallization issues have a more fundamental nature, since this process is based on the slow diffusion of atoms and, hence, the rearrangement of the atomic system takes a certain time.

The first reports on compounds formed in the GST system date back to the 1960s when publications of Abrikosov and Danilova-Dobryakova[50,51] on phase equilibria appeared; later their results were made more specific and were extended.[52–61] The principal conclusions did not basically change: three stable chemical compounds are present in the $GeTe-Sb_2Te_3$ quasi-binary section (Fig. 6), with the general formula $(GeTe)_n(Sb_2Te_3)_m$ and different $n:m$ ratios: GST225 (2 : 1), GST124 (1 : 1) and GST147 (1 : 2). They are formed by the peritectic reaction during incongruent melting. Shelimova *et al.*[54] noted the possibility of formation of also other intermediate compounds with $n:m$ ratios differing from those noted above, particularly, $Ge_7Sb_2Te_{10}$ (7 : 1), $Ge_6Sb_2Te_9$ (6 : 1), $Ge_5Sb_2Te_8$, (5 : 1), $Ge_4Sb_2Te_7$ (4 : 1), $Ge_3Sb_2Te_6$ (3 : 1), $GeSb_6Te_{10}$ (1 : 3) and $GeSb_8Te_{13}$ (1 : 4).

Apart from the thermodynamically stable compounds, other phases can also be found in the GST system, *e.g.*, $Ge_3Sb_3Te_6$,[55] $Ge_3Sb_2Te_6$,[56] $Sb_2Te_3(GeTe)_n$ ($n = 3-19$),[57] which are probably metastable. These phases are detected by high-resolution transmission electron microscopy, (HRTEM) or by high-angle annular dark field scanning transmission electron microscopy (HAADF-STEM) after the appropriate heat treatment of the initial polycrystalline films. Despite quite a number of structural studies of compounds in GST system (the first publications in the USSR appeared back at the end of 1960s),[58] many issues related to their structures and structural rearrangements are still debated. However, the basic conclusions 1–3 listed below are undoubted.

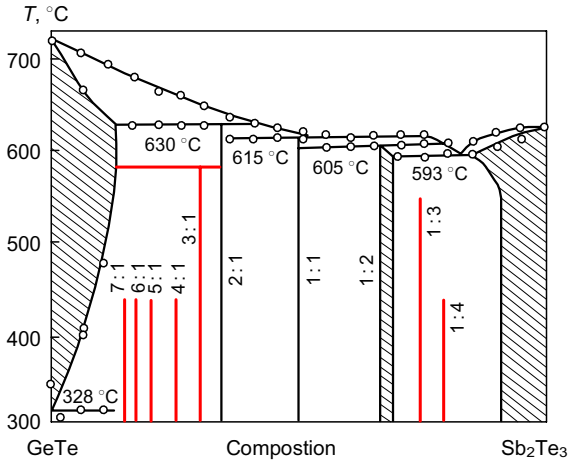


Figure 6. Equilibrium state diagram of $GeTe-Sb_2Te_3$[50,51,59] supplemented by data of Ref. 54. Published with permission from John Wiley and Sons.

1. Compounds formed in GST system have a stable layered crystal structure with a hexagonal close-packed (HCP) lattice (space group $P\bar{3}m1$ or $R\bar{3}m$, see Fig. 7 *a*)[55] consisting of two sublattices — antimony telluride Sb_2Te_3 and germanium telluride GeTe; each layer contains atoms of one sort and germanium and/or antimony cationic layers alternate with telluride anionic layers. The layers are arranged along the crystallographic *c* axis, thus forming unit cells separated by a van der Waals gap, which is located between the corresponding tellurium layers.[60] Depending on the composition, unit cells contain different numbers of layers: nine layers for GST225, seven layers for GST124 and twelve layers for GST147; inside the cell, there is one more van der Waals gap between the fifth and seventh layers. The structure of stable phases in GST system is illustrated by Fig. 7 *a*.

2. Compound GST225 has both a stable hexagonal phase and a metastable cubic phase with a NaCl type structure (space group $Fm\bar{3}m$), which forms upon crystallization of the amorphous phase. In the cubic phase, tellurium atoms occupy anionic sites, while the germanium and antimony atoms are randomly distributed over cationic sites.[62,63] The unit cell of the cubic phase consists of six alternating tellurium and Ge–Sb layers. The main structural differences between the crystal phases are in the fact that the hexagonal phase has pairs of neighbouring tellurium layers separated by a van der Waals gap, but no such structure is present in the cubic phase containing ~10–20% vacancies in the Ge–Sb layers (see Fig. 7 *b*,*c*).[61] A high concentration of vacancies is important for these PCM materials (see below).

3. The interest of researchers in the vacancies and their role in the superfast phase transition from the amorphous to metastable crystalline phase is stimulated by the desire to understand the nature of this transition. Some authors are prone to believe that vacancies play the key role in this process. For example, Wuttig *et al.*[64] showed that the higher the concentration of vacancies and the degree of local disorder of the metastable phase of GST system in a thin

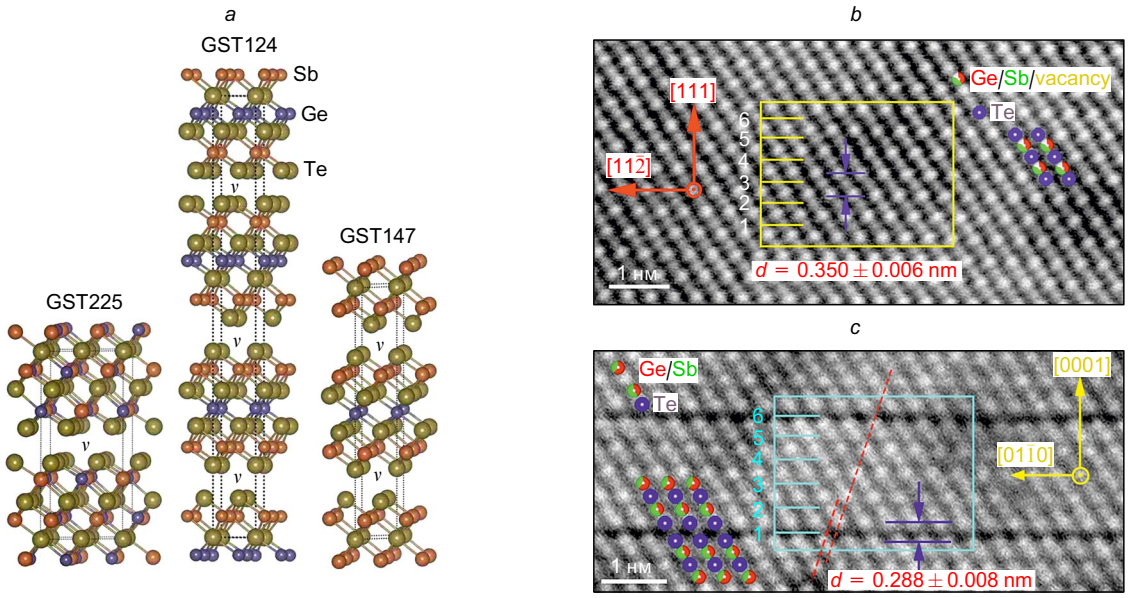


Figure 7. Unit cells of stable compounds along the $GeTe-Sb_2Te_3$ quasi-binary section (*a*)[55] and HAADF-STEM images of metastable cubic (*b*) and stable hexagonal (*c*) phases of GST225.[61] *v* is van der Waals gap. In Fig. *b*, numerals 1–6 designate cationic layers; in Fig. *c*, numerals 1 and 6 mark the van der Waals gaps, while 2–5 are cationic layers; the red dashed lines indicate the positions of anions. Figure 7 *a* is published with permission from the American Physical Society; Figures 7 *b*,*c* are published in accordance with the Creative Commons CC license.

film [the calculation was carried out by quantum chemistry methods, particularly, by density functional theory (DFT)], the greater the optical contrast between the amorphous and crystalline states. In the authors opinion, this is due to the fact that as a result of annihilation effect, vacancies can counterbalance the energetically unfavourable electronic interactions between germanium and tellurium atoms, as well as between antimony and tellurium atoms, the electrons of which occur in antibonding orbitals. Lee and Elliott,[65,66] who used molecular dynamics simulation techniques, showed that vacancies mainly have tellurium sites as neighbours, while diffusion of germanium and antimony atoms towards vacancies in the amorphous phase during crystallization at the crystal/glass interface promotes the formation of stable crystal nuclei, which is favourable for high crystallization rate. This provided the conclusion that the crystal nuclei mainly border vacancies.[65,66]

Apart from modelling, other approaches taking account of structural details and specific properties related to the electronic subsystem are also used to interpret the superfast phase transitions in GST materials. The most popular approaches are based on the following assumption: since PCM materials are $A^{IV}B^{VI}-A^{V}B^{VI}$ type quasi-binary compounds consisting of p-elements with partially filled outer electron shells and the covalent bonds involve p valence electrons, the bonds that are formed in the amorphous and crystalline phases are different (first of all, this concerns the bond lengths). In the metastable cubic structure, long and short Ge–Te chemical bonds are possible. A number of mechanisms have been proposed for stabilization of these bonds such as resonant bonding[67] and Peierls distortion.[68]

The GST225 compound, the structure of which comprises sublattices of antimony and germanium tellurides (see above), combines several advantages such as fast crystallization inherent in the Sb_2Te_3 phase and thermal stability of the amorphous GeTe phase. This makes GST225 one of the most practically promising PCM materials.[38,59] However, some functional properties of this compound still need to be improved, *e.g.*, it is necessary to decrease power consumption and increase the durability of characteristics.[69,70]

Apart from GST materials, which receive the primary attention in this review, some other compositions used as PCM materials are also worth mentioning. In some cases, these are fairly structurally similar materials, while in other cases, they significantly differ, which seems a curious fact.

First of all, mention should be made of antimony telluride Sb_2Te_3, which is a promising binary PCM material owing to the ability of antimony to improve the crystallization properties in comparison with pure tellurium (see below) and, hence, to increase the rate of switching between the states under the action of electric pulse.[71] The crystal structure of Sb_2Te_3 is composed of layers (Fig. 8), like that of other GST compounds,[72] but as distinct from other compounds, the predominant crystallization mechanism in antimony telluride is the growth of crystal nuclei, which provides for greater resistance contrast between the crystalline and amorphous phases. However, simultaneously low crystallization temperature is a problem regarding the stability of data storage, because spontaneous uncontrolled crystallization of the amorphous phase may result in the loss of information.[73,74] A general approach to modification of antimony telluride is doping with metals and semiconductors (Ag, In, Ge, Bi),[75] which does not change the layered structure of the material, but increases the thermal stability and simultaneously maintains crystallization rate at an acceptable level.

There are several studies in which antimony telluride was doped with binary compounds such as Sb_2S_3 and Sb_2Se_3.[76] This method is promising for photonic applications, in particular for the design of integrated optical devices and metasurfaces operating with radiation near the telecommunication wavelength.[76] In view of their main benefit, high transparency in the IR range near 1550 nm,

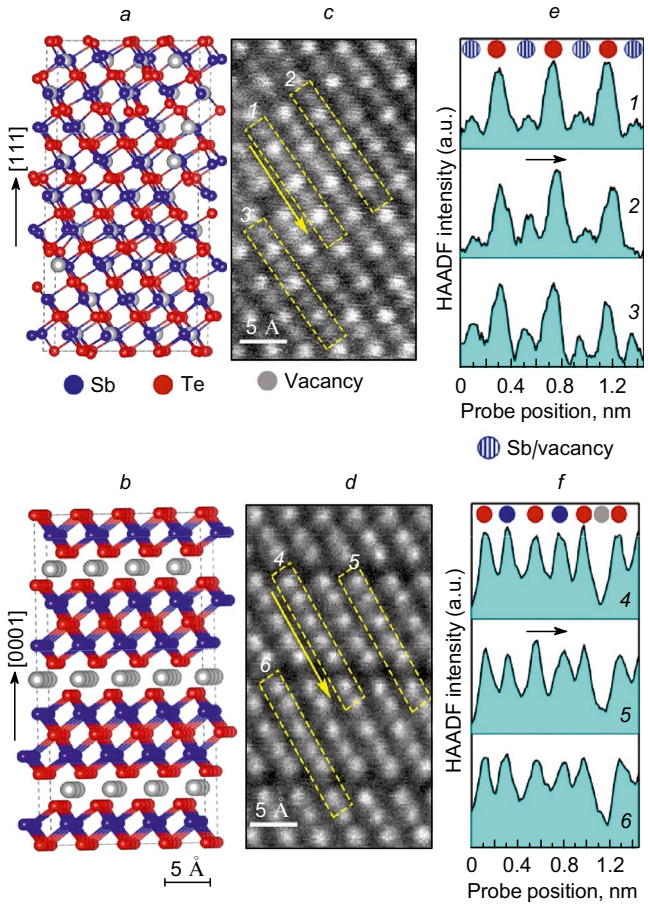


Figure 8. Structures (*a*, *b*), HAADF-STEM images (*c*, *d*) and variations of the signal intensity along the regions *1*–*6* enclosed by dashed lines (*e*, *f*) for the metastable cubic (*a*, *c*, *e*) and stable hexagonal (*b*, *d*, *f*) structures of Sb_2Te_3.[72] Published with permission from Springer Nature.

this opens up the possibility of designing devices characterized by significantly lower losses compared to the GST-based devices. In addition, the similarity of refractive indices of these materials and silicon allows them to be integrated into photonic systems manufactured using silicon-on-insulator (SOI) technology.

A relatively new trend is the study of chalcogenide compounds containing no tellurium.[77–81] The appearance of this trend is due to two factors: the desire to reduce the environmental impact of the industrial manufacture of PCM materials by eliminating toxic tellurium and the prospects for increasing the number of data writing–rewriting cycles. It is known[82] that upon appropriate initiation of crystallization, pure antimony demonstrates so-called explosive crystallization where the reaction follows a cascade mechanism and the crystallization time is $< 10^{-6}$ s even at room temperature. Therefore, relevant tasks are to increase the thermal stability of this phase and to improve the morphology in the phase transition. Often, this can be attained using antimony alloys such as $In_{1-x}Ga_xSb$ rather than pure antimony.[83]

A separate group of PCM materials is formed by Ga–La–S (GLS) alloys, including doped alloys, *e.g.*, GaLaSCu (GLSC) or GaLaSO (GLSO).[84–86] Characteristics of indicated compounds are quite attractive; for example, the resistivity is ~4 Ω m, which allows effective use of Joule heat for electrical switching; the crystallization time of GLSC is 150 ns and depends on the percentage of copper in the alloy: as the copper content grows by 30 at.%, the crystallization time increases to 350 ns. Therefore, GLSC has a potential as a PCM material. However, an obvious drawback of these alloys are relatively high softening, crystallization and melting temperatures: T_g = 640 °C, T_c = 730 °C and T_m = 830 °C. This sharply increases the power consumption of devices based on these alloys compared with devices based on GST materials, although the thermal stability simultaneously increases. Another important factor is more complex synthesis of these compounds compared with the synthesis of GST alloys.

2.3. Functional properties of phase change memory materials

Despite the commercial success and obvious application prospects of devices based on PCM materials,‡ their manufacturing and studying ARE faced with a number of difficulties that prevent more extensive commercial development of this field. These difficulties include

— structure-relaxation processes and drift of the key parameters of the functional regions of amorphous thin films of PCM materials;

— high power consumption;

— failures during data writing and erasing because of insufficient knowledge of structural transformations and, as a consequence, problems in the selection of programming pulses;

— insufficiently high writing speed; the GST225 crystallization time is ~50 ns; for comparison, in the use of 1T-1C DRAM volatile memory, the writing time is ~10 ns;

— the necessity to improve the property contrast between the amorphous and crystalline states; the property contrast directly affects the signal-to-noise ratio and the possibility of further increasing the number of logical states that can be written in one cell.

The listed challenges that are faced by specialists who develop such devices and their solutions depend on many requirements imposed on functional materials (which may often contradict one another) and on the possibility of controlling characteristics of the materials. For example, the power consumption can be reduced by decreasing the energy needed to write data, *i.e.*, the activation energy of crystallization; however, this may simultaneously decrease the stability of the amorphous state and increase the probability of spontaneous crystallization at the operating temperatures, *i.e.*, may lead to information loss. Thus, it is not some single parameter, but the whole set of physicochemical characteristics that are to be optimized. This requires development of an efficient method for control of the properties of PCM materials.

The significance of thermal properties of the materials should be emphasized. The parameters that deserve attention include not only obvious values such as melting, crystallization and glass transition temperatures and the corresponding thermodynamic characteristics (thermal and temperature conductivity), but also, for example, the Seebeck coefficient (S) and thermo-optic coefficients. It should be noted that the non-uniform temperature distribution in a separate nanosized cell and the arising temperature gradient

‡ According to the estimate of *Reports and Data*, the market of PCM devices amounted to 290 million US dollars in 2018, and, by 2026, according to an optimistic scenario, the market would reach 46.52 billion US dollars.[87]

give rise to thermoelectric processes, in addition to the Joule heat released upon data writing–erasing.[88,89] In other words, data writing–erasing processes in the cell are affected by the Thomson (thermoelectric) effect. Since for most PCM materials, the Seeback coefficient is positive and the temperature coefficient is negative, the Thomson coefficient $T(\partial S/\partial T)$ is also negative. Depending on the polarity of the electric pulse acting on the cell, heat is either released or withdrawn; the differences in the input power needed to perform the operation may reach 10%.

The switching dynamics of integrated nanophotonic devices may depend on the thermo-optical effect, as demonstrated by Stegmaier *et al.*[90] in relation to Mach–Zehnder devices based on GST225. At high temperatures, the refractive indices n and k vary by a few percent (real part) and by up to hundreds of percent (imaginary part). Furthermore, after crystallization of amorphous films, the thermo-optical coefficient describing the variation of the real part of the dielectric permittivity changes the sign. Thus, the considerable heating and change in the phase state may induce malfunctioning of devices, especially when a temperature gradient appears. This should be taken into account for the design of on-chip photonic circuitry.

An important aspect is the crystallization kinetics of the amorphous phase and the associated parameters, which influence the response speed of devices. These parameters include the activation energy of crystallization, nucleation rate, critical radius of the nucleus, crystal growth rate and viscosity of both the melt and the metastable phase above the softening temperature. This is due to the fact that the SET operation is slower than the other two operations — READ and RESET. A typical crystallization time for modern GST-based PCM materials is in the range from tens to hundreds of nanoseconds in the temperature range from $\sim$500 to 600 K, which is lower than the melting points of the corresponding compositions.[13] Thus, the overall operating speed of the device is determined by the slowest stage. Naturally, it is necessary to develop approaches to increase the crystallization rate based on understanding of the mechanisms of this process.

The generally accepted point of view is that the nucleation rate in GST materials prevails over the crystal growth rate, whereas in doped antimony tellurides, *e.g.*, $Ag_4In_3Sb_{67}Te_{26}$ (AIST), the driving force of crystallization is the growth of crystal nuclei.[13] While considering crystallization, one should take into account the fact that in nanosized spaces such as one electrical memory cell, the effects of the two mentioned processes may differ from their effects in bulk materials in the GST system, in which the role of nucleation decreases, while crystallization is mainly determined by the growth of nuclei in the cells.[91]

The following fundamental questions are related to the crystallization kinetics of PCM materials:

— Can the growth of crystal nuclei be described by an Arrhenius type model, *i.e.*, where the nucleus growth rate is maximum in the temperature range of existence of metastable liquid (at temperatures markedly below T_m but above T_g) and the temperature dependence of the viscosity is described by the Arrhenius equation?[92]

— what is the role of structural relaxation and rigidity of the glass network in the crystallization kinetics?[93]

— what is the softening point and what is its significance for PCM materials?[94]

Apart from the listed issues, there are also specific problems related to initiation of the crystallization by external stimuli, for example, by strong electromagnetic field, which is the case for electrical memory devices,[95,96] or by laser radiation, which takes place in optical discs.[97]

The electrophysical properties of PCM materials are of key importance for the performance of electric memory. It is known that in disordered semiconductors, charge carriers are transported either over the localized states in the band gap or over the extended states.[6] Correspondingly, the conduction in amorphous materials can be described in terms of the model of transport over the extended states at temperatures > 200 K and a field strength below the threshold switching field strength; at low temperatures, the principal role is played by conduction over traps in the band gap.[98,99] This model adequately explains the experimental results obtained for most PCM materials; for the amorphous phase, the activation energy for conduction is approximately equal to half the optical band gap and is in the range from 0.2 to 0.4 eV.[100]

The current–voltage characteristics for the amorphous and crystalline states of a PCM material measured by applying various voltage pulses are shown in Fig. 9. In the crystalline state, the cell demonstrates the ohmic behaviour over the whole range of low voltages, whereas in the amorphous state, the current variation as a function of the applied voltage follows a complex pattern: when the voltage

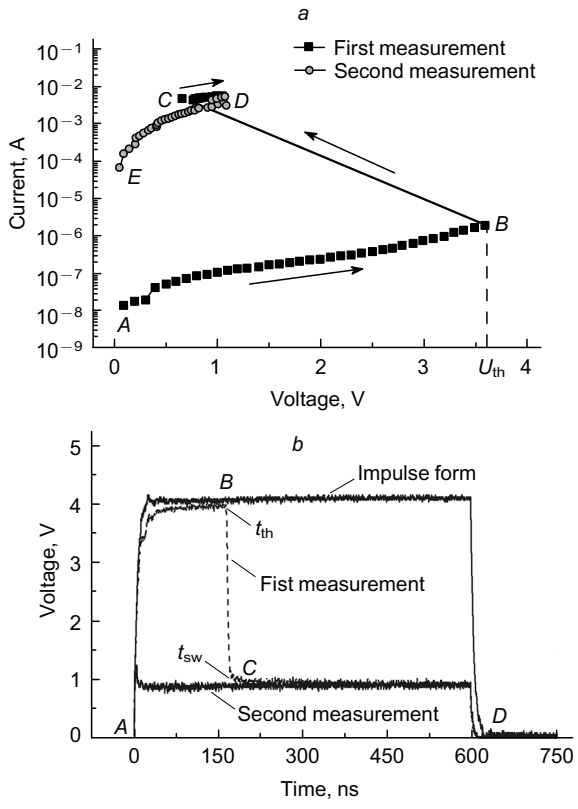


Figure 9. Current–voltage characteristics of the amorphous ($A-B$) and crystalline ($D-E$) states of a PCM material obtained by application of a constant (*a*) and rectangular voltage pulse (*b*).[101] Range $A-B$ is the high-resistance amorphous state; $B-C$ is electrical switching; $C-D$ and $D-E$ are current–voltage characteristics for the low-resistance state measured during increase and subsequent decrease in the voltage. The arrows show direction of characteristics; t_{th} is the time of the start of switching, t_{sw} is the time of the end of switching. Published with permission from AIP Publishing.

is below the threshold value, the cell demonstrates the ohmic (linear) dependence, while at higher voltage, the current–voltage dependence is exponential.[101] Above the threshold switching voltage, the cell conductivity rapidly increases due to the feedback mechanism, resulting in a negative differential resistance.

As the threshold voltage is exceeded (threshold switching), the state in which crystallization has not yet took place is attained. Only after a certain period of time, crystallization occurs due to the relatively high current and heat evolution. Note that the threshold switching effect is very important for devices based on PCM materials. Presumably, these devices could not have existed without this effect: switching of the material from the high-resistance amorphous state to low-resistance crystalline state would have required too high voltage; as a result, the device would have been too power consuming and in low demand. The mechanism of threshold switching is still a debated subject, starting from the discovery of this effect. The key issue is the following: whether switching is thermal electron (*i.e.*, switching is due to the thermal electron instability in the bulk, that is, in the cord when the current is passed) or purely electronic?[102–106] It is noteworthy that new approaches to interpretation of the switching effect have appeared in the last two decades, *e.g.*, tunnelling between deep and shallow traps, where under instability conditions the tunnelling current exceeds the thermally activated current,[107] and the above-mentioned electric field-initiated nucleation model.[105]

Since the READ operation in devices based on PCM materials is induced by current pulses with parameters differing from those for SET and RESET, stable operation requires that the resistances of the amorphous and crystal phases be considerably different. The devices should have a pronounced electrical contrast between the resistances for SET and RESET operations, in order to exceed the possible noises during fast data reading and to ensure the possibility of reading (actually recognizing) the resistance states without disrupting the phase states. The difference between the resistivities largely determines other important functional characteristics such as the durability of the device with large number of SET–RESET switching cycles, data retention time (usually, a period of 10 years is indicated at some elevated temperature) and the SET operation speed (the time needed for cell recrystallization from the RESET state). As a rule, data retention depends on the ability of the cell to exist in the amorphous state without spontaneous crystallization. One more aspect that may be significant is the possibility to store more than one bit of data in one cell for a long period of time, which would increase the effective data density without decreasing the size of the element.

The phase transition between the amorphous and metastable crystalline phases (*i.e.*, between two thermodynamically unstable states), which underlies functioning of PCM-based devices, results in the so-called resistance drift in PCM materials, which means that resistance increases with time. This refers, first of all, to the high-resistance state (amorphous phase); in addition, considerable resistance fluctuations (noises) can be observed in this state; this is especially critical for the functioning of multilevel memory systems. It is considered that the resistance drift is accelerated at elevated temperature and that it is caused by both the temperature dependence of the activation energy of conduction (ΔE_σ) (associated with the change in the Fermi level position) and the change in the optical band gap (E_g) (Fig. 10).[99, 108, 109]

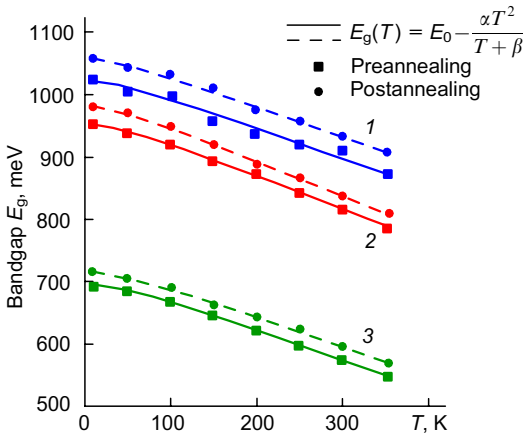


Figure 10. Effect of the heat treatment at 353 K for 27 h on the temperature dependence of the optical band gap for chalcogenide thin films.[109] (*1*) GeTe, (*2*) GST225, (*3*) AIST, α and β are fitting parameters; for other designations, see the text. Published in accordance with the Creative Commons CC license.

In the case of amorphous GST225, a decrease in E_g is equal to the difference $(E_0 - \zeta T^2)$, where E_0 is the optical band gap at 0 K, and the temperature coefficient ζ is 1.43×10^{-6} eV K^{-2} (Ref. 108). From the microscopic standpoint, the resistance drift is due to spontaneous structural relaxation of the amorphous film to energetically more favourable configuration, 'ideal glass'.[110–112] Le Gallo *et al.*[110] used the collective structural relaxation model, which implies successive relaxation between two neighbouring states driven by the energy difference (Δ_b) between local minima (Fig. 11). The closer the system to the equilibrium state, the smaller this difference, but the higher the energy barrier for the subsequent relaxation (E_s). It is noteworthy that because of the observable change in the optical band gap, the drift of functional parameters is manifested as a change in both the resistivity and the dielectric permittivity and, hence, also in the refractive index and the light absorption coefficient, which may affect the operation of optical and optoelectronic devices.[109]

A very important characteristic of materials used as optical data storage media is the optical contrast, which

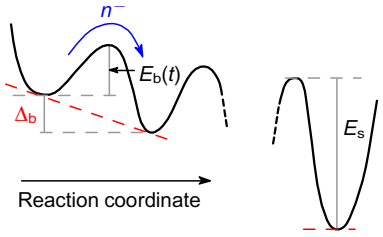


Figure 11. Collective relaxation model according to which the as-deposited film in the metastable amorphous state tends to energetically more favourable state *via* a sequence of transitions, while remaining amorphous. The activation energy of relaxation $E_b(t)$ increases after each transition associated with movement of atoms and subsequent stabilization of their positions.[110] Here n is the relaxation rate towards the equilibrium, t is time, Δ_b is the energy difference between the local minima of two neighbouring states (driving force of relaxation). Published in accordance with the Creative Commons Attribution license.

includes the difference between the optical coefficients n and k of the amorphous and crystalline phases in the integral form. The values of the optical contrast of PCM materials characterizing the efficiency of optical memory and nanophotonic devices are not entirely clear.

The most popular PCM materials, their optical constants and density changes upon the phase transition are summarized in Table 1. Analysis of the data provides the conclusion that materials most promising for optical recording are NaCl type metastable cubic phases with substantially different n and k and a noticeable change in the density between two phases (5% and more).

The question arises of why the optical contrast is relatively high for some compositions (in particular, GST alloys) and is small for other compositions (see Table 1). Several approaches were proposed to explain this fact. Martinez *et al.*[113] showed in relation to Sb_2Te_3 that the factors responsible for high optical contrast include the crystal field and spin–orbit coupling and abnormally high refractive index of the crystalline phase. Transfer to the amorphous phase is accompanied by metal–dielectric type second order phase transition associated with the electronic subsystem, which gives rise to a large optical gap at relatively small electronic band gap. Li *et al.*,[114] who analyzed GeTe and Sb_2Te_3 binary phases and ternary phases of the GST system, showed the essential role of defects such as vacancies and structure stiffness and their effect on the optical contrast and the thermal stability of optical properties of materials. The best characteristics were found for germanium telluride in which the concentration of vacancies is markedly lower than those in GST compounds [115] and the structure is most stiff.

As can be seen from the data of Table 1, there is a clear correlation between the change in the material density and the optical contrast: the greater Δd, the higher the optical contrast, and, hence, the more this compound is suitable as the active material for optical phase change memory devices. This relationship is due to the fact that the phase transition is accompanied by a pronounced local rearrangements in the material. It is of interest that compositions that have no polymorphs, but have only one stable structure (*e.g.*, chalcopyrite type structure) have low optical contrast.[116]

Table 1. Parameters n and k (at 650 nm) wavelength and density changes (Δd) upon phase transition for some PCM materials.[28]

Material	Amorphous state		Crystalline state			Δd (%)
	n	k	structure	n	k	
GeTe	3.6	1.5	Cubic NaCl type	6.1	0.2	–
GST124	4.1	2.1	Cubic NaCl type	3.6	4.2	7.5
			(metastable);			
			hexagonal (stable)	–	–	8.2
GST225	4.1 to	1.9 to	Cubic NaCl type	4.4	4.3	6.8
	4.5	2.3	(metastable);			
			hexagonal (stable)	3.9	4.3	8.2
$Ge_4Sb_1Te_5$	3.8	1.3	Cubic NaCl type	3.2	3.9	9.3
$AgSbTe_2$	3.2	2.8	Cubic NaCl type	2.7	3.5	4.3
$AuSbTe_2$	3.3	3.2	Cubic NaCl type	3.1	4.2	5.0
$AgInTe_2$	3.3	0.6	Chalcopyrite type	3.3	0.7	1.7
$AuInTe_2$	3.8	1.1	Chalcopyrite type	3.3	1.2	2.0

Spectral ellipsometry is used most often to determine optical constants of PCM thin films; the method makes it possible to calculate n and k values using model views on the layered structure and roughness of films as well as experimental data — ellipsometric angles ψ and Δ.[116–118] This method provides a higher accuracy than spectrophotometric techniques, since there is no need to measure the transmission and reflection coefficients of thin films possessing high absorption. The optical band gap can also be determined by spectral ellipsometry; hence, it is possible to compare the result with a similar characteristic found from optical transmittance of the thin film (this approach is also often used to study PCM materials).[116,119] It should be borne in mind that the results of optical measurements for formally the same chemical composition of thin film may differ, which is attributable to both the preparation and subsequent heat treatment conditions and the applied model and analytical methods used for processing of experimental data (see, for example, Ref. 116). The results of ellipsometric measurements of amorphous thin films, in particular GST225 thin films, are most often interpreted using the Tauc–Lorentz and Cody–lorentz models. The former model is quite popular for interpretation of the optical properties of disordered semiconductors, this is actually a classical approach [120] known for several decades. A specific feature of the Cody–Lorentz model proposed in 2002 by Ferlauto *et al.*,[121] is taking account of the Urbach energy, which characterizes tails of the density of states in the mobility gap of an amorphous semiconductor.

The above examples lead to the conclusion that now there is no general approach to interpretation of some important effects inherent in PCM materials. Thus, a number of key questions have not yet been answered by fundamental science, despite the obvious success in the commercial application of these materials.

2.4. Application areas

It is beyond doubt that the discovery of PCM materials in the GST system has played an important role in the development of electronic technology; however, one more circumstance should also be borne in mind. It is known that high power consumption for programming of memory cells was a key drawback of the phase change memory devices designed in the 1970s (they are conventionally called first-generation PCM devices). The linear dimension of one cell (a few micrometres) was dictated by the potential of photolithographic processes of that time; therefore, the relatively high energy needed for switching the state of a PCM material was actually determined by the volume of the active region. However, at the turn of the millennium, owing to achievements in the lithography, the size of the element decreased from 10 μm to 180 nm, *i.e.*, ~56-fold, while the corresponding volume of the active region thus decreased 171 468-fold (!). This led to a sharp drop of the power consumption for programming and made it possible to fabricate elements that were quite competitive and found use in various nanodevices.

2.4.1. Optical data storage systems

The design of rewritable optical discs is one of the first commercially successful applications of PCM materials.[122–124] The principle of recording data to a disc is based on considerable changes in the reflection coefficient of a local region of the data layer as a result of phase transition. The sequence of operation stages is the follow-

ing. Initially, the active layer of the material is usually in the polycrystalline state. The amorphous local regions (so-called pits) in the data layer of the disc are generated using local heating by laser pulses above the melting point; then the material transforms into the amorphous state as a result of fast cooling. Switching to the crystalline state is induced by heating the material to a temperature below the melting point but above the crystallization temperature by using a longer but less intense pulse (see Fig. 2). The duration of the initiating action for discs based on GST materials is ~10 ns. Reading is performed by laser radiation the intensity of which should not initiate phase transitions. The parameters of the read laser beam reflected from the data layer depend on the phase state of the material; this may be identified by a detector, which converts the obtained data to a digital flow consisting of logical zeros and ones.

Phase state memory materials are used to manufacture CD (compact disc), DVD and BD optical discs. The structures of these discs are, in essence, identical (Fig. 12 *a*); the major differences are in the numbers and thicknesses of the layers and in the composition of the PCM material. The change in the optical system on going from CD to DVD and then to BD is due to the decrease in the laser radiation wavelength (780, 650 and 405 nm) and increase in the numerical aperture (0.45, 0.6 and 0.85), which ensures a decrease in the pit lateral dimension (see Fig. 12).[122] By improvement of the optical system, it is possible to better focus the laser beam and obtain a higher resolution and, hence, to achieve a higher data density on a disc. Transition from a single-layer DVD to a single-layer BD increased the disc capacity from 4.7 to 25 GB. It is noteworthy that this was not accompanied by a change in the energy density needed to form an amorphous pit, while the cross-section of a laser beam decreases. As a result, power consumption for data recording to BD is equal to 1/4 of the power consumption for recording to DVD (see Fig. 12).[123, 124]

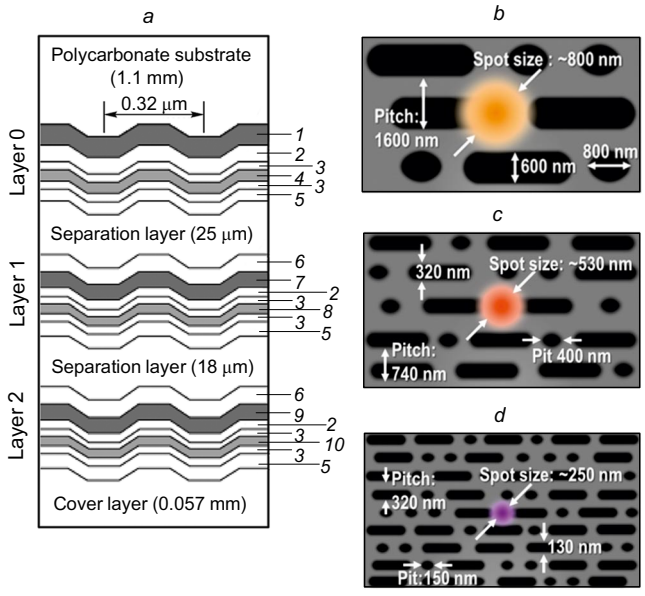


Figure 12. Structure of a multilayer BD disk (*a*)[123] and a change in the size of the laser spot focused on the surface of CD (*b*), DVD (*c*) and BD (*d*) disks.[124] (*1*) 100 nm silver layer; (*2*) dielectric film; (*3*) interfacial film; (*4*) $GeTe-Sb_2Te_3$ film, 10 nm; (*5*) $ZnS-SiO_2$ film; (*6*) TiO_2-based film; (*7*) 9 nm silver layer; (*8*) $GeTe-Sb_2Te$ film, 7.5 nm; (*9*) 7 nm silver layer; (*10*) $GeTe-Sb_2Te_3$ film, 6 nm. Figure 12 *a* is published with permission from Springer Nature; Figures 12 *b–d* are published with permission from ACS Publications.

The change in the wavelength in the data recording systems with the goal of decreasing the size of the laser spot brought about the need to adjust the elemental composition of the PCM material to optimize the optical contrast. Whereas GST225 is one of the most popular compounds for DVD discs, in the case of BD discs, $Ge_8Sb_2Te_{11}$ is used most often.[122] Currently, multilayer BD discs are manufactured using analogous PCM materials, which increased their recording capacity severalfold.[123]

2.4.2. Electrical data storage systems

The development of electronic devices, including the most recent advances in the design and wide use of portable and wearable electronic devices maintains the stable growth of demand for the fabrication of new and upgrading of existing compact data storage and transfer systems. Data storage devices based on flash memory technology are most popular among users of electronics. However, flash memory devices possess certain drawbacks, which considerably hamper further development of computation systems, *e.g.*, insufficient number and low speed of write–erase cycles. In addition, increase in the operating stability of such systems is associated with limitations manifested upon increase in the leak current due to radiation exposure and upon further decrease in the geometric dimensions of the cells.

In view of the foregoing, the design of a power efficient, radiation-resistant, high-speed and non-volatile memory device is a scientific and engineering challenge, solution of which would increase the capability of electronic devices. The enhancement of the above-listed parameters in comparison with the parameters of flash memory devices may be attained by using PCM materials. A specific feature of the design of modern cells is the presence of initial polycrystalline PCM layer in which the active region is formed spontaneously upon the application of a specified voltage pulse to the bottom electrode (BE).

Initially, PCM devices were designed using circuitry solutions based on 1T–1R (one transistor–one resistor) logic where the transistor served to control signal parameters and ensured access to the cell.[125] The electrical circuit for a memory storage device in which each cell has a resistive element based on a PCM-material and a control field effect transistor is depicted in Fig. 13 *a*. A cell design is shown in Figs 13 *b*,*c*. In this cell, the phase state changes in a limited part of the chalcogenide material. The electrical contact with this part is provided by the bottom electrode made of a refractory material. The rest of the PCM material remains in the crystalline state.

In these circuits, transistors can be separated by trench isolation (Fig. 13 *c*).[125–127] Each cell has conductor paths, word line (WL) and a bit line (BL), which provide the electrical connection to other functional blocks of the memory storage device (decoding circuit, selection system and so on). A drawback of this design is relatively high cell switching current, which imposes certain requirements on the operation of the selection transistor, restricts the possibility of decreasing its size and, hence, the size of the whole cell.

A variety of cell designs were tested with the goal to find electrophysical characteristics optimal for data writing and to decrease the applied currents.[126, 127] Despite the consid-

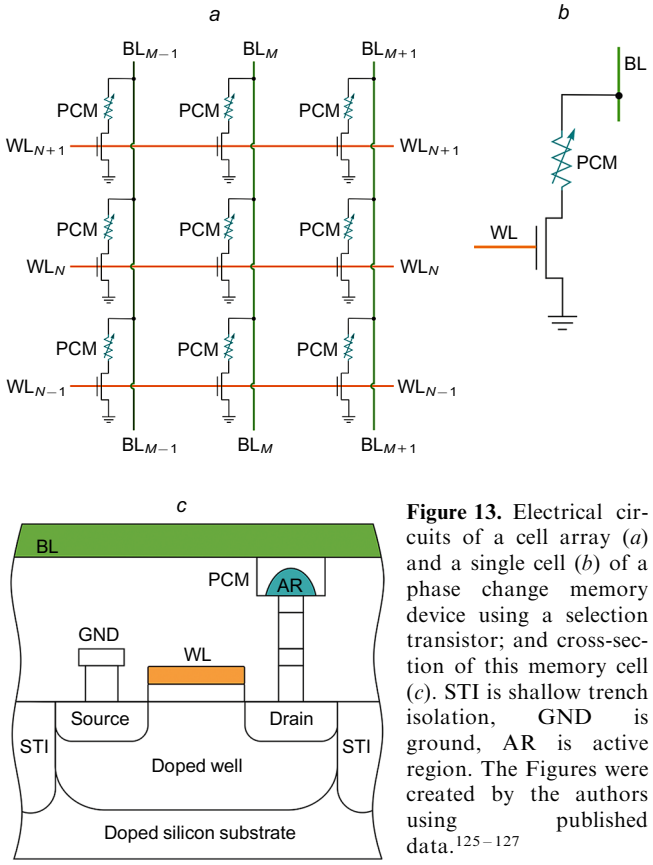


Figure 13. Electrical circuits of a cell array (*a*) and a single cell (*b*) of a phase change memory device using a selection transistor; and cross-section of this memory cell (*c*). STI is shallow trench isolation, GND is ground, AR is active region. The Figures were created by the authors using published data.[125–127]

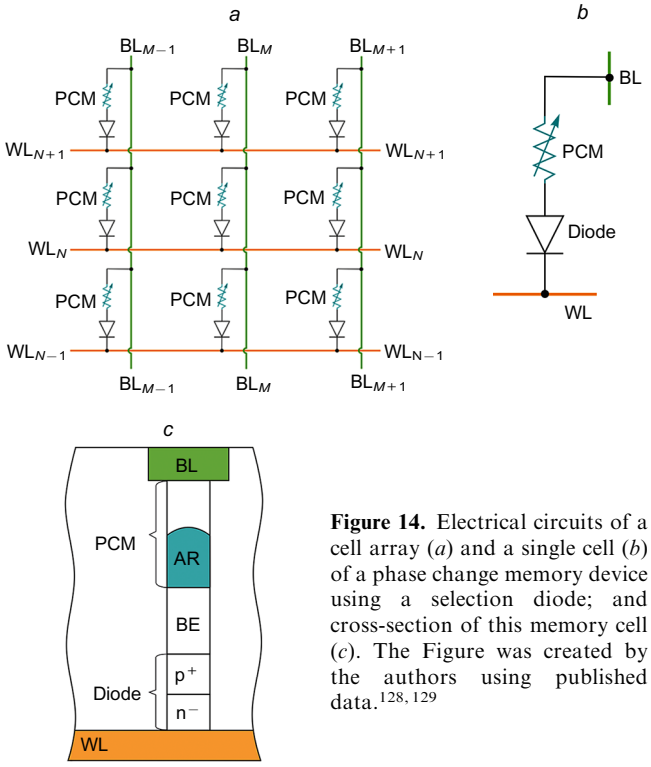


Figure 14. Electrical circuits of a cell array (*a*) and a single cell (*b*) of a phase change memory device using a selection diode; and cross-section of this memory cell (*c*). The Figure was created by the authors using published data.[128, 129]

erable differences between the designs, some key solutions used in all types of these cells can be listed:

— Chalcogenide semiconductors of the GST system are used most often as programmable phase change memory materials; this is due to the high speed of switching, stability and great resistance contrast between the amorphous and crystalline states;

— refractory metals that withstand heat treatment to 700 °C are used as current-conducting materials;

— the electrical characteristics of the cells are varied by varying the design and size of the bottom electrode;

— the cells are formed using conventional techniques applied in microelectronics.

A change in the design and size of the bottom electrode makes it possible to optimize SET and RESET operation parameters, but does not completely solve the problem of further miniaturization of PCM cells. A progress along this line was attained by designing 1D–1R (one diode–one resistor) type cells. As a result, the selection transistor was removed from the cell to a control line (Fig. 14).[128, 129] This approach provided a quantum leap in the design of memory storage devices based on electrical phase change memory. Indeed, in 2010, Samsung[129] manufactured a prototype memory cell with $4F^2$ size, where F corresponds to the technology level applied to design the cell (Kim *et al.*[129] used a sub-20-nm technology); subsequently, Intel used the 3D-XPoint technology[40] to design a non-volatile memory device Intel Optane, which found commercially successful application as SCM class memory.[42]

Currently, further development of the electrical phase change memory technology is mainly hampered by the drift of electrical parameters in the functional region of a PCM material in the amorphous state. This complicates manufacturing of multilevel memory cells and increases the time of crystallization, which restricts the operation speed of elements based on GST compounds. In commercially successful PCRAM type electrical memory devices, crystallization is initiated by ~30 ns current pulses,[130] which makes it non-competitive in the writing speed with DRAM type memory, for which the writing time is ~10 ns.

2.4.3. Prospects for application in nanophotonic and optoelectronic devices

The modern achievements of nanophotonics and microelectronics and the above-noted benefit of PCM materials, that is, existence of two relatively stable states with large contrast of properties, resulted in the development of a number of electrical, electro-optical and optical devices for various purposes (Fig. 15). In the last several years, there have been publications discussing types of thin-film reflective displays (see Fig. 15 *b*,*c*),[22, 131] near-IR metasurfaces (Fig. 15 *j*),[132] thermal camouflage (Fig. 15 *l*),[133] nanophotonic (Fig. 15 *d*–*f*,*i*)[134–137] and plasmonic devices (Fig. 15 *g*,*h*)[138, 139] and other applications (Fig. 15 *a*,*k*).[17, 140]

A highly promising trend is the design of multilevel nanophotonic devices, which operate due to formation of different ratios of phase fractions in the functional regions of GST thin films. These processes can be initiated by heat treatment (Fig. 16 *a*),[116] electrical current (Fig. 16 *b*)[141] or laser radiation (Fig. 16 *c*).[142] Variation of parameters of the initiating stimulus may give rise to fully amorphous and/or fully crystalline (FCC or HCP structure) or a partially crystallized state with different amounts of amorphous and crystalline material in the functional region. The possibility of obtaining states with different degrees of crystallinity and pronounced optical and electrical contrast between these states provides a multilevel change in the parameters with an acceptable signal-to-noise ratio. Li *et al.*[143] demonstrated

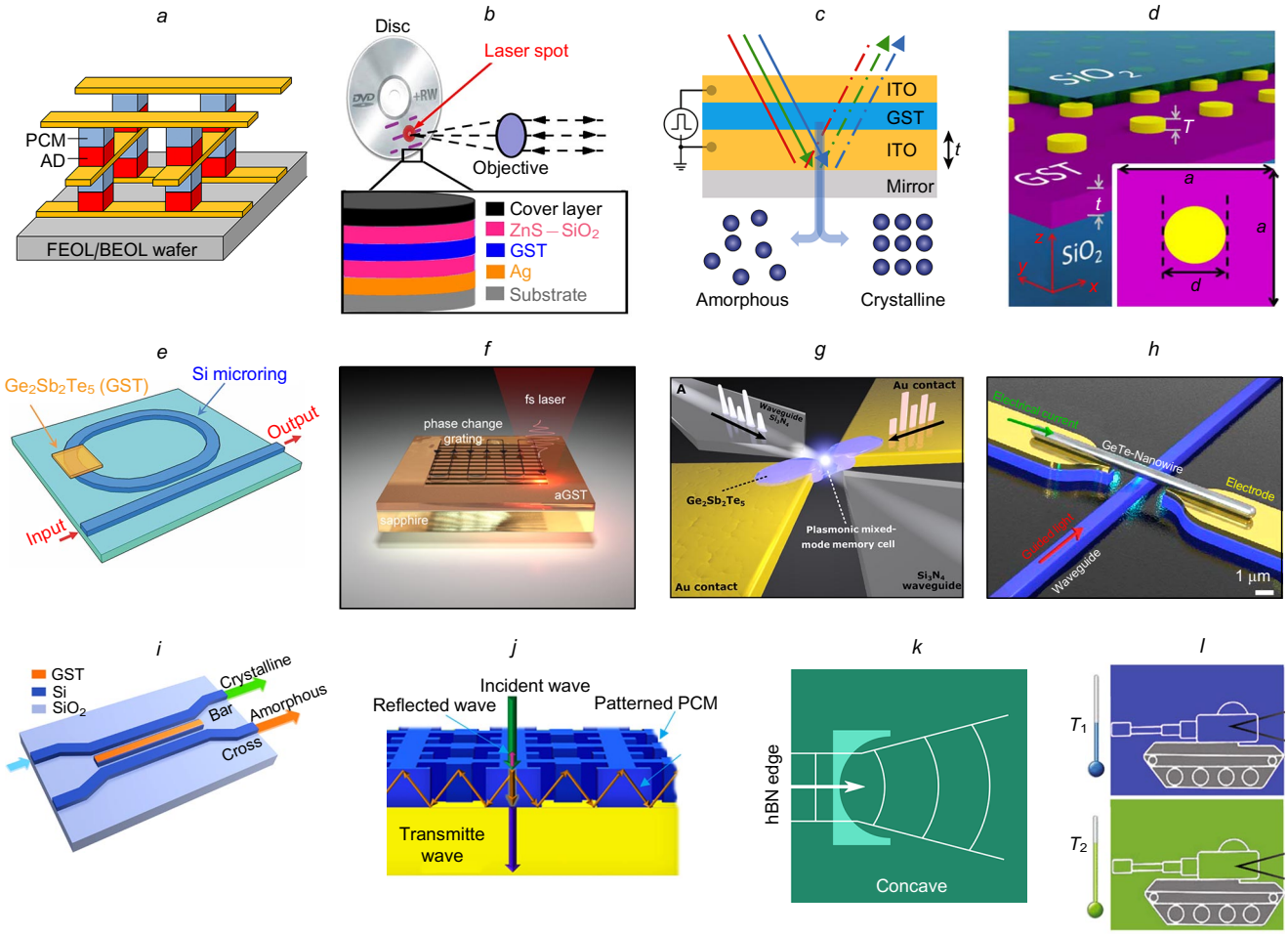


Figure 15. Schematics illustrating operating principles of various reconfigurable non-volatile devices based on phase change memory materials. (*a*) 3D-Xpoint electrical memory;[17] (*b*) optical discs;[22] (*c*) reflective displays;[131] (*d*) hybrid plasmonic crystals;[137] (*i*) racetrack microresonators;[134] (*f*) diffraction elements;[135] (*g*) electro-optical element based on plasmonic waveguide;[138] (*h*) optoelectronic integrated cell based on thin film waveguides;[139] (*i*) waveguide switch of the radiation direction;[136] (*j*) near-IR metasurfaces;[132] (*k*) lenses, prisms and other elements for the control of parameters of surface waves;[140] (*l*) thermal camouflage.[133] Figure 15 *a* is published with permission from IOP Publishing; Fig. 15 *b* is published in accordance with the Creative Commons license; Fig. 15 *c* is published with permission from Springer Nature; Fig. 15 *d*,*j*–*l* is published in accordance with the Creative Commons license (CC BY); Fig. 15 *e* is published with permission from AIP Publishing; Fig. 15 *f*,*h*,*i* is published with permission from the American Chemical Society; Fig. 15 *g* is published in accordance with the Creative Commons Attribution 4.0 license (CC BY).

the conceptual possibility of manufacturing a 5-bit non-volatile fully optical memory cell (> 34 non-volatile states in a single cell) functioning as a result of modification of optical properties under laser irradiation.

The design of multilevel integrated nanophotonic devices would improve and significantly expand the capabilities of integrated optical circuits. Unlike implementations in a free space where optical switching is induced by a focused far-field laser beam, multilevel devices operate in the near field, which allows miniaturization of waveguide-integrated cells to nano size, without being restricted by the diffraction limit. A promising application of such reconfigurable multilevel optical devices in the integrated design is the fabrication of photonic synapses and neurons in order to implement neuromorphic computing systems (Fig. 17).[144] These systems are capable of efficient solution of complex problems such as image processing, speech recognition, artificial vision, deep learning and some other. Non-volatility, multilevel nature, the possibility of generating a continuum of states, low power consumption, high operation speed and prospects for further miniaturization of devices based on GST compounds make them more competitive that the existing analogues.

In the last several years, a number of approaches to the design of fully optical neuromorphic systems have been proposed. Chakraborty *et al.*[146] designed a photonic synapse based on ring-shaped resonators partly coated by GST225 . Cheng *et al.*[144] proposed application of waveguide elements with discrete GST225 islands as an isolated photonic synapse, which is connected to neurons at the input and output of the waveguide. A similar approach was used by Feldmann *et al.*,[145] who integrated photonic synapses to optical neuronal circuits, also formed on the basis of GST225. The authors demonstrated the possibility of manufacturing a fully optical neuromorphic system (see Fig. 17 *b*) and its controlled and uncontrolled training.

Thus, the conceptual possibility of designing photonic neuromorphic computing systems based on GST225 has been proved. The next stage in the development of this field should be determination of the limiting achievable characteristics of the integrated optical elements based on PCM

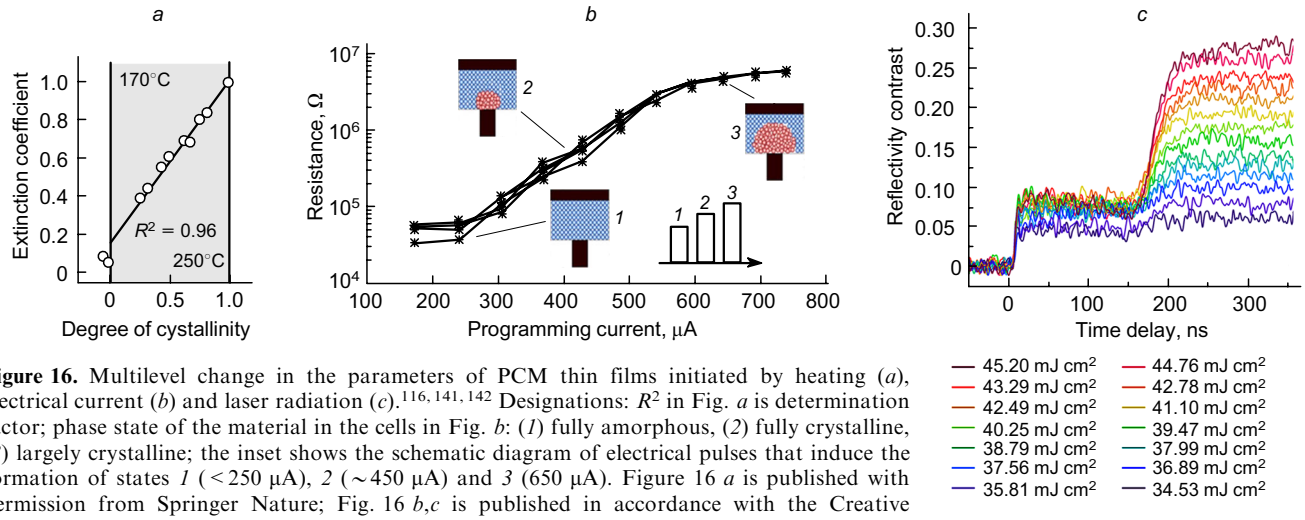


Figure 16. Multilevel change in the parameters of PCM thin films initiated by heating (*a*), electrical current (*b*) and laser radiation (*c*).[116, 141, 142] Designations: R^2 in Fig. *a* is determination factor; phase state of the material in the cells in Fig. *b*: (*1*) fully amorphous, (*2*) fully crystalline, (*3*) largely crystalline; the inset shows the schematic diagram of electrical pulses that induce the formation of states *1* (< 250 μA), *2* (~450 μA) and *3* (650 μA). Figure 16 *a* is published with permission from Springer Nature; Fig. 16 *b*,*c* is published in accordance with the Creative Commons Attribution license.

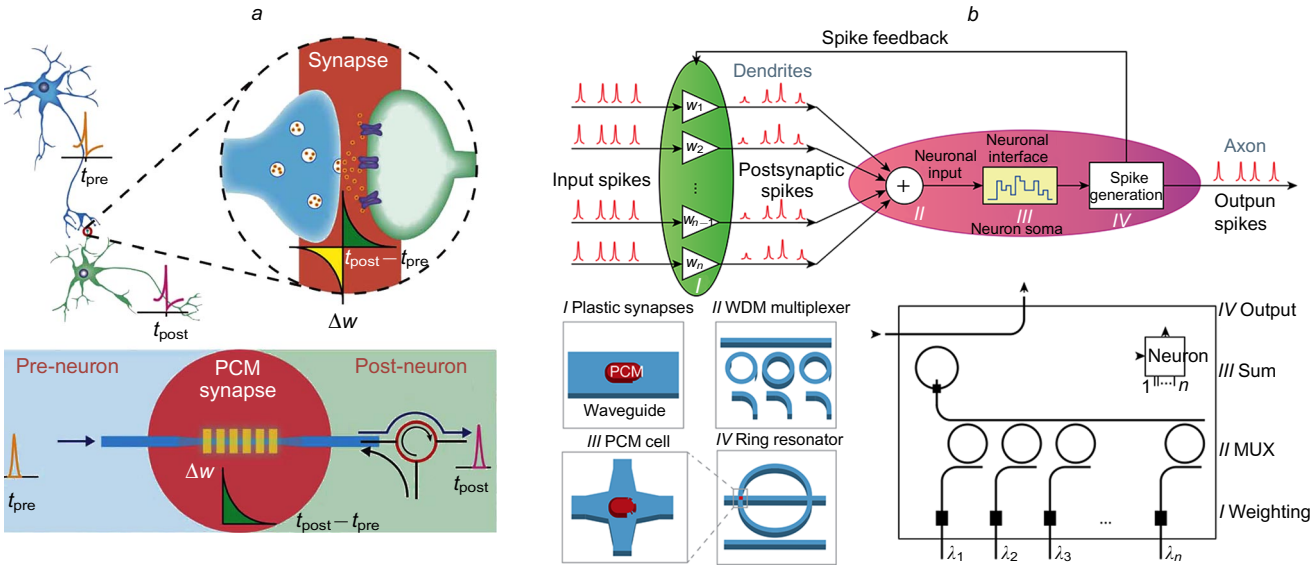


Figure 17. Schemes illustrating the principles of functioning of neurons and synapses (*a*) [144] and fully optical neuromorphic system made of PCM-based cells of different configuration (*b*).[145] *w* is the synaptic weight, t_{pre} and t_{pos} are pre-neuron and post-neuron signal parameters, respectively; the arrows in the lower panel of Fig. *a* indicate the direction of light propagation through the circulator; WDM is multiplexing with separation according to the wavelength, MUX is a multiplexer. Figure 17 *a* is published in accordance with the Creative Commons Attribution 4.0 license; Fig. 17 *b* is published with permission from Springer Nature.

materials, in particular, the scalability, speed of operation and power consumption.

Reconfigurable metasurfaces formed using chalcogenide semiconductors as functional materials are also promising for the development and commercialization. Metasurfaces based on films of the GST system can serve for optical modulation [147] (*e.g.*, to control the shape and propagation direction of a light beam [148] or absorption of optical systems) [132] and are of interest for polarization transformation.[149] In addition, these metasurfaces can be used to design diffraction optical elements (in particular, rewritable holograms).[150] Until recently, the development of this trend was hampered by problems associated with initiation of the change in the phase state and, hence, reconfiguration of metasurfaces, and with high level of optical loss.

The phase transitions of metasurfaces in functional PCM materials were initiated by laser radiation or by electrical current. This requires the use of a large laser system or numerous additional process operations in the manufacture of metasurfaces to ensure local heating of nanosized areas. This problem can be solved, in particular, by using the approach proposed by Abdollahramezani *et al.*,[151] who used an external microheater to induce switching of GST metasurface elements (Fig. 18).

Meanwhile, the problem of optical losses can be solved by changing the composition of the PCM material with the goal to attain the maximum transparency of the amorphous state, while retaining a sufficient optical contrast in the wavelength range needed for operation of the device. Promising compounds for this purpose are, for example, Sb_2S_3 and Sb_2Se_3, which possess a high transparency in the telecommunication range (~1550 nm) and a refractive index consistent with parameters of silicon photonics components.[76]

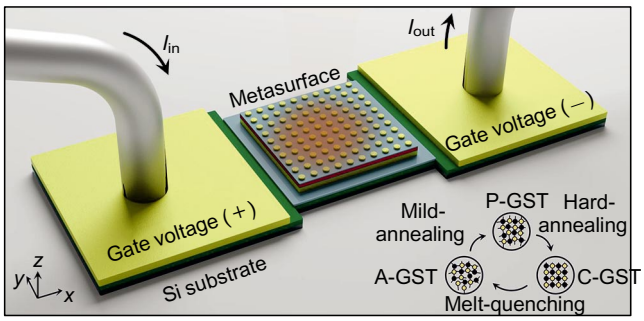


Figure 18. Schematic view of a metasurface integrated to an external microheater. A-GST, C-GST, P-GST are the amorphous, fully crystallized and partly crystallized states of the GST region, respectively.[151] The arrows indicate the direction of the electrical current. Published in accordance with the Creative Commons Attribution 4.0 license.

Thus, the application prospects of PCM materials of the GST system in various data storage devices and nanophotonic and optoelectronic devices are now obvious; however, for further development of this field, optimization of their physicochemical characteristics is required.

3. Chemical modification

The performance characteristics of PCM-based devices (speed of operation, power consumption, contrast between levels, optical losses at operating wavelengths, *etc*.) can be improved using several approaches listed below

— search for compositions other than GST225 in the Ag—In—Sb—Te,[152] Se—Sb—Te,[153] Sb_2Se_3,[76] *etc*. systems;

— change in the ratios of elements in the compounds of the GST system (GeTe,[154] $GeSb_4Te_7$, $GeSb_2Te_4$, $Ge_2Sb_2Te_5$,[155] $Ge_8Sb_2Te_{11}$,[156] *etc*.);

— application of thin films formed from alternating GeTe and Sb_2Te_3 monolayers;[157]

— doping of GST225; this is one of promising methods for the control over the properties of non-crystalline semiconductors (see below).

3.1. Methods of dopant introduction for chemical modification of thin films

The lack of sensitivity of properties of chalcogenide glassy semiconductors to substitutional impurities is due to the relaxation of the atomic structure of the material. To preserve the electrical activity of impurity atoms, it is desirable to avoid relaxation of the glass structure. For this purpose, the impurity atoms must be introduced under conditions where restructuring of the material is hampered, *i.e*., at temperatures below the softening temperature of the basic material.

These conditions can be implemented by at least two methods, either by ion implantation of impurity atoms into the film or by simultaneous ion-plasma sputtering of chalcogenide glassy semiconductors and the impurity on a substrate the temperature of which is lower than the softening temperature. The latter method was used [158, 159] to develop and implement a method for chemical modification of films. It is noteworthy that in this approach, the density of localized states caused by intrinsic defects remains high in the semiconductor band gap. Therefore, effective control of the electrophysical properties of the material requires relatively large concentrations of impurity atoms (a few tenths of a percent or a few percent).

The efficiency of this approach is exemplified by Fig. 19 *a*, which shows the temperature dependences of the specific conductivity (σ) of $(Ge_{32}Te_{32}Se_{32}As_4)_{1-x}Ni_x$ films and in Table 2, which presents parameters of films with various nickel contents.[159] It can be seen that for nickel-free samples, the temperature dependence of the electrical conductivity is a straight line with a slope corresponding to the activation energy of 0.74 eV, which attests to a Fermi level position close to the middle of the semiconductor band gap.

When the above conditions are met, the introduction of nickel into films not only increases the electrical conductivity by several orders of magnitude, but also changes the shape of this dependence: an impurity conduction segment appears in the plot. The slope of this segment decreases with increasing nickel concentration, which corresponds to a decrease in the activation energy of conduction down to 0.18 eV; this may be due to either a change in the position of the Fermi level in the band gap or a decrease in the band gap width. However, studies of the effect of material modification on the spectral dependences of the optical absorption coefficient showed that the band gap width changes insignificantly (Fig. 19 *b*). It can be seen that increase in the nickel concentration in the film causes mainly an increase in the density of localized states in the Urbach tails of the band gap. Thus, the observed changes in the electrophysical characteristics of chalcogenide glassy semiconductor films upon modification with nickel are caused by the change in the Fermi level position in the semiconductor band gap.

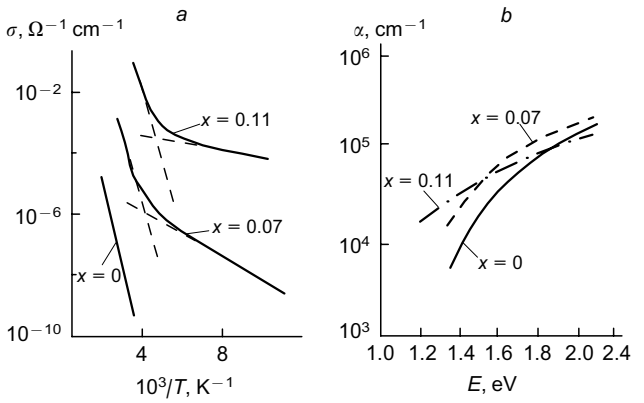


Figure 19. Temperature dependences of the specific conductivity (*a*) and spectral dependence of the optical absorption coefficient (*b*) of the $(Ge_{32}Te_{32}Se_{32}As_4)_{1-x}Ni_x$ film. The Figures were created by the authors using data of Ref. 159.

Table 2. Effect of chemical modification on the electrophysical properties of $Ge_{32}Te_{32}Se_{32}As_4)_{1-x}Ni_x$ films.[159]

x	E_σ, eV	$\sigma_{293\,K}$, Ω^{-1} cm^{-1}	S, μV K^{-1}
0	0.74	4×10^{-10}	2000
0.07	0.33	1.4×10^{-5}	54
0.09	0.25	6.5×10^{-4}	−82
0.11	0.18	3.8×10^{-2}	−84

Note. $\sigma_{293\,K}$ is the specific conductivity at 293 K, S is the thermo-emf coefficient.

Chemical modification can induce a change in the sign of thermo emf from plus to minus (see Table 2), which is indicative of a change in the type of conduction.[159] This also confirms that the observed changes in the electrical characteristics, with the band gap width being virtually invariable, are caused by the shift of the Fermi level. Studies of other semiconductor compositions and other modifying metals showed analogous results.[159]

Ion implantation, which is based on bombardment of a film surface with an ion beam followed by ion incorporation into the material, is widely used owing to its benefits, in particular

— the possibility of doping virtually any material with any impurity, because there is no need to take into account the solubility, thermodynamic issues and so on;

— the process can be conducted at any temperature, including low temperatures;

— the depth of ion penetration into near-surface layers can be varied over wide limits, with the bulk material itself remaining unchanged;

— by varying the irradiation dose, it is possible to attain a high density of defects in the layers.

The two last-mentioned issues are somewhat contradictory to each other, and finally they comprise the limitation of this method.

In relation to chalcogenide glassy semiconductors, ion implantation is used to control their electrical and optical properties. In particular, ions of d-elements (Fe, Co, Ni) implanted into binary arsenic selenides change the conductivity by several orders of magnitude, whereas main group metals such as tin induce a much smaller effect.[160] Interesting results were obtained by various authors who attempted to change the type of conduction in CGS thin films by bismuth or lead implantation;[161] furthermore, in GeTe thin films, the sign of the Seebeck coefficient changed at a markedly lower concentration of implanted bismuth ($\sim$0.6 at.%) than in the case of melts with the same composition.

The idea of doping of melts and subsequent sputtering of the synthesized PCM materials does not appear sufficiently promising for a number of reasons (see above); nevertheless, this method is used in research practice. First, it is least costly regarding both the experimental time and the economic expenses, if this refers to exploratory research where it is necessary to obtain materials with different contents of the dopant. Second, this method is applicable for studying not only thin films, but also bulk materials, which is in some cases important, because analogous measurements for thin-film structures may be either impossible or difficult.

Among approaches to the formation of thin films of doped compounds (most often, vacuum thermal deposition and ion plasma sputtering), isomorphous replacement of the major components should be noted.[162–164] The essence of this approach is as follows. The GST225 metastable cubic phase has 10 to 20% cationic vacancies; therefore, heterovalent isomorphous substitution using components with covalent radii close to the covalent radius of one of major components can affect the concentration of vacancies, without introducing considerable deformations into the short- and medium-range order of the material. Since purely covalent chemical bonds are rarely encountered in chalcogenide compounds (in which the bonds are always partly ionic; see, for example, Ref. 165), ionic radii of elements should also be taken into account.

It was assumed that impurity atoms would change the optical and electrical properties of bulk polycrystalline samples, and these changes would affect characteristics of amorphous thin films and also crystallization kinetics. It is important that particularly polycrystalline materials are used as sources for thermal deposition, because the formation of bulk amorphous GST phases is almost impossible at the cooling rates attained to date. The approach is based on the idea of isomorphous substitution, according to which the substitutional atoms occupy positions of original atoms; in this case, substitutional solutions, in which the inserted atoms occupy positions of original atoms, are not fundamentally differentiated from the interstitial solutions, in which they occupy voids (vacancies).[166] The dopants were either isoelectronic elements with atomic sizes close to that of the original component or heterovalent elements with similar covalent radii.

As substitutional impurities, Bi, As, Ag, Sn, In and Ti were proposed, while germanium or antimony served as original elements to be replaced. The impurity elements were chosen considering the valency compensation principle. Hence, isomorphisms with subtraction (formation of vacancies) and with insertion (filling of the interatomic space) are considered. For example, the stable titanium species is Ti^{IV}, and layered titanium dichalcogenides $TiTe_2$ are known. Hence, the introduction of titanium into a GST phase would result in isomorphism accompanied by subtraction

$$2\,Ge^{2+} \longrightarrow Ti^{4+} \quad (1)$$

or

$$4\,Sb^{3+} \longrightarrow 3\,Ti^{4+} \quad (2)$$

which should result in increasing concentration of vacancies relative to their concentration in the initial compound. In the case of heterovalent insertion of silver(I), the isomorphous substitution is expected to result in filling of the interatomic space according to the scheme

$$Ge^{2+} \longrightarrow 2\,Ag^{+} \quad (3)$$

i.e., it is assumed that the concentration of vacancies would decrease. In the case of isovalent substitution, the concentration of vacancies is expected to remain unchanged, which could hypothetically allow one to differentiate between effects of vacancy concentration and type of impurity.

3.2. Modifying dopants

The efficiency of a modifying dopant is based on the following statements. First, it should provide a change in the characteristics of thin films of chalcogenide semiconductors in the amorphous state. Modification should envisage the changes that this dopant would make to the characteristics of the crystalline state. The second important statement is that not only should particular parameters of different phases change, but also an overall beneficial effect of these changes is required. The introduction of a dopant should improve the stability of the phase composition of the material over a broad range of operating temperatures of the cell, including temperatures above T_m. Stability of a PCM material is significant for device characteristics such as the number of write–rewrite cycles and the time drift of functional parameters. The introduced dopant should not induce the separation of a second phase or a local segregation of atoms during operation of the device.

The results of modification of GST225 properties with C,[167, 168] Ni,[169] Al,[170] Ag,[171] In,[172] N,[173] Si,[174] Cu,[175] Zn,[176] As,[177] Se,[69] Sn,[178] Sm,[179] Bi,[180] Mg,[181] Si,[182] Sc,[183] V,[184] Cr,[185] Mo (Ref. 186) and Al (Ref. 187) have been reported to date. The large number of dopants is due to the complexity of selection of the optimal modifying component that would have a beneficial effect on the functional properties of GST225.

In some studies, attempts were made to summarize the experimental results on implantation of impurity ions. For example, Kang and Chen [23] analyzed the data on the effect of dopants on the properties of GST225 and also plotted the dependences of some parameters (in particular, crystallization temperature, resistance contrast, crystallization activation energy) on the type of modifying dopant (Fig. 20).

Comparative analysis revealed the effect of tungsten and nickel doping on the increase in the crystallization temperature and decrease in the switching time. Choi *et al.*[176] studied the lattice distortions and the energy of formation of bonds and demonstrated that the zinc-doped sample is more promising for increasing the stability and resistance of the crystalline phase compared to the samples with thirteen other doping elements.

However, as noted above, PCM materials are subject to contradictory requirements. On the one hand, tungsten and nickel doping leads increases the crystallization temperature, which is an obvious advantage since this decreases the probability of spontaneous crystallization of the amorphous material, but, on the other hand, this results in a higher power consumption. The introduction of zinc into GST phases increases the resistivity and decreases the power consumption; however, the contrast between the amorphous and crystalline states becomes less pronounced, which has an adverse effect on the performance of multilevel devices.

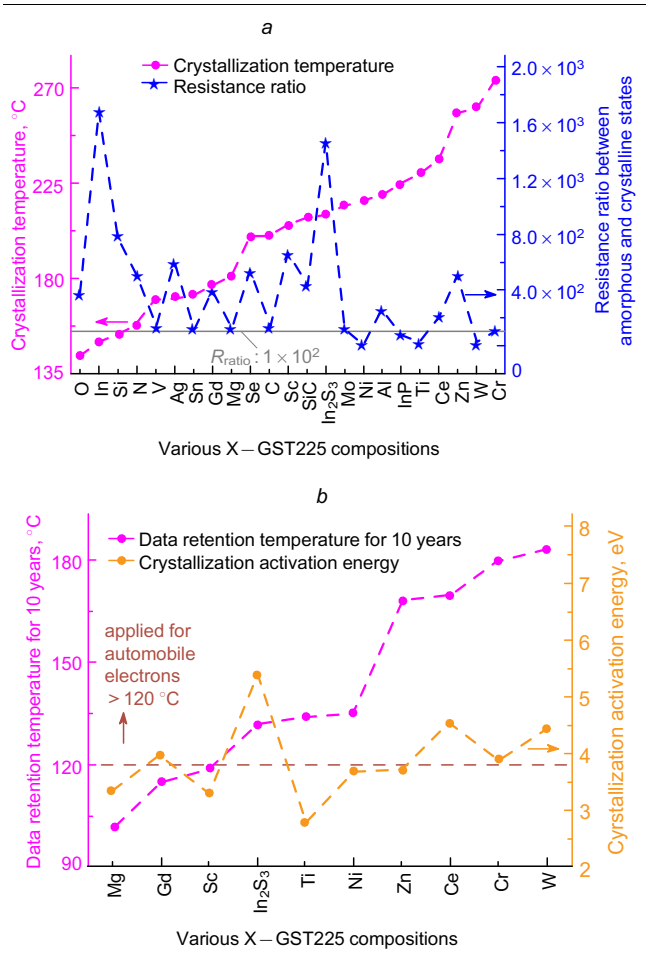


Figure 20. Dependences of the crystallization temperature and resistivity contrast (*a*), activation energy of crystallization and temperature ensuring stability of the amorphous state of GST225 for 10 years (*b*) on the type of modifying dopant.[23] Published with permission from Springer Nature.

Depending on the type of device being developed (electrical memory, integrated photonic devices, information display elements, metasurfaces, *etc.*) and the functional purpose, the requirements to the material and the priority between them may change. Thus, chemical modification can be considered as a method for controlling the properties of PCM materials suitable for targeted selection of a dopant to meet the imposed requirements. Below we consider doping with bismuth, tin, oxygen, nitrogen and refractory tungsten and titanium.

3.2.1. Isomorphous impurities

According to the Goldschmidt rule,[188] the formation of isomorphous mixtures is possible over a broad range of concentrations at temperatures below T_m provided that the difference between the ionic radii of exchanging components does not exceed 15%. If the doping element and one of the original elements of the material have similar covalent or atomic radii, a minimum deformation of the lattice is expected. The introduction of a smaller ion or an ion with a higher charge may strengthen the lattice, which would be energetically favourable (polarity rule). Furthermore, the choice of a doping element must comply with the valency compensation principle; correspondingly, subtraction or insertion isomorphism alternatives should be considered in the case of heterovalent substitution; also, the electronegativity difference between the exchanging atoms should be considered (the smaller this difference, the wider the range of isomorphism).

Analysis of published data [69, 169, 173–180, 189] showed that to change the properties of GST225, the doping atoms should have parameters close to the parameters of one component of this PCM material; in this case, the insertion of impurity atom into the lattice causes little stress. Bismuth, tin, indium, titanium and some elements were proposed as isomorphous impurities for cationic substitution. However, fulfilment of this condition does not ensure the success of chemical modification of GST225, since the change in the properties depends on the substitution mechanism, the sites occupied by the doping atoms and characteristics of the formed chemical bonds. For example, titanium has a valency of 4 in chalcogen compounds; hence, in the case of titanium doping, subtraction isomorphism can be expected [see processes (1) and (2)]. This should result in higher vacancy concentration relative to that in the initial compound.

Replacement of germanium atoms by tin atoms. Tin and germanium are isovalent and isomorphous elements with similar electronegativities [χ(Sn) = 1.96, χ(Ge) = 2.01].[190] Hence, it can be expected that replacement of germanium (cationic unit) with tin to give Sn–Te bonds would not induce a pronounced lattice deformation; this is consistent with conclusions drawn from DFT calculations of stability [176] and with X-ray photoelectron spectroscopy data.

For a solid material, the replacement of germanium with tin would be accompanied by a decrease in the bond energy from 180.3 kJ mol^{-1} for the Ge—Te bond [8, 191, 192] to 179.3 kJ mol^{-1} for the Sn—Te bond.[193] In this case, even a minor amount of tin impurity in the GST225 thin film may change switching characteristics, in particular, the energy of initiation of phase transition may decrease, which would entail a decrease in the power consumption by the devices. This assumption is indirectly confirmed by the observed decrease in the temperature and laser radiation energy needed for crystallization.[156, 194–196] However, in some publications (see, *e.g.*, Refs 197–199), it was stated that introduction of tin into a phase change material such as GST225 leads to higher temperature of crystallization. Furthermore, the tin doping of amorphous thin films of GST compounds decreases the laser pulse duration.[200] Zalden *et al.*[201] observed an increase in the laser crystallization rate and demonstrated the possibility of switching between states under the action of femtosecond laser pulses.

According to Raman spectroscopy [202] and X-ray diffraction [178] data, the introduction of tin atoms into GST225 thin films leads to a change in the vibrational modes and parameters of film structures both in the amorphous and crystalline states. This may bring about a pronounced increase in the optical contrast, in particular, due to increase in the optical reflectivity of doped GST225 in the crystalline state.[156, 178, 194, 195, 203]

An important characteristic of device operation is thermodynamic stability of a PCM material. Phase separation and segregation of elements may disrupt SET and RESET properties. According to DFT calculations of the formation energy of structural fragments, tin has the highest thermodynamic stability in GST225 among elements used for doping of GST compounds. Despite the increase in the lattice parameters of crystalline states [200] caused by the difference between the covalent radii of tin (1.44 Å) and germanium (1.22 Å), the introduction of low concentrations of tin should not considerably affect the stability. Yin and Chen [178] confirmed that phase separation into GST225 and SnTe during crystallization takes place only when the tin concentration is >11.6 at.%. However, even if the two-phase system is formed, the FCC lattice of GST225 and the cubic lattice of SnTe have similar structures; therefore, doping should not significantly influence the phase stability and, hence, the number of writing cycles in devices based on PCM materials.[178]

Thus, tin doping can serve for increasing the operation speed and decreasing the power consumption of nanophotonic devices and reflective display elements based on GST compositions operating at moderate temperatures.

Replacement of antimony atoms by bismuth atoms. The addition of bismuth is of interest for control of the electrophysical properties of PCM materials; the effects of bismuth doping have been considered in detail.[164, 196, 204, 205] Bismuth and antimony are isoelectronic elements of Group 15 of the Periodic Table with three electrons in the outer p-orbitals. The elements have similar atomic (R_{Sb} = 0.161 nm, R_{Bi} = 0.1547 nm) and ionic radii ($R_{Sb^{3+}} = 0.082 \pm 0.003$ nm, $R_{Bi^{3+}} = 0.102 \pm 0.007$ nm) and virtually equal electronegativity [χ(Sb) = 2.05, χ(Bi) = 2.02].[190] The Bi—Te and Sb—Te bond energies in the gas phase are 230.12 and 276.1 kJ mol^{-1} (Ref. 206). The bond energy in glasses differs from that in the gas phase, for example, the mean Sb—Te bond energy in glass is 195 kJ mol^{-1} (Ref. 8). However the trend of decreasing bond energy with increasing atomic number of the element of the same group holds. Hence, the Bi—Te bond energy can be expected to be lower than 195 kJ mol^{-1}. The replacement of some of the antimony atoms by bismuth *via* the isomorphous substitution mechanism was confirmed, first, by Raman scattering data,[207] which demonstrated that the introduction of bismuth into GST225 gives Bi_2Te_3 groups in addition to Sb_2Te_3, and, second, by *ab initio* calculations, which predicted the probable formation of defective octahedral $BiTe_n$ complexes.[205]

The introduction of bismuth atoms makes a significant contribution to the electrical conductivity of GST225. The increase in the bismuth concentration is accompanied by a decrease in the resistivities of the amorphous and crystalline states and the ratio of these values (Fig. 21). This restricts the applicability of this material for the design of electrical multilevel phase change memory devices. However, the optical contrast virtually does not change.[205] A study of GST225 thin films modified with bismuth in high concentration showed the absence of sharp step in the temperature dependences typical of crystallization. This result was obtained for objects formed both by magnetron co-sputtering of chalcogenide glassy semiconductor and bismuth targets (see Fig. 21 *a*) [196] and by ion implantation (see Fig. 21 *b*).[208]

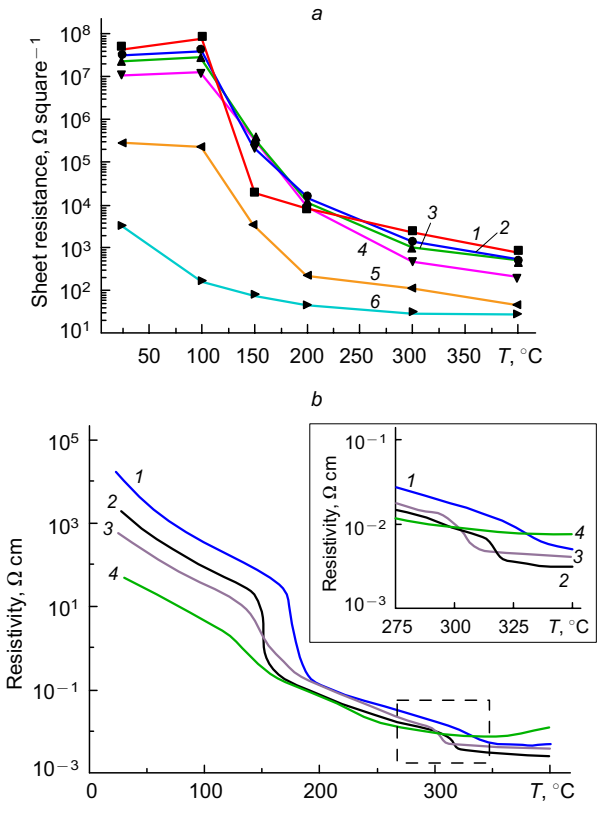


Figure 21. Effect of annealing temperature on the resistivity of GST225 thin films doped with various bismuth concentrations obtained by co-sputtering of several targets (*a*) [196] and by ion implantation (*b*).[208] Designations in Fig. *a*: Bi concentration, at.%: (*1*) 0, *2*–3.8, (*3*) 4.4, (*4*) 5.9, (*5*) 9.8, (*6*) 19.6; Fig. *b*: degree of sample doping: (*1*) none, (*2*) minimum, (*3*) medium, (*4*) maximum. Figure 21 *a* is published with permission from Elsevier; Fig. 21 *b* is published in accordance with the Creative Commons Attribution 3.0 license.

It is noteworthy that the dependences describing the variation of semiconductor properties with increasing bismuth concentration are not linear. Schottmiller *et al.*[209] showed the presence of two different ranges in the concentration dependences of the optical properties of amorphous Se–Bi films (Fig. 22 *a*), while Elliott and Steel[210] experimentally demonstrated four ranges with different patterns of variation of the activation energy of conduction *versus* bismuth concentration (ranges I–IV in Fig. 22 *b*) in the $Bi_xGe_{20}X_{80-x}$ systems (X = S, Se). Non-linearity of these dependences was also found for GST225 thin films:[164] the addition of low bismuth concentrations (~0.5 at.%) gave rise to a local extremum in the curves.

Tohge *et al.*[211] demonstrated switching of p-type conduction to the n-type conduction for GST compositions and a change in the charge transport mechanism upon the introduction of large concentrations of bismuth (>10 at.%). A similar effect was also observed for other chalcogenide glassy semiconductors containing germanium, *e.g.*, GeSe (Ref. 212) and GeTe.[213] Upon analysis of the change in the electron state density, Skelton *et al.*[205] suggested that a change in the type of conduction is attributable to the shift of the valence and conduction bands to lower energy and delocalization of states at the band edges; this may change the mobility of charge carriers. This effect, in combination with a change in the heat conductivity of the material in the amorphous state upon the introduction of bismuth, may be of interest for specialists engaged in the development of thermoelectric devices.[214]

The addition of bismuth increases crystallization rate of the amorphous GST225 phase. This was attributed[205,215] to increase in the free volume and decrease in the viscosity, which facilitate atomic diffusion in early stage of crystallization. However, Ren *et al.*[216] noted that crystallization of $Ge_{1.3}Bi_{0.5}Sb_{1.5}Te_3$ is accompanied by a much less pronounced density change ($\Delta d = 4.6\%$) than that of the undoped GST225 ($\Delta d = 6.8\%$); therefore, the mechanical stress arising during switching of the device may decrease, which has a beneficial effect on the number of switching cycles. The possibility of creating T-shaped cells based on $Ge_{1.3}Bi_{0.5}Sb_{1.5}Te_3$ with endurance of at least 10^5 write–rewrite cycles was demonstrated in the same study.

Thus, bismuth-modified PCM materials can be promising for the use in optoelectric devices that control the optical signal *via* a phase transition and in low-temperature thermoelectric applications where the change in the type of conduction depending on the phase state can be used for the control.

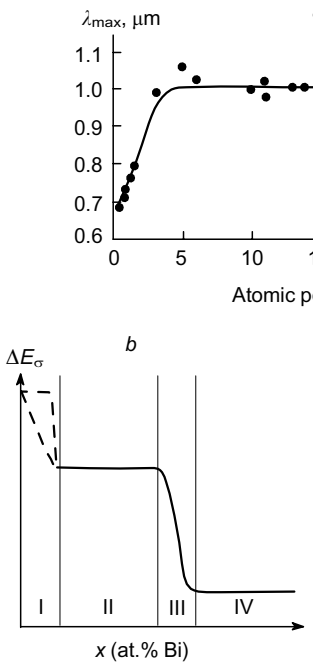


Figure 22. Effect of bismuth concentration on the results of spectral photometry of Bi–Se films (*a*)[209] and on the activation energy of conduction of $Bi_xGe_{20}X_{80-x}$ glasses (X = S, Se) (*b*).[210] The dashed lines show the possible changes in the activation energy in this range. Figure 22 *a* is published with permission from AIP Publishing; Fig. 22 *b* is published with permission from IOP Publishing.

3.2.2. Light elements

Studies of the chemical modification of PCM materials with light elements are mainly concerned with the role of nitrogen and oxygen in GST compounds, which is due to the following circumstances:

— oxygen is located in Group 16 of the Periodic Table, together with chalcogens, and, hence, it has a similar electronic structure, including two lone pair electrons, which play an important role in the energy band structure of chalcogenide glassy semiconductors, since they form the top of the valence band and make a contribution to the physicochemical properties of these materials;[217]

— oxygen and nitrogen have a significant chemical affinity for the main components of the GST system, the heats of formation of their oxides are positive and relatively high;

— since the main method for the preparation of PCM thin films is the ion plasma sputtering of a target, chemical modification with light elements can be easily accomplished by varying the composition of the gas mixture in the working chamber; and the impurity concentration can be controlled by varying the percentages of elements in the gas mixture;

— the nitrogen and oxygen impurity atoms considerably influence the performance of phase change memory devices; for example, doping with nitrogen increases the stability of GST225, in particular, by decreasing the diffusion ability of germanium;[218] meanwhile, the presence of oxygen in thin films of this material may induce the segregation of atoms, formation of oxides GeO_x and additional phases depleted in germanium relative to GST225.[219]

Oxygen as an uncontrolled impurity. While analyzing the effect of oxygen on the properties of PCM thin films, several circumstances should be taken into account. First, oxygen is present almost in all cases at least at film edges; therefore, it is important to know how oxygen influences both the physicochemical properties of a PCM material and performance of devices based on these materials. Second, analytical determination of oxygen concentration and distribution across the thin film is a separate challenging task, which often complicates comparison of the data reported in different sources. Third, the targeted introduction of oxygen for studying the properties of a doped material implies that the initial sample is undoped, but this is most often unknown.

Data on the effect of oxygen on the electrophysical, optical and thermodynamic properties of GST225 thin films can be found in a number of publications.[220–224] This Section is focused on the works where oxygen was considered as an uncontrolled impurity, since the change in the properties in the presence of oxygen may substantially hamper the manufacturing technology and operation of phase change memory devices.

Above, it was noted above that chalcogenide glassy semiconductors based on tellurides are readily oxidizable materials. When the GST225 thin film gets in contact with an oxygen-containing atmosphere, for example, with air, natural oxide appears in the near-surface layer of the film. Studies of films after exposure to air for three months and two years, respectively, by angle-resolved photoelectron spectroscopy[224] and by low-energy ion scattering[225] showed that the thickness of the continuous natural oxide layer does not exceed ~5–7 nm. After heat treatment, the oxide layer thickness may increase to 20 nm.[226]

It was suggested[224,227] that oxidation in the GST films is selective, involving first of all germanium atoms, because they has the highest chemical affinity for oxygen. This is in line with the results of a detailed study of GeTe films by X-ray photoelectron spectroscopy,[228] which provided grounds for a four-step oxidation mechanism, including

— formation of germanium oxide;

— formation of the germanium-enriched $Ge^{4+}_{1+a}Te^{0}_{1-a}O^{2-}_{2(1+a)}$ layer where a varies from 0 to 0.5;

— expansion of the formed enriched layer;

— formation of $m\,GeO_2 \cdot n\,TeO_2$.

In addition, the studies of GST225 films without a protective layer provide the conclusion that in the presence of oxygen, germanium is separated from the GST matrix as amorphous GeO_2 inclusions, while the initial GST matrix is thus converted to germanium-depleted inclusions with locally observed Sb_2Te_3 fragments[218] or to a mixture of phases corresponding to various compounds of the $GeTe-Sb_2Te_3$ quasi-binary section.[227,229] Some publications (see, for example, Refs 224, 225, 227) report the possible formation of SbO_x structural units, apart from GeO_x.

The state of the boundaries of the amorphous thin films of GST-based PCM materials, in particular the presence of oxygen in the near-surface area,[227] considerably affects crystallization, which was repeatedly confirmed by measurement of temperature dependences of the electrical and optical parameters. The presence of surface oxide leads to a considerable decrease in the crystallization temperature, which may vary from 5 (Ref. 225) to 20 °C,[227] depending on the time of air exposure of the film and the presence of a protective layer. The process of thin film crystallization can be conventionally divided into two stages separated by a step in the temperature dependence reflecting the variation of functional properties of oxidized GST225 thin films (Fig. 23).[227] It should be noted that this pattern of variation of properties during crystallization is rather widespread.[168,230–234]

The first stage of variation of the resistivity and reflectivity of the GST225 thin film around 150 °C is related to the material crystallization near the surface. During this stage, nucleation and crystallization take place only in the near-surface part of the film (~15–20 nm), while the rest remains amorphous.[227,235–238] The second stage, accompanied by the subsequent drop in the resistivity near 175 °C, is related to the appearance of crystal nuclei in the amorphous bulk of the film and subsequent crystallization. It is noteworthy that the second stage is reflected most clearly in the electrophysical properties since optical properties defined for the spectral range near the absorption edge would be limited by the crystallized surface. The fact that the nucleation on the oxidized surface of the GST225 film occurs at a low temperature than the nucleation in the bulk can be attributed to the difference between the energy barriers for

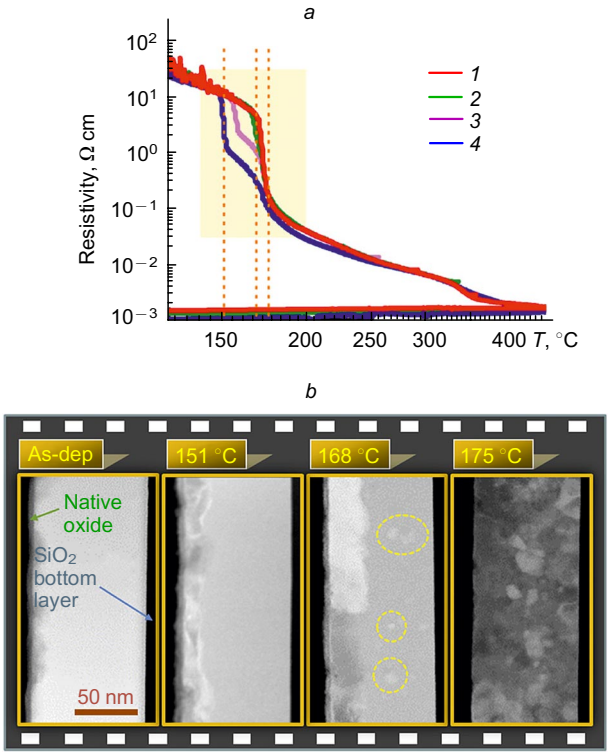


Figure 23. Temperature dependences of the resistivity of GST225 thin films with and without SiN protective layer (*a*) and TEM images of the cross-section of GST225 films treated at different temperatures (*b*).[227] (*1*) with SiN coating; (*2*, *3*) with SiN coating formed after exposure to air for 1 and 48 h, respectively; (*4*) without protective coating. TEM is transmission electron microscopy. Published with permission from Elsevier.

nucleation in a homogeneous material (homogeneous crystallization) and near some surface or defect (hetergeneous crystallization);[239] in the latter case, the activation energy for nucleation is lower.

The amorphous GST225 film without an oxidized surface layer crystallizes in one stage *via* homogeneous nucleation in the film bulk at temperatures of ~170–175 °C. This is close to the temperature range of the second crystallization stage in oxidized films, which corresponds to bulk nucleation. The crystallization is accompanied by phase separation due to local oxidation and formation of tellurium-rich regions. During the second stage, this will be manifested as appearance of various phases in the $GeTe-Sb_2Te_3$ quasi-binary section, in particular, $GeSb_2Te_4$.[240] It is noteworthy that these temperature ranges may somewhat shift depending on the film thickness,[229,241] boundary materials,[242] heating conditions,[243] *etc*.

The presence of germanium oxide in the near-surface layer was established for GST225 thin films both exposed to air and coated by a protective layer of, *e.g.*, Ta_2O_5 immediately after deposition.[227] The appearance of the oxide can be attributed to the use of oxygen-containing gas mixture to form tantalum oxide, which does not rule out diffusion of oxygen atoms between layers. Thus, the formation of the surface layer that contains oxygen does not rule out the probability of oxidation of boundary regions of GST thin films and accompanying effects. A similar situation can also be observed in other stages of formation of phase change

memory devices, for example, during lithographic processes (resist development in alkaline inorganic compounds or resist stripping in oxygen-containing plasma) and plasma chemical etching in a gas medium with oxygen, which passivates the side wall of the object being etched and gives rise to a uniform etching profile. While developing process data books and choosing the design for phase change memory devices, it is necessary to consider and exclude whenever possible the entry of oxygen into GST225 films.

Note that despite the above-indicated drawbacks, studies of the applicability of GeSbTeO layers in PCM-based cells are continued. Kraft *et al.*[244] attained an enhancement of properties compared to GST by fabricating a nanocomposite of GeSbTeO and LaSrMnO.

Nitrogen as a stabilizer of migration processes. A problem hampering further technology development and expansion of the applicability range of electrical and optical PCM devices based on GST225 is susceptibility of some cells to malfunction upon repeated switching. This is caused by thermal diffusion[245] and electric migration of atoms of some elements in GST225[246] and also by mutual diffusion of elements and interfacial reactions between a given PCM material and the material of adjacent layers.[227] These processes disrupt the uniformity of element distribution in the bulk of programmable region and induce composition segregation, phase separation and formation of macroscopic defects and voids in the GST225 bulk (Fig. 24).[246] This changes the functional cell parameters and, as a consequence, the material warms-up non-uniformly and, in some cases, it is even impossible to perform the phase change in the functional region.[246] In the presence of nitrogen, stability of GST225 increases and its properties change. This distinguishes nitrogen from other light elements.

The introduction of nitrogen into GST225 increases the crystallization temperature and activation energy, which leads to higher stability of the amorphous phase and, hence, increases performance reliability of PCRAM devices in comparison with the devices based on undoped GST225.[247–251] As the nitrogen concentration increases, the GST225 crystallization temperature rises considerably,[252–255] which is visible even at low concentrations of nitrogen.[255] Studies of crystallization kinetics and microstructure evolution of GST thin films[256–258] showed that the increase in the thermal stability of the amorphous GST225 phase is due to the formation of Ge–N bonds, resulting in a decrease in the diffusion coefficient of germanium and retarding crystallization. By introducing different concentrations of nitrogen, it is possible to control crystallization kinetics; this can be used to optimize the operation of devices.[258]

The thermal annealing carried out as a part of standard microelectronic processes to form the upper metallization layers gives rise to large crystal grains in the functional regions of undoped GST225, which hampers the RESET operation[259] and the subsequent data reading.[29, 260, 261] The inhibition of thin film crystallization due to nitrogen doping is accompanied by decreasing rates of crystallization and crystallite growth,[257] which results in a smaller size of crystal grains[254, 255] and lower melting point of the material.[257] Ahn[262] showed the possibility of decreasing the RESET current by nitrogen doping of GST material due to increase in the Joule heating efficiency. Furthermore, the decrease in the grain size increases the uniformity of the electrical and optical properties,[257] which is important for reliability of the data reading operation.

It is noteworthy that nitrogen doping can also serve to control the crystal grain size in non-stoichiometric GST materials, in particular germanium-enriched ones.[173] Since the germanium concentration in the films of these materials exceeds the concentration of germanium atoms in the lattice, heating is accompanied by phase separation; according to Luong *et al.*,[257] this process starts at 380 °C. After the phase separation, germanium crystallizes as fine grains, the size of which gradually increases. This locally decreases the concentration of germanium in the remaining part of the film until all germanium atoms occupy their sites in the crystal lattice, which would induce crystallization at a temperature above 400 °C.[257] The authors[257] also showed that the introduction of nitrogen into a germanium-rich material (as well as into stoichiometric GST225) may markedly decrease the size of crystallites formed after annealing at 500 °C from values comparable with the film thickness (in this study, hundreds of nanometres) to a few tens of nanometres. The combination of increasing germanium concentration and introduction of nitrogen enhances the resistivity contrast between the amorphous and crystalline states of GST materials,[263–265] which makes them promising for various high-temperature applications. However, while modelling the electrical characteristics of devices based on these materials, one should bear in mind that switching to the conductive (crystalline) state is non-uniform and the crystalline material consists of grains of two different phases, one being a chalcogenide compound and the other being elemental germanium, possibly with nitrogen impurity.

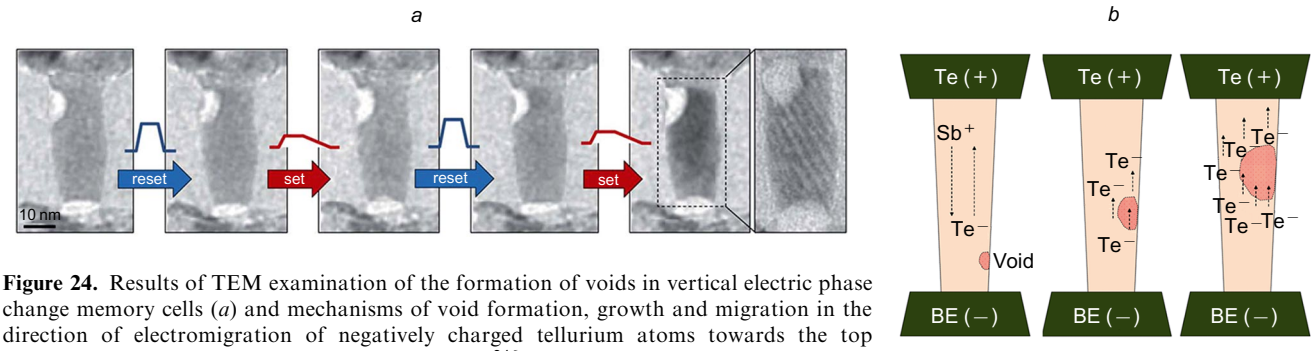


Figure 24. Results of TEM examination of the formation of voids in vertical electric phase change memory cells (*a*) and mechanisms of void formation, growth and migration in the direction of electromigration of negatively charged tellurium atoms towards the top electrode with an applied positive potential (*b*).[246] Published in accordance with the Creative Commons Attribution license.

The introduction of nitrogen into GST phases influences not only parameters of switching of the amorphous to crystalline state with a cubic structure, but also the subsequent phase transitions. For example, no hexagonal phase was detected after annealing at 500 °C in a sample doped with 10 at.% nitrogen, whereas in an undoped sample the transition to hexagonal structure was observed at 350 °C.[257] When the formation of the hexagonal phase, which has the lowest resistance in GST system, is suppressed, the power consumption of the electrical memory cells may decrease, because there is no need to reduce the resistivity of the crystalline cell material and to increase the pulse power for material melting. However, this precludes the possibility of utilizing cubic to hexagonal transition to increase the number of logic levels in the devices. However, the effect of nitrogen on the second phase transition deserves a more detailed investigation, because Yao *et al.*,[266] conversely, obtained a stable hexagonal structure at a lower temperature after the introduction of nitrogen than in the case of undoped sample.

Crystallization of GST225 thin films decreases their volume by 6–10% (Refs 267, 268) due to increase in the material density by 6–7%;[268, 269] consequently, mechanical stress appears and is accumulated,[258, 270, 271] which significantly affects the performance reliability of the devices.[272] An X-ray reflectivity study demonstrated that introduction of up to 1.6% nitrogen reduces the density change upon crystallization. In combination with a decrease in the grain growth rate caused by the reduced diffusion ability of elements in highly nitrogen doped materials, this may ensure a uniform morphology of the surface of GST225 thin films after thermal crystallization. In addition to the foregoing, it was noted[266] that nitrogen doping may improve adhesion between a PCM material and a substrate. This enhances the stability of the contact with the bottom electrode and decreases the probability of high resistance in the cell in the amorphous state, thus being a beneficial factor.

Doping with nitrogen decreases the extinction coefficient, while the refractive index remains virtually invariable;[273] this opens up the possibility of application of nitrogen for tuning parameters of optical elements. Nitrogen compounds (*e.g.*, titanium nitride) have application prospects in GST-based reconfigurable plasmonic structures as diffusion barrier layers. The key criterion for functioning of these structures is the proximate arrangement of chalcogenide semiconductor and metal layers: as the distance between them increases, the intensity of plasmonic effects and, hence, the optical response exponentially decrease. It was shown[274] that gold and silver, which are metals used most often in plasmonics, can actively diffuse in GST225. In the case of ultrathin chalcogenide films (< 10 nm thick),[275] this can be a severe problem for multiple rewriting. However, when the TiN layer with a dielectric function similar to that of gold is used in a GST225-based plasmonic structure, no mutual diffusion of atoms between the layers takes place. Titanium nitride can be used as a diffusion barrier layer in electrical and optical phase change memory devices to prevent diffusion and interfacial reactions between the PCM material and adjacent layers.

Thus, the introduction of nitrogen proved to be an approach for increasing the endurance and reliability of phase change memory devices based on GST225. As unfavourable consequences of introducing nitrogen, note the decrease in the rate of crystallization, increase in the crystallization energy and decrease in the extinction coefficient contrast between the amorphous and crystalline states, which may have an adverse effect on the operation speed, power consumption and the number of logic levels for data writing.

3.2.3. Refractory metals

Elemental tungsten and its compounds are used to design electrically switched devices as materials for one of the contacts.[276–278] Most often, materials of this type are used to fabricate the contact conventionally called the bottom electrode , or heater , near which the functional region of the cell is warmed up.

Tungsten is a refractory material, which has relatively high thermal and electrical conductivity and a thermal expansion coefficient close to that of silicon. In combination with the well-developed techniques for the fabrication of tungsten-based thin films and nano-sized objects, this accounts for the wide use of tungsten for the manufacture of semiconductor devices, in particular, as metallization materials for DRAM and PCM devices.

However, in order to establish the possibility of mutual diffusion of the atoms of tungsten and the functional region material at high temperatures during the RESET operation, it is necessary to assess the probable changes in the properties of these spontaneously doped materials. As will be shown below, the introduction of tungsten may considerably modify the properties of GST compounds; this can be used for task-oriented optimization of characteristics of PCM materials and improving the parameters of manufactured devices.

An important consequence of tungsten doping of GST materials is considerable increase in the crystallization temperature.[279–281] A gradual increase in the tungsten concentration in GST225 thin film up to 7.1 at.% raises the crystallization temperature to 220 °C,[279] which is 40 °C higher than the value obtained upon the introduction of nitrogen in the same concentration[256] (see Section 3.2.2). This is not the highest temperature of crystallization: as the tungsten content is increased to 10.8 at.%, this temperature reaches 277 °C.[256] The results of comparative analysis reported by Kang and Chen,[23] which are shown in Fig. 20, indicate that tungsten, like chromium or zinc, has the most pronounced effect of this characteristic of GST225 thin films.

Guo *et al.*,[279] who investigated the temperature dependences of the Raman spectra, concluded that most of tungsten atoms are incorporated into the crystal lattice as substitutional impurities, which is facilitated by the similarity of the atomic radii of tungsten (139 pm), tellurium (140 pm) and antimony (145 pm), while some tungsten atoms occur as interstitial impurity. This disrupts the crystal structure of GST225, which prevents a change in the positions of Ge, Sb and Te atoms upon phase transition and, hence, increases the temperature of crystallization.

Tungsted-doped GST225 thin films (up to 0.08 at.% W)[281] crystallize to a NaCl type stable face-centred cubic phase with uniform crystal grains. This was confirmed by powder X-ray diffraction[280] and transmission electron microscopy (TEM) and selected area electron diffraction (SAED) data.[281] The amorphous GST225 thin films doped with tungsten in concentration of > 3.2 at.% cannot be converted to a hexagonal structure even after heat treatment at 450 °C, although in the case of undoped

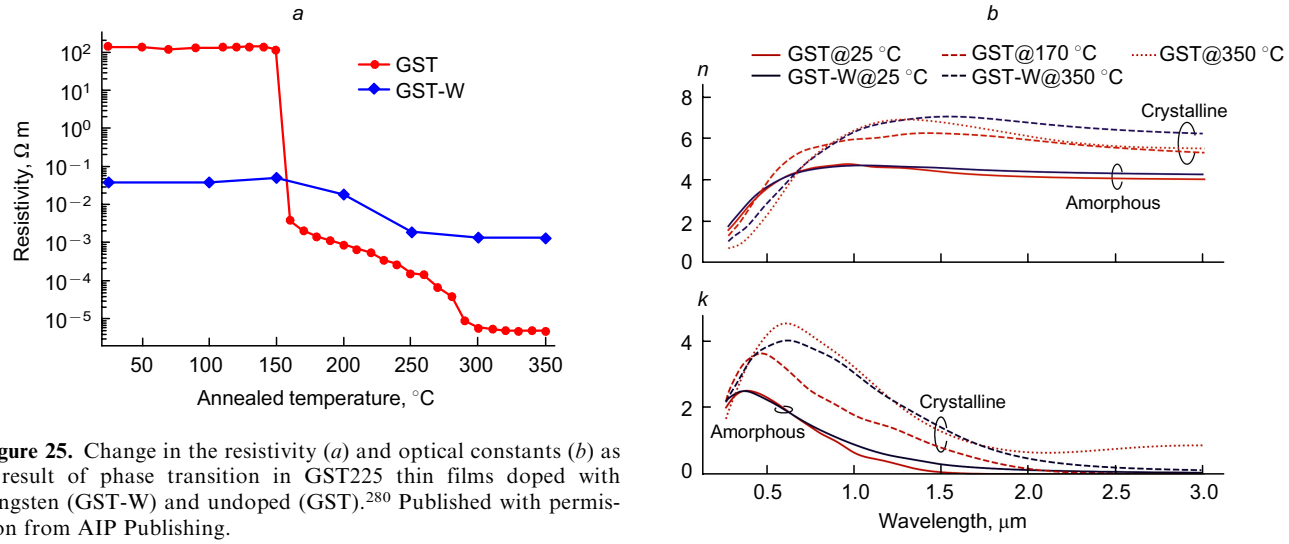


Figure 25. Change in the resistivity (*a*) and optical constants (*b*) as a result of phase transition in GST225 thin films doped with tungsten (GST-W) and undoped (GST).[280] Published with permission from AIP Publishing.

GST225, this structure is formed at a temperature of ~300 °C.[279]

An increase in the crystallization temperature is favourable for increasing the thermal stability of the amorphous phase, decreasing the probability of spontaneous crystallization and increasing the data retention in the high-resistance state of PCM-based devices. Stability of the amorphous phase can be characterized by the activation energy of crystallization and the temperature that ensures data storage for 10 years.[243] Upon the introduction of 10.8 at.% tungsten into GST225, these values increase from 2.99 to 4.57 eV and from 89 to 214 °C, respectively.§ Note that the values for pure GST225 may somewhat differ depending on the manufacturing details and investigation conditions (see Section 3.1).

However, too pronounced increase in the activation energy of crystallization may necessitate the increase in the power and duration of programming pulses in the SET operation, and, hence, the power consumption of the whole device. Thus, while choosing the concentration of the tungsten impurity, it is necessary to consider the operation conditions of memory elements. For example, for operation in automotive vehicles, the International Organization for Standardization (ISO)[282] and the Automotive Electronics Council (AEC) standards,[283] which regulate the environmental conditions and testing conditions for electrical and electronic equipment for road transport, require that stable operation of electronic devices be ensured in the temperature range from −40 to 125 °C. From this standpoint, the appropriate concentration range is 3–7 at.%. Meanwhile, GST225 with a higher content of tungsten, which shows higher data storage temperatures, in view of high radiation stability of GST materials,[46] could be of interest for application in devices operating in the near-Earth orbit and in middle and deep space.

Despite the increase in the temperature of crystallization, electrical memory cells based on $W_{0.08}(Ge_2Sb_2Te_5)_{0.92}$ are switched by shorter pulses (10 ns)[281] than memory cells based on undoped GST225 (50 ns), with the endurance (6×10^5 cycles) being comparable with that for flash memory cells.

§ These values were found under identical conditions by Guo *et al.*[279]

In the design of devices, the effect of impurities on the performance characteristics, including electrophysical and optical characteristics, should be taken into account. The resistivity of amorphous GST225 doped with 4 at.% W is three orders of magnitude lower than that of the undoped material. Meanwhile, the resistivity is higher for crystalline GST-W than for crystalline GST. In combination, this leads to a considerable decrease in the resistivity contrast between the phases (Fig. 25).[280] Low resistivity contrast makes inappropriate the use of tungsten for the fabrication of multilevel electrical memory cells and neuromorphic computing systems. However, by increasing the resistivity of the crystalline phase, it is possible to decrease the power consumption of devices.

The performance characteristics of the electrical phase change memory devices are affected by contact resistance (Fig. 26).[162, 163, 280] Guo *et al.*[280] used the transfer length method (TLM) to demonstrate that the introduction of tungsten decreases the contact resistance by almost four orders of magnitude compared with the contact resistance of undoped GST225. This opens up the opportunity for more reliable carrying out and prediction of electrical switching.

After annealing at 350 °C, tungsten-doped GST225 thin films have a higher refractive index and somewhat lower extinction coefficient in the long-wavelength range (> 2 μm) than the undoped material, which may provide for lower optical losses for nanophotonic devices in the IR range. The

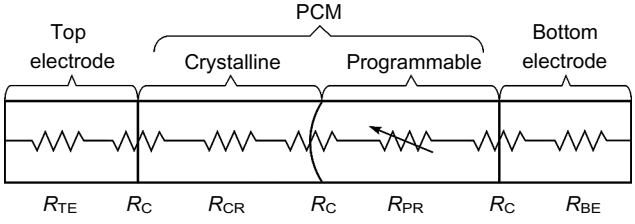


Figure 26. Phase change memory cell. R_{TE} and R_{BE} is the resistance of top and bottom electrode materials, respectively, R_C is the contact resistance between materials, R_{CR} and R_{PR} are resistances of the crystalline and programmable regions of the semiconductor chalcogenide layer, respectively. Created by the authors using published data.[162, 163, 280]

introduction of tungsten barely affects the optical contrast near the telecommunication wavelength (1550 nm).

Thus, by using the tungsten impurity for chemical modification of GST225, it is possible to combine the stability of the amorphous state and high electrical switching speed with a broad optical contrast. This attests to good prospects of tungsten-doped GST compounds for the design of non-volatile multilevel devices, providing control over optical signal characteristics by changing the phase composition upon electrical switching and reliable operation over a broad temperature range, which complies, in particular, with requirements of the automotive industry.

4. Structural modification

4.1. Control of the properties of semiconductor materials by changing their structure

Apart from the development of methods for chemical modification of properties of chalcogenide glassy semiconductors (see Section 3), development of efficient methods for the control of the properties of these materials is a relevant task. The absence of long-range order in the positions of atoms in non-crystalline phases opens up new opportunities in the control of properties by changing the atomic structure, with the chemical composition remaining intact. This fact formed the basis for structural modification: a new method for the control of properties of PCM materials.[284] Modification of the atomic structure of non-crystalline semiconductors during their synthesis (or after the synthesis) gives rise to materials in various metastable states with different properties.[285]

The variation of methods and intensity of external action on a non-crystalline material induces a change in its structural characteristics, namely, parameters of the short- and medium-range order in the arrangement of atoms, material morphology and heterogeneity, and the type and concentration of structural defects.[286] The listed changes influence various physical and chemical properties of a non-crystalline material. Therefore, in the framework of the control of properties of semiconductor materials by changing their structure without changing the chemical composition, four levels of structural modification of properties are usually considered.

4.2. Levels of structural modification

4.2.1. First level: change in the short-range order parameters

A treatment of a material that changes characteristics of the short-range order in the positions of atoms would affect the electronic structure, which determines the fundamental properties of the material. A classic example of the effect of the short-range order on the properties is existence of allotropes of crystalline carbon, that is, diamond, graphite, carbyne, with different orbital hybridization (sp^3, sp^2 and sp, respectively).

Studies of the atomic structure of films of amorphous carbon and hydrogenated amorphous carbon a-C : H showed the presence of structural units with different types of electron orbital hybridization; the concentration ratio of hybridization types markedly depends on the film preparation method and conditions.[287] For example, by varying the power of the sputtering discharge and the substrate temperature during the preparation of a-C : H films, it is possible to change the band gap width by up to two orders of magnitude and to change the electrical conductivity by more than 10 orders of magnitude.[286]

Under certain operating conditions of the synthesis, changes in the short-range order parameters were also observed in the films of amorphous silicon and hydrogenated amorphous silicon a-Si : H,[288–290] selenium,[291, 292] in a tellurium melt[293] and in a glassy GeS_2 under pressure.[294] This suggests that a change in the parameters of the short-range order in the positions of atoms of non-crystalline semiconductors, including chalcogenide glassy semiconductors, is an efficient method for the control of their properties.

4.2.2. Second level: change in the medium-range order parameters

Unlike modification at the level of short-range order, which affects the electronic structure of the semiconductor, changes in the medium-range order in the positions of atoms affect mainly the mechanical properties of the material, although some publications (*e.g.*,[295, 296]) note the change of also electrical and optical properties of non-crystalline films of the As–Se system.

The possibility of modifying the properties of a non-crystalline semiconductor depends on the rigidity of the structural network of the material, which increases with increasing number of covalent bonds per atom and decreases with increasing number of lone pair electrons per atom. Phillips[297, 298] introduced the notion of rigidity threshold for the structural network defined as the point where the number of force constants (N_{con}) is equal to the number of degrees of freedom of the atom (N_d):

$$N_{con} = N_d \tag{4}$$

The N_{con} value depends on the type of chemical bonds in the material and on the number of chemical bonds per atom. Compounds with predominantly covalent type of bonds are characterized by chemical bond stretching–compression and bending force constants and N_{con} is defined as

$$N_{con} = \frac{K^2}{2} \tag{5}$$

where K is the average coordination number.

Since in purely covalent materials the number of degrees of freedom of an atom $N_d = 3$, the rigidity threshold is attained when $K = 2.4$. This suggests that the control of properties of non-crystalline semiconductors by affecting the medium-range order in the positions of atoms would be effective for materials with $K < 2.4$ and of little unility for materials with $K > 2.4$.

The results of experimental studies of chalcogenide glasses $A_x^{IV}(A_x^{V})B_{1-x}^{VI}$ (Refs 299, 300) prompt the conclusion that the rigidity threshold of the structural network for these compounds is considerably shifted towards higher K. The causes for the discrepancy in the rigidity threshold data were analyzed by Popov,[301] who demonstrated that correct calculation of the coordination number corresponding to the rigidity threshold should take into account the degree of ionicity and metallization of chemical bonds in the compound. For this purpose, the average coordination number should be replaced by the expression $K(1 - I_c - M)$, where I_c is the average bond ionicity coefficient, M is the degree of bond metallization.

The necessity to take into account the rigidity threshold is also dictated by the fact that chalcogenide glassy semiconductors, like other inorganic glasses, are subject to physical ageing. This is caused by the fact that any disordered system formed upon fast cooling has excess enthalpy,

free volume and configurational entropy in comparison with either the crystalline analogue or the extrapolated equilibrium state of a supercooled liquid at an invariable temperature. Over time, such thermodynamic system tends to equilibrium of the supercooled liquid provided that the structural matrix of the liquid allows the required relaxation processes,[302] and the relaxation kinetics appreciably depends on K.[303] Note that natural ageing may be accelerated by external stimuli such as γ-irradiation [304] or irradiation with high- or low-absorbed light.[305, 306] Naturally, this should be taken into account when chalcogenide glassy semiconductors are used in devices.

4.2.3. Third level: change in the morphology and/or heterogeneity

The synthesis of a non-crystalline solid is a thermodynamically non-equilibrium process accompanied by appearance of inhomogeneities (columnar structures, globules, *etc.*) separated by boundaries, which is characteristic of heterogeneous systems. The existence of boundaries between inhomogeneities attests to disruption of the continuous covalent structural network of the material. A certain heterogeneity was first found in a-Si : H,[307] and then in other tetrahedral amorphous semiconductors. Meanwhile, no heterogeneity is usually present in high-quality glassy semiconductors. Since the synthesis of glassy materials, like the synthesis of other non-crystalline solids, is also a non-equilibrium process, one can assume that these materials do contain inhomogeneities, which nevertheless do not produce a heterogeneous structure, but give rise to regions of medium-range order in the positions of atoms [308] bound to each other (or to the surrounding matrix) without breaking the continuous structural network. Thus, inhomogeneities are inherent in non-crystalline solids and may be manifested as either structure heterogeneity or the presence of ordered regions of atomic structure beyond unit cells (medium-range order in the positions of atoms).

The appearance of the former or latter type of inhomogeneity in a particular non-crystalline material is determined by the structural network rigidity. The formation of medium-range order regions, with the continuous structural network being retained, is possible for materials in which the average coordination number taking account of bond ionicity and metallization is smaller than the rigidity threshold of the structural framework. There is no heterogeneity in such materials, and the third level of structural modification is ineffective in this case. If the average coordination number is greater than the rigidity threshold, then the presence of inhomogeneities breaks the continuous covalent structural network, thus giving rise to the heterogeneity. In the latter case, the properties (optical and electrophysical) sensitive to inhomogeneities can be controlled by changing the morphology (heterogeneity) of materials.

4.2.4. Fourth level: changes in the subsystem of defects

This structural modification level implies an impact on the defects of a non-crystalline solid in order to change the concentration and distribution of localized states and Fermi level position in the semiconductor band gap. The subsystem of defects can be affected by changing the conditions of material synthesis or by additional material treatment after the synthesis or after fabrication of the device.

The effects of pseudo-doping of hydrogenated amorphous silicon, *i.e.*, varying the spectrum of the localized states by changing the conditions of film preparation, have been described by Golikova.[309] In order to change the spectrum of localized states after the synthesis, it is necessary to carefully choose the modifying stimulus, because this stimulus should mainly affect the defect subsystem. Popov [310] used UV radiation to affect hydrogenated amorphous silicon. Under UV irradiation at a 10^{19} cm^{-2} dose, the concentration of Si–H_3 sites in the amorphous silicon considerably decreased, while the concentration of Si–H sites increased. This induced changes in the spectrum of localized states in the band gap of a-Si : H (Fig. 27).[310] The practical consequences were higher stability of properties of hydrogenated amorphous silicon and enhanced parameters of thin film transistors based on this material.[311]

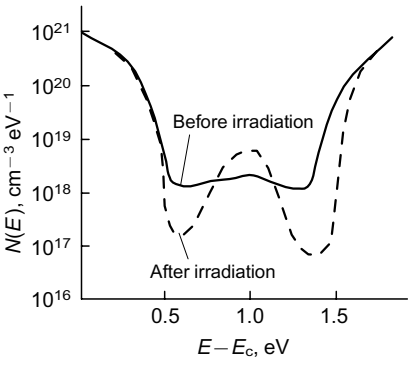


Figure 27. Change in the density of localized states [$N(E)$] in the band gap of a-Si : H relative to the bottom of the conduction band (E_c) under UV irradiation with a dose of 10^{19} cm^{-2}. The Figure was created by the authors using data of Ref. 310.

The structural modification of properties at the level of defect subsystem is also effective for chalcogenide glassy semiconductors. Weak magnetic and electrical fields were found to influence the quasi-molecular defect subsystem and the properties of elemental chalcogens (selenium, sulfur) and chalcogen compounds (As_2S_3 and As_2Se_3).[312, 313] The fourth level of structural modification was experimentally observed both in compounds with a rigid tetrahedral structural network and in chalcogenide glasses based on Group 15 and 16 elements.

Thus, the considered four levels of modification of properties of non-crystalline semiconductors differ in the scale in which the structural changes take place. The control of the properties of non-crystalline semiconductors by changing the structure at the level of short-range order and by affecting the subsystem of defects is possible for all considered materials. The control of properties by changing the medium-range order in the positions of atoms is possible for glassy semiconductors characterized by high values of the criterion of structural modification efficacy; the limit of applicability of this level corresponds to the rigidity threshold of the structural network calculated with allowance for the chemical bond ionicity and metallization. For materials with a rigid structural network, structural modification including a change in the morphology (heterogeneity) is possible.

4.3. Structural modification induced by laser radiation

This Section considers some aspects of laser modification of GST materials, particularly, the change in their properties and phase transitions, first of all, effects of laser crystallization and reamorphization induced by laser radiation. The experiments demonstrating the formation of laser-induced periodic surface structures (LIPSS), so-called ripples, are also discussed. This corresponds to the third level of structural modification, which is related to the change in the material morphology (heterogeneity), according to the previously proposed classification.

4.3.1. Thermal and athermal aspects of phase transformations under pulsed laser irradiation

The influence of laser radiation on the crystallization of amorphous PCM thin films is the subject of numerous papers, reviews and monographs. While preparing this review, the authors did not intend to describe this effect in detail, but focused on some key aspects.

The amorphous to crystalline transition (SET) is the slowest process in PCM devices; hence, it determines the operation speed of the device (see Fig. 2). For some time, attempts have been made to find methods and approaches to decrease the crystallization time. In this respect, the use of pulse lasers, including femtosecond lasers, is a modern trend and an efficient method for addressing this issue.

Crystallization is a diffusion process in which the reorganization of atoms in a solid requires relatively high amounts of energy and time. Analysis of the results obtained by Tominaga *et al.*[314] mainly by differential scanning calorimetry indicates that the activation energy of crystallization of GST225 varies from 2.23 to 2.9 eV. According to the model developed by the authors, this is well correlated with the energy of Ge–Te bond switching upon transformation of the amorphous to crystalline state and confirms reorganization of the germanium atoms during phase transition. The structural rearrangement that accompanies crystallization takes some time; in order to determine this time, the minimum laser pulse duration that provided the amorphous to crystalline transition was determined. Wiedenhof *et al.*[315] concluded that this shortest time for GST225 is 100 ns (when the pulse is shorter, the phase transition does not take place); hence, this value corresponds to the minimum time needed for the formation of crystal nuclei of the critical size in an amorphous matrix.

The specific character of GST225 is that this compound can be synthesized in the amorphous state only as a thin film, and this imposes additional requirements on the studies of crystallization. It is necessary to take into account that crystallization is a multifactorial process depending on characteristics of the material (film thickness, type of the substrate, the presence of protective layers, *etc.*) and on the degree of non-equilibrium of the phase transition (isothermal or non-isothermal crystallization; in the latter case, the heating/cooling rate is critical). An important issue is the experimental method used to determine the crystalline fraction in the amorphous film (the method sensitivity is significant). As applied to PCM materials, of interest are data obtained for nano-sized objects (for which the size factor plays a role) and at heating rates of $\sim 10^6$ K s^{-1}; therefore, the problem is quite complicated and must be addressed using non-trivial experimental approaches and special equipment.

A widely used approach to determine the phase state of PCM materials is to measure the refractive index. In the case of GST225, this value markedly changes upon phase transition, and the higher refractive index inherent in the crystalline phase (both metastable and stable hexagonal phases) compared to the amorphous phase[117,316] determines a greater reflectivity coefficient in the visible range and, correspondingly, a lighter image in an optical microscope for the crystallized region. Thus, by following the changes in the reflectivity coefficient, it is possible to estimate the proportion of the crystalline material; this is done using laser testers.[317] However, GST materials have a high optical absorption coefficient ($\sim 10^6$ cm^{-1}) in the visible region. Thus, the penetration depth of the visible light is ~ 10 nm, and crystallization occurs with certainty only in a thin near-surface layer.

It was noted above that a time of 100 ns may be critical for studying crystallization of GST225; therefore, a key question is whether the crystallization can be induced using single pulses of < 100 ns duration. Analysis of the experimental studies does not provide an unambiguous answer to this question, since different conclusions have been drawn. For example, Wang *et al.*[318] found that a 100 nm-thick GST124 film has crystallized under the action of a femtosecond pulse at 800 nm wavelength; GST225 thin films with a thickness of 90 nm crystallized on exposure to a single pulse in the UV range (248 nm wavelength; 500 fs duration),[319] and Zhang *et al.*[320] observed crystallization of thin films of a similar composition on exposure to a 120 fs pulse at 800 nm wavelength. Meanwhile, iegel *et al.*[321] did not observe crystallization of GST225 thin film when used the same pulse laser characteristics; a similar result was reported by Kunkel *et al.*[322] These contradictory results indicate that crystallization is a complex multifactorial process, and the absence of the desired result can be due to the fact that some important factors were neglected. For example, consider the conclusions drawn by Kunkel *et al.*,[322] who showed that crystallization depends not only on the number of pulses, but also on the type of substrate (conductor or dielectric) and on the film thickness (Fig. 28). When fluence has the threshold value that induces crystal-

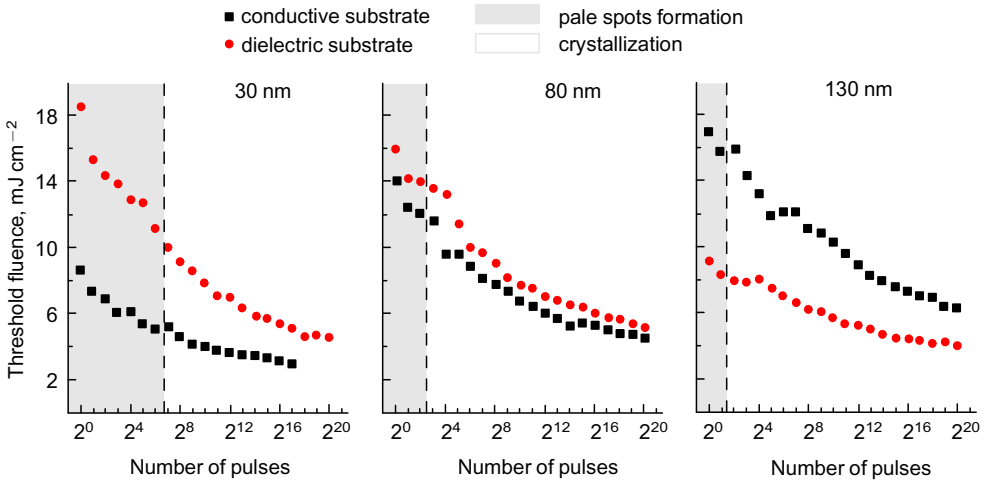


Figure 28. Threshold fluence *vs.* the number of pulses for 30, 80 and 130 nm thick GST225 thin films on various types of substrates.[322] Published with permission from Elsevier.

lization, but is insufficient for ablation of the film material, crystallization can be induced by a single pulse if the film thickness is 200 nm or more and the substrate is a dielectric.[323]

While considering the phase transition of a PCM material from the crystalline to amorphous state, one should bear in mind that a thermal treatment of the system excites a fairly broad spectrum of vibrational modes; therefore, the purely thermal process is not optimal as regards the switching efficiency, since only those modes that disrupt ordering of the atomic structure contribute to triggering of the phase transition. An important issue is how efficient the energy brought into the system *via* a conventional non-thermal channel can be, in comparison with the thermal energy. Experimental studies demonstrating the high efficiency of femtosecond laser pulses [321, 324] or coherent phonons [325, 326] indicate that the non-thermal mechanism is possible for PCM materials. For example, Tiwari *et al.*,[327] who studied the composition of Sb_2Te_3 by non-adiabatic molecular dynamics simulation, concluded that in the presence of ~10% photoexcited valence electron–hole charge carriers, amorphization of the crystalline phase takes place due to changes in the electronic structure associated with virtually instantaneous (~4 ps, Fig. 29) [327] charge (electron) transfer from the tellurium valence p-orbital to the antimony p-orbital.

A change in the electronic subsystem may lead to higher diffusion of atoms, destabilization of the crystal structure and, hence, to the irreversible loss of the long-range order. Approximately the same proportions of photoexcited charge carriers (10%) were found in GaAs;[328, 329] the authors found that it is sufficient to excite 10% of valence electrons to the conduction band by a femtosecond laser pulse to induce structure disordering (amorphization) by the shift of ions from the initial crystal positions.

However, experiments with polycrystalline films of pure tellurium led researcher to conclusion that amorphization induced by femtosecond laser pulses has the thermal nature.[330] This discrepancy can be attributed to structural features of the materials. Tellurium has a trigonal structure composed of helical chains in which each atom is bound not only to two other atoms in the chain, but also to four atoms of neighbouring chains; binary and ternary compounds are layered structures, such as crystalline gallium arsenide films obtained by molecular beam epitaxy in which the unit cells are separated by van der Waals gaps.

In the framework of traditional thermal paradigm of phase transitions, the required level of intense excitation is dictated by the necessity of heating the material above its melting point. Models of non-thermal, or athermal mechanism, which take into account the excitation of electronic subsystem and the subsequent electron – phonon relaxation, propose several approaches that explain the existence of the intensity threshold. In this regard, note publications by Kolobov *et al.*,[331, 332] who considered the amorphous phase as a purely covalently bonded disordered matrix, while the crystalline phase was represented as being composed of resonance bonds.¶ The covalently bonded part located within the resonantly bonded crystalline phase and containing long and short bonds is taken to be a defect.

The crystalline phase of PCM materials is a degenerate p-type semiconductor with the Fermi level located above the top of the valence band (or within this band). The total energies of the GST225 alloy containing germanium atoms in the octahedral and tetrahedral symmetry positions are very similar; therefore, it was assumed [335] that the energy levels of particular tetrahedrally coordinated germanium atoms (and the corresponding cationic vacancies) should be located closer to the top of the valence band. At room temperature and at low degrees of excitation, the levels of complex defects are located above the chemical potential level and, hence, they are vacant. In this situation, a single excitation leads to instability of the tetrahedral Ge level, which easily decays and relaxes to the initial structure. Upon intense optical excitation, the chemical potential level moves towards the centre of the band gap; the defective states may happen to be located below the chemical potential level; thus, they will be occupied and therefore stable. Under certain conditions, the concentration of these defects becomes rather high, their wave functions overlap, and the electronic structure transforms into the state corresponding to the amorphous phase.

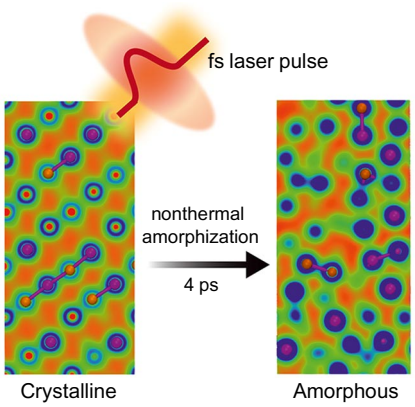


Figure 29. Scheme of fast amorphization of Sb_2Te_3 as a result of instantaneous charge transfer from the tellurium p-orbital to antimony p-orbital upon femtosecond laser excitation of Sb_2Te_3.[327] Published with permission from American Chemical Society.

4.3.2. Periodic surface structures in phase change memory materials

Recent years have seen intense studies devoted to the periodic surface structures that arise in the focal spot of a linear-polarized laser beam in various materials with highly different electronic subsystems. The formation of laser-induced periodic surface structures (LIPSS) was observed in metals,[336] semiconductors [337] and dielectrics;[338] they were studied as thin films on various substrates [339–341] and as bulk materials, *e.g.*, SiO_2 type inorganic glasses.[342, 343] The mechanism of formation of LIPSS is actively discussed in the literature (see a review [344] and the bibliography cited therein), but is not yet entirely clear. The appearance of ripples appreciably depends on the material and laser treatment conditions. As a rule, the ripples are classified in terms of the relationship between their period and laser radiation wavelength: there are ripples with high and low spatial frequency and orientation of the resulting pattern relative to the laser beam polarization (parallel or perpendicular).[345, 346] Materials with high optical absorption, for example metals, tend to form LIPSS with an orientation perpendicular to the polarization vector; the formation of structures of this type is usually attributed to the spatially non-uniform absorption of electromagnetic energy caused by interference of the incident wave with the surface plasmon polariton. In materials with a low optical absorption, for example, dielectric glasses such as quartz glasses, the formed periodic structures have a period smaller than the laser wavelength, and they are parallel to the polarization vector. In semiconductors, various types of LIPSS

¶ Lately, these bonds have been called metavalent.[67, 333, 334]

are possible, which is mainly determined by laser pulse absorption and, hence, by generation of non-equilibrium electrons and the subsequent electron–phonon relaxation.

According to the above classification (see Section 4.1), the appearance of periodic surface structures may imply the third level of structural modification *i.e.*, the morphology (heterogeneity) level. The formation of amorphous thin films of PCM materials is accompanied by change in the morphology and gives rise to two-phase heterogeneous structures with a clear boundary between the amorphous and crystalline phases (see below). From our standpoint, the possibility of formation of two-phase periodic structures is a characteristic feature of phase change memory materials, which could serve for several new applications in the future.

Structural modification of this type induced by the radiation of pulse (mainly femtosecond) lasers was observed for both binary and ternary GST compounds. Katsumata *et al.*,[347] who exposed GeTe thin films to a femtosecond laser (λ = 800 nm), observed the formation of periodic structures as alternating crystal fringes in the amorphous matrix with a period of ~600 nm (which is smaller than the irradiating laser wavelength). Li *et al.*[348] showed that laser irradiation (λ = 1580 nm, pulse duration of 100 fs) of highly absorbing crystalline Sb_2Te_3 films epitaxially grown on a sapphire substrate may give rise to periodic nanostructures with a period approximately equal to the laser wavelength.

It was shown[349–351] that femtosecond laser irradiation of amorphous GST225 thin films gives rise to two-phase LIPSS, characteristics of which are sensitive to radiation parameters (wavelength, pulse duration and frequency, direction of the polarization vector). The micrographs of the resulting surface structures, which look like ridges with a height ranging from a few nanometres to tens of nanometres and valleys of different phase compositions with sharp boundaries are shown in Fig. 30.[351]

The STEM-based explicit evidence for the shape, geometric size and phase composition of ripples (Fig. 31) is well correlated with the results of optical microscopy and atomic force microscopy (AFM).[350] Stability for a long time is an important feature of the observed periodic surface structures, which allows predicting their practical application and also preparation under irradiation conditions that do not deteriorate the material, as LIPSS are formed at radiation powers markedly lower than the laser ablation threshold for GST225, *i.e.*, where the liquid phase has not

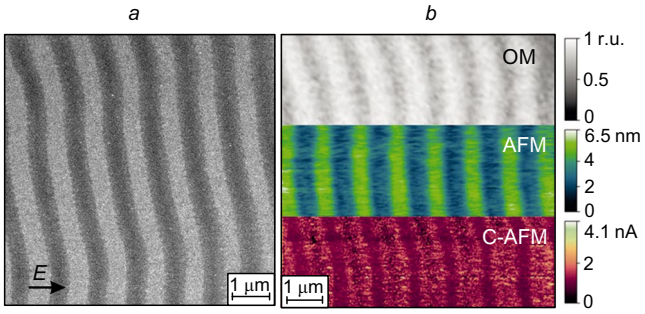


Figure 30. SEM (*a*) and AFM (*b*) images demonstrating the change in the profile and image of the profile of a thin film obtained using conductive AFM mode (*b*).[351] SEM is scanning electron microscopy, OM is optical microscopy, C-AFM is conductive atomic force microscopy. Published with permission from John Wiley and Sons.

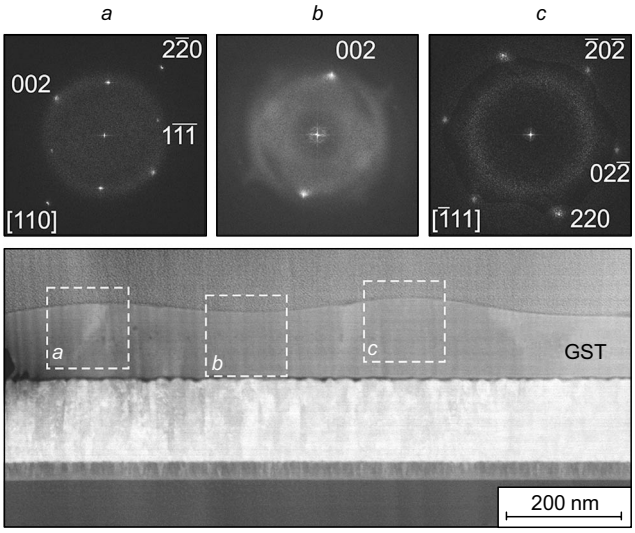


Figure 31. STEM images of formed LIPSS (lower panel) and Fourier transformations of marked regions (*a*–*c*) (upper panel).[350] STEM is scanning transmission electron microscopy. Published with permission from Elsevier.

appeared as yet and intense diffusion of the material with the subsequent microexplosion does not take place. The key importance of these irradiation conditions for the formation of ripples is that the prospects of practical use of this effect require not only preparation of periodic structures, but also the possibility of erasing them, which is similar to the reversible SET–RESET process in optical discs.

As noted above, the mechanism of formation of periodic surface structures under pulsed laser irradiation is a debated issue, which is largely due to different nature of the modified materials. The authors of a recent review[344] presented a classification of LIPSS formation models (Fig. 32). The numerous theoretical models can be split into two large groups. The first group includes the electromagnetic theories of LIPSS formation based on the fact that an incident electromagnetic wave is scattered on microscopic surface roughness, and under certain conditions,

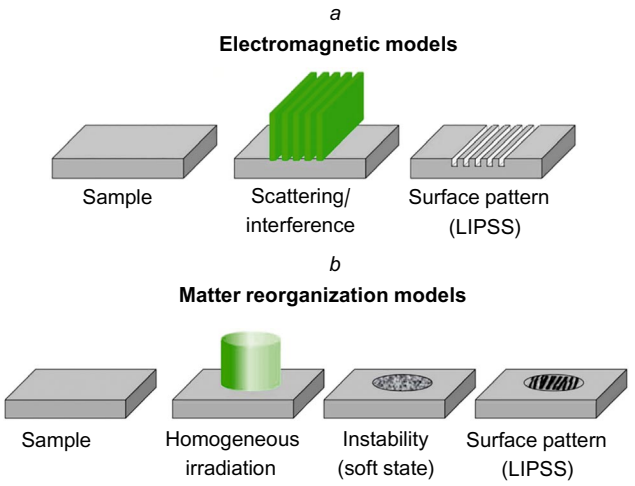


Figure 32. Fundamental processes involverd in the formation of LIPSS according to electromagnetic models (*a*) and material reorganization models (*b*).[344] Published in accordance with the Creative Commons Attribution license.

this leads to generation of a surface plasmon polariton electromagnetic wave. This wave can interfere with the incident radiation wave, which leads to spatial modulation of local energy distribution and is reflected as periodic surface structures (see Fig. 32 *a*). Second group models are based on reorganization of the material induced by laser radiation; it is assumed that under highly non-equilibrium conditions of laser pulse, various hydrodynamic effects give rise to periodic surface structures, which are frozen as the material is hardened (see Fig. 32 *b*).

The mechanism of formation of LIPSS in narrow band gap semiconductors is apparently related, to a higher extent, to the electromagnetic theory, particularly the Sipe – Drude theory according to which non-equilibrium pulse irradiation conditions are likely to generate surface plasmon polaritons.[352, 353]

Trofimov *et al.*[135] demonstrated the possibility of covering extended surfaces of GST225 thin films by the laser-induced surface structures and their subsequent erasing and rewriting. The LIPSS characteristics, in particular, the period and orientation of the structures, were varied by varying the laser radiation wavelength. The results showed the good prospects of the development of non-volatile fast rewritable photonic elements based on PCM materials, including elements for the control of optical signal parameters.

4.3.3. Photostructural transformation effects under laser irradiation

The studies of photostructural transformations in chalcogenide glassy semiconductors were started approximately in the first half of the 1970s. These materials are characterized by relatively low chemical bond energy; therefore, the intense light irradiation at the absorption edge may modify the short-range order, which corresponds to the first level of structural modification. For example, the thoroughly studied photoinduced transformations in the chalcogenides As_2X_3 (X = S, Se) were interpreted in terms of the views of cleavage of the As – X heteroatomic bonds and, correspondingly, the formation of As – As and X – X type homoatomic bonds, which are improper for these stoichiometric compounds, and also in terms of polymerization of isolated molecular groups.[354, 355] The effect consisted in the long-wavelength shift of the absorption edge upon irradiation, which increases with decreasing temperature.[356] This effect was reversible: annealing at temperatures close to the softening temperature resulted in restoration of the absorption spectrum. This reversibility was confirmed by X-ray diffraction.[357] For further acquaintance with the diverse effect of photostructural transformations in chalcogenide glassy semiconductors, refer to monographs,[358 – 360] which consider this effect in most detail.

Special mention should be made of photocrystallization effect in chalcogenide amorphous semiconductors, because in some publications it is shown than crystallization rate can be increased by not only local thermal heating caused by illumination, but also purely electronic effect, *i.e.*, a sharp increase in the concentration of charge carriers upon illumination.[361, 362] The latter is very important, since it indicates that the structural modification may be due to impact on the electronic subsystem of the material, including the defects; this also corresponds to one of the structural modification levels.

Traditionally, it is believed that crystallization in PCM materials may be due to thermal heating induced by laser radiation or a current pulse. However, it was shown in some studies that coherent photon excitation in the superlattices composed of alternating GeTe and Sb_2Te_3 layers may induce switching of these structures between two states and the energy spent for this is lower than the crystallization energy of the material. The effect of the time delay between two pulses that cause the change in the state is illustrated in Fig. 33.[325] When the delay reaches 276 fs, *i.e.*, the value equal to the vibrational frequency of the crystal mode, the harmonic oscillations are resonance-enhanced. The peak of the A_1 local mode shifts from the 3.84 THz frequency corresponding to the amorphous phase to 3.68 THz characteristic of the crystalline phase.

Makino *et al.*[325] concluded that a pair of pump pulses selectively modulates the Ge – Te bonds in the covalently bonded parts of the amorphous phase, which forces germanium atoms to migrate to octahedrally symmetric positions located along the [111] direction of the crystal, which is schematically shown in Fig. 34.

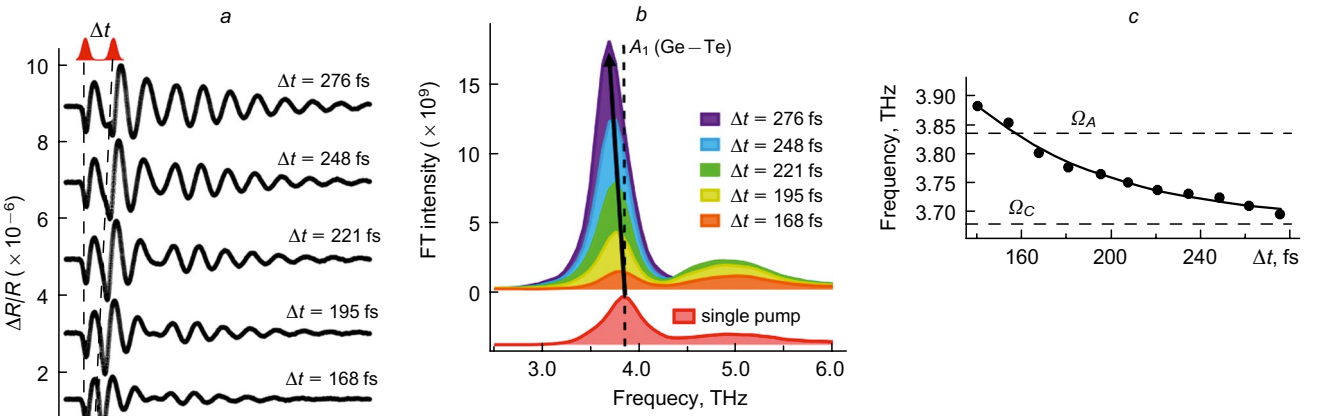


Figure 33. Time dependence of the non-stationary reflection of coherent oscillations excited in the amorphous phase by a pair of pump pulses with variation of time delay (Δt) between the pulses (*a*). The Fourier transformed spectra (*b*) derived from the data shown in Fig. *a* demonstrate that the A_1 local mode shifts to lower frequency upon increase in the flux density; The single pump dependence is given for more clear visualization of the peak frequency shift. The frequency shift (from Ω_A to Ω_C) caused by superfast crystallization is illustrated in Fig. *c*.[325] Published in accordance with the Creative Commons Attribution license.

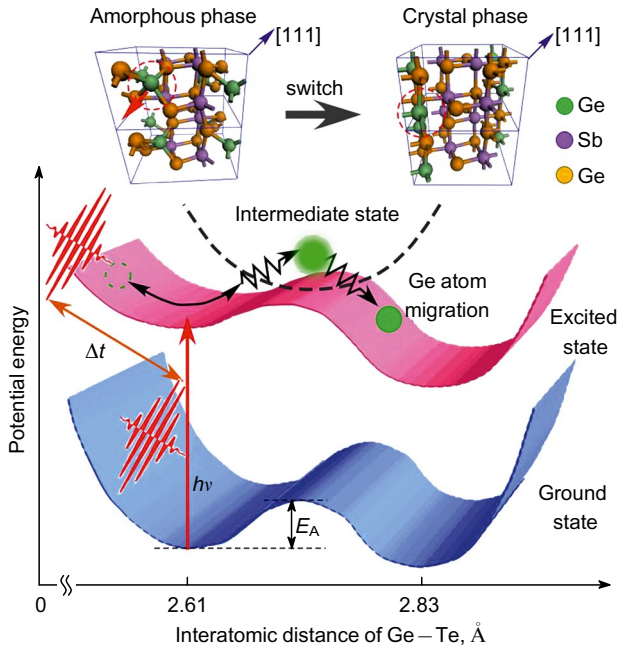


Figure 34. Potential energy surface upon excitation with two successive pump pulses (lower drawing) and local structural changes in the GST superlattice (upper drawing). E_A is the activation energy where phase transition is a thermal (non-coherent) process. The positions of germanium atoms can be rearranged by the coherent selective excitation of the $GeTe_4$ local vibration accompanied by rearrangements of the surrounding atoms (Sb and Te) *via* an intermediate state (dashed line). The local structures of two phases are constructed on the basis of DFT calculations. The red colour marks the $GeTe_4$ local structures (in the amorphous phase) and $GeTe_6$ structures (in the crystalline phase); red arrow indicates the atomic displacement of the germanium atom along the [111] direction.[325] Published in accordance with the Creative Commons Attribution license.

It is assumed that the above state switching process requires little energy, since the chemical bonds are more easily reorganized in the excited state than in the ground state.[363]

The structural changes caused by the laser radiation lead to modification of properties of the material, which was established in a number of studies. For example, it was shown[364] that continuous laser irradiation of GST225 thin film at $\lambda = 405$ nm changes the optical constants n and k of the material, with these changes being non-linearly dependent on the radiation power (at high powers, the thin film material melts).

Shanmugam *et al.*[365] observed giant circular dichroism in thin films of the initially achiral amorphous GST225 upon irradiation with circularly polarized light at 532 nm. The dichroism was detected by synchrotron circular dichroism spectroscopy, which is often used to derive structural information about chiral biological objects using UV and visible light. The chirality was induced by film irradiation by a pulsed circularly polarized laser for < 2 μs; the signal depended on the laser fluence and film thickness. The correlations of the optical results and structural data with theoretical modelling suggested that the alignment of the reamorphized fragments in the crystallized film along the electric field vector of the light give rise to centres responsible for the chirality. Optical activity was also observed in nitrogen-doped GST225 films upon irradiation with circularly polarized light.[366] Thus, these experiments indicate that optically active media can be obtained by laser modification of amorphous films of GST materials.

5. Conclusion

The chemical and structural modification methods (or a combination of both) developed for glassy chalcogenide semiconductors can be used to effectively control the performance characteristics of PCM materials without deteriorating their unique properties (for example, radiation stability) and without complicating the process of their manufacturing. Doping impurities used for chemical modification can be chosen considering the data on physicochemical processes induced by low-energy external stimuli and basic notions of the isomorphism theory. The theory of structural modification, which implies that the structure of non-crystalline materials with a soft structural network can be modified at four levels, is applicable to phase change memory materials, which was confirmed by experiments with laser radiation. The PCM materials demonstrate specific features caused by their ability to undergo reversible phase transitions, *e.g.*, form two-phase laser-induced periodic surface structures. These features can be used to fabricate laser micro-optical phase change cells.

The prospects of development of PCM materials are based on the possibility of formation of not only two stable phase states, differing by unique optical and electrical contrast, but also intermediate metastable states under low-energy external stimuli. This allows the use of these materials as efficient components for the multilevel control. Understanding the fundamentals of the control of performance characteristics would provide approaches to solving the existing problems, *e.g.*, to reduce the drift of parameters of PCM materials, increase the stability of their intermediate states and increase the robustness of multilevel devices. The development of this research area would result in the design of new-generation device for the hardware implementation of fully optical neuromorphic computating and for modern radiophotonic integrated devices, requiring compact switches for high-speed telecommunication data transfer and access.

This review was financially supported by the Russian Foundation for Basic Research (Project No. 20-13-50295). The authors are grateful to M.E.Fedyanina for the help in technical formatting of the review.

6. List of abbreviations and symbols

AFM — atomic force microscopy,
AD — as-deposited (film),
BD — Blu-ray disk,
BE — bottom electrode,
BL — bit line,
CD — compact disc,
DFT — density functional theory,
DRAM — dynamic random access memory,
DVD — digital versatile disc,
GST — Ge – Sb – Te system,
GST124 — $GeSb_2Te_4$,
GST147 — $GeSb_4Te_7$,
GST225 — $Ge_2Sb_2Te_5$,
HAADF-STEM — high-angle annular dark field scanning transmission electron microscopy,

HRTEM — high-resolution transmission electron microscopy,
LIPSS — laser-induced periodic surface structures,
NAND — NOT – AND flash memory,
PCM — phase change memory,
PCRAM — phase change random access memory,
READ — data reading operation,
RESET — operation providing transition to the amorphous state,
SCM — storage-class memory,
SEM —scanning electron microscopy,
SET — operation providing transition to the crystalline state,
STEM — scanning transmission electron microscopy,
TEM — transmission electron microscopy,
WL — word line,
E_c — conduction band bottom,
E_F — Fermi level,
E_g — optical band gap width,
E_0 — optical band gap width at 0 K,
E_s — energy barrier for the subsequent relaxation,
E_v — valence band top,
I_c — average band ionicity coefficient,
k — absorption coefficient,
K — average coordination number,
M — degree of bond metallization,
n — refractive index,
N — distribution density,
T_{cr} — crystallization temperature,
T_g — glass transition temperature,
T_m — melting point,
Δ_b — energy difference between local minima,
Δd — change in the material density,
ΔE_σ — activation energy of conduction,
λ — emission wavelength,
$\sigma_{293\,K}$ — electrical conductivity at 293 K,
χ — electronegativity.

7. References

1. A.Wilson. *Proc. R. Soc.*, **133**, 458 (1931)
2. A.Wilson. *Proc. R. Soc.*, **134**, 277 (1931)
3. B.T.Kolomiets, N.A.Gorunova. *Gosudarstvennyi Reestr Otkrytii SSSR. Otkrytie No. 98 s Prioritetom ot Yanvarya 1955. Poluprovodnikovye Svoistva Khal'kogenidnykh Stekol. (State Register of Discoveries of the USSR. Discovery No. 98 with Priority Dated January 1955. Semiconducting Properties of Chalcogenide Glasses)*; http://ross-nauka.narod.ru/06/06-098.html; http://www.decoder.ru/list/topic_373 (Last access 31.08.2022)
4. N.A.Gorunova, B.T.Kolomiets. *Bull. Russ. Acad. Sci. Phys.*, **20**, 1496 (1956)
5. W.E.Spear, P.G.Le Comber. *Solid State Commun.*, **17**, 1193 (1975)
6. N.F.Mott, E.A.Davis. In *Electron Processes in Non-Crystalline Materials*. (Oxford: Clarendon Press, 1979)
7. B.T.Kolomiets. *Phys. Status Solidi*, **7**, 359 (1964)
8. A.Feltz. In *Amorphe und Glasartige Anorganische Festkorper*. (Berlin: Akademie Verlag, 1983)
9. M.H.Brodsky. In *Amorphous Semiconductors*. (Ed. M.H.Brodsky). (Berlin: Springer-Verlag, 1979). P. 3
10. A.I.Popov. In *Fizika i Tekhnologiya Neuporyadochennykh Poluprovodnikov. (Physics and Technology of Disordered Semiconductors)*. (Moscow: Izd. Dom MEI, 2008). P. 272
11. P.Guo, A.M.Sarangan, I.Agha. *Appl. Sci.*, **9**, 530 (2019)
12. N.A.Bogoslovskiy, K.D.Tsendin. *Fiz. Tekhn. Poluprovod.*, **46**, 577 (2012)
13. W.Zhang, R.Mazzarello, M.Wuttig, E.Ma. *Nat. Rev. Mater.*, **4**, 150 (2019)
14. X.B.Li, N.K.Chen, X.P.Wang, H.B.Sun. *Adv. Funct. Mater.*, **28**, 1803380 (2018)
15. A.Lotnyk, M.Behrens, B.Rauschenbach. *Nanoscale Adv.*, **1**, 3836 (2019)
16. M.L.Gallo, A.Sebastian. *J. Phys. D*, **53**, 213002 (2020)
17. H.-Y.Cheng, F.Carta, W.-C.Chien, H.-L.Lung, M.J.BrightSky. *J. Phys. D*, **52**, 473002 (2019)
18. G.W.Burr, M.J.Brightsky, A.Sebastian, H.-Y.Cheng, J.-Y.Wu, S.Kim, N.E.Sosa, N.Papandreou, H.-L.Lung, H.Pozidis, E.Eleftheriou, C.H.Lam. *IEEE J. Emerg. Select. Top. Circ. Syst.*, **6** (2), 146 (2016)
19. M.Wuttig, H.Bhaskaran, T.Taubner. *Nat. Photon.*, **11**, 465 (2017)
20. S.Abdollahramezani, O.Hemmatyar, H.Taghinejad, A.Krasnok, Y.Kiarashinejad, M.Zandehshahvar, A.Alu, A.Adibi. *Nanophotonics*, **9**, 1189 (2020)
21. T.Cao, R.Wang, R.E.Simpson, G.Li. *Prog. Quantum Electron.*, **74**, 100299 (2020)
22. J.Wang, L.Wang, J.Liu. *IEEE Access*, **8**, 121211 (2020)
23. L.Kang, L.Chen. *J. Electron. Mater.*, **50**, 1 (2021)
24. C.Y.Zhao, G.H.Zhang. *Renew. Sustain. Energy Rev.*, **15**, 3813 (2011)
25. K.Pielichowska, K.Pielichowski. *Prog. Mater. Sci.*, **65**, 67 (2014)
26. W.E.O'Connor, R.Warzoha, R.Weigand, A.S.Fleischer, A.P.Wemhoff. *Appl. Energy*, **132** 496 (2014)
27. M.C.Floros, K.L.C.Kaller, K.D.Poopalam, S.S.Narine. *Solar Energy*, **139**, 23 (2016)
28. E.R.Meinders, A.V.Mijiritskii, L.van Pieterson, M.Wuttig. In *Optical Data Storage. Phase-Change Media and Recording*. (Springer, 2006). P. 174
29. M.Wuttig, S.Raoux. In *Phase Change Materials. Science and Applications*. (Springer, 2009). P. 430
30. A.Redaelli. In *Phase Change Memory. Device Physics, Reliability and Applications*. (Ed. A.Redaelli). (Cham: Springer International Publishing, 2018). P.65
31. A.D.Pearson, W.R.Northover, J.F.Dewald, W.F.Peck Jr. *Adv. Glass Technol.*, **2**, 357 (1962)
32. B.T.Kolomiets, E.A.Lebedev. *Radiotekhn. Elektron.*, **8**, 2097 (1963)
33. S.R.Ovshinsky. *Phys. Rev. Lett.*, **21**, 1450 (1968)
34. E.I.Evans, J.H.Helbers, S.R.Ovshinsky. *J. Non-Cryst. Solids*, **2**, 33 (1970)
35. R.G.Neale, D.L.Nelson, G.E.Moore. *Electronics*, **43**, 56 (1970)
36. J.Feinleib, J.de Neufville, S.C.Moss, S.R.Ovshinsky. *Appl. Phys. Lett.*, **18**, 254 (1971)
37. N.Yamada, M.Otoba, K.Kawahara, N.Miyagawa, H.Ohta, N.Akahira, T.Matsunaga. *Jpn. J. Appl. Phys.*, **26**, 61 (1987)
38. N.Yamada, E.Ohno, K.Nishiuchi, N.Akahira. *J. Appl. Phys.*, **69**, 2849 (1991)
39. N.Yamada. *MRS Bull.*, **21** (9), 48 (1996)
40. B.Tallis. *Intel Announces Optane Memory M15 : 3D XPoint On M. 2 PCIe 3.0 x4*; https://www.anandtech.com/show/14437/intel-announces-optane-memory-m15-3dxpoint-on-m2-pcie-30-x4 (Last access 31.08.2022)
41. *Intel and Micron Produce Breakthrough Memory Technology*; https://newsroom.intel.com/news-releases/intel-and-micron-produce-breakthrough-memory-technology/#gs.wv45wi (Last access 31.08.2022)
42. S.W.Fong, C.M.Neumann, H.S.P.Wong. *IEEE Trans. Electron Devices*, **64**, 4374 (2017)
43. O.I.Shpotyuk. In *Semiconducting Chalcogenide Glass I: Glass Formation, Structure, and Simulated Transformations in Chalcogenide Glasses*. (Eds R.Fairman, B.Ushkov). (Cambridge: Academic Press, 2004). P. 215
44. S.Gerardin, A.Paccagnella. *IEEE Trans. Nucl. Sci.*, **57**, 3016 (2010)

45. A.L.Serra, T.Vogel, G.Lefevre, S.Petzold, N.Kaiser, G.Bourgeois, M.C.Cyrille, L.Alff, C.Trautmann, C.Vallee, D.Sylvain, C.Charpin-Nicolle1, G.Navarro, E.Nowak. *France: Virtual Conference. RADECS*; https://hal.archives-ouvertes.fr/cea-03086407 (Last access 31.08.2022)
46. K.Konstantinou, T.H.Leea, F.C.Mocanua, S.R.Elliott. *Proc. Nat. Acad. Sci. USA*, **115**, 5353 (2018)
47. M.Wuttig, N.Yamada. *Nat. Mater.*, **6**, 824 (2007)
48. J.-J.Wang, Y.-Z.Xu, R.Mazzarello, M.Wuttig, W.Zhang. *Materials*, **10**, 862 (2017)
49. P.I.Lazarenko, Yu.V.Vorobiev, A.A.Sherchenkov, S.A.Kozyukhin, A.O.Yakubov, A.V.Kukin, Yu.S.Sybina, I.V.Sagunova. *Inorg. Mater.: Appl. Res.*, **11**, 330 (2020)
50. N.Kh.Abrikosov, G.T.Danilova-Dobryakova. *Neorg. Mater.*, **1**, 204 (1965)
51. N.Kh.Abrikosov, G.T.Danilova-Dobryakova. *Neorg. Mater.*, **6**, 475 (1970)
52. B.Legendre, B.Hancheng, S.Bordas, M.T.Clavaguera-Mora. *Thermochim. Acta*, **78**, 141 (1984)
53. V.I.Kosyakov, V.A.Shestakov, L.E.Shelimova, F.A.Kuznetsov, V.S.Zemskov. *Inorg. Mater.*, **36**, 1004 (2000)
54. L.E.Shelimova, O.G.Karpinskii, M.A.Kretova, V.I.Kosyakov, V.A.Shestakov, V.S.Zemskov, F.A.Kuznetsov. *Inorg. Mater.*, **36**, 768 (2000)
55. J.L.F.Da Silva, A.Walsh, H.Lee. *Phys. Rev. B*, **78**, 224111 (2008)
56. A.Lotnyk, U.Ross, S.Bernutz, E.Thelander, B.Rauschenbach. *Sci. Rep.*, **6**, 26724 (2016)
57. T.Rosenthal, M.N.Schneider, C.Stiewe, M.Doblinger, O.Oeckler. *Chem. Mater.*, **23**, 4349 (2011)
58. I.I.Petrov, R.M.Imamov, Z.G.Pinsker. *Kristallografiya*, **13**, 417 (1968)
59. N.Yamada. *Phys. Status Solidi B*, **249**, 1837 (2012)
60. P.Urban, M.N.Schneider, L.Erra, S.Welzmiller, F.Fahrnbauera, O.Oeckler. *CrystEngComm*, **15**, 4823 (2013)
61. Y.Zheng, Y.Wang, T.Xin, Y.Cheng, R.Huang, P.Liu, M.Luo, Z.Zhang, S.Lv, Z.Song, S.Feng. *Commun. Chem.*, **2** (13), 1 (2019)
62. N.Yamada, T.Matsunaga. *J. Appl. Phys.*, **88**, 7020 (2000)
63. T.Matsunaga, N.Yamada, Y.Kubota. *Acta Crystallogr., Sect. B*, **60**, 685 (2004)
64. M.Wuttig, D.Lusebrink, D.Wamwangi, W.Welnic, M.Gilleben, R.Dronskowski. *Nat. Mater.*, **6**, 122 (2007)
65. T.H.Lee, S.R.Elliott. *Phys. Rev. B*, **84**, 094124 (2011)
66. T.H.Lee, S.R.Elliott. *Adv. Mater.*, **29**, 1700814 (2017)
67. K.Shportko, S.Kremers, M.Woda, D.Lencer, J.Robertson, M.Wuttig. *Nat. Mater.*, **7**, 653 (2008)
68. A.Kolobov, P.Fons, A.Frenkel, A.L.Ankudinov, J.Tominaga, T.Uruga. *Nat. Mater.*, **3**, 703 (2004)
69. E.M.Vinod, K.Ramesh, K.S.Sangunni. *Sci. Rep.*, **5**, 8050 (2015)
70. Z.Y.Li, Y.F.Hu, T.Wen, J.W.Zhai, T.W.Lai. *J. Appl. Phys.*, **117**, 135703 (2015)
71. S.Fujimori, S.Yagi, H.Yamazaki, N.Funakoshi. *J. Appl. Phys.*, **64**, 1000 (1988)
72. Y.Zheng, M.Xia, Y.Cheng, F.Rao, K.Ding, W.Liu, Z.Song, S.Feng. *Nano Res.*, **9**, 3453 (2016)
73. Y.Zhang, J.Feng, Z.F.Zhang, B.C.Cai, Y.Y.Lin, T.A.Tang, B.Chen. *Appl. Surf. Sci.*, **254**, 5602 (2008)
74. C.Z.Wang, S.M.Li, J.W.Zhai, B.Shen, M.C.Sun, T.S.Lai. *Scr. Mater.*, **64**, 645 (2011)
75. R.E.Simpson, D.W.Hewak, P.Fons, J. Tominaga, S.Guerin, B.E.Hayden. *Appl. Phys. Lett.*, **92**, 141921 (2008)
76. M.Delaney, I.Zeimpekis, D.Lawson, D.W.Hewak, O.L.Muskens. *Adv. Funct. Mater.*, **30**, 2002447 (2020)
77. Z.Zhang, Y.F.Gu, S.N.Song, Z.T.Song, Y.Cheng, B.Liu, Y.Q.Zhu, D.Zhou, S.L.Feng. *J. Appl. Phys.*, **116**, 074304 (2014)
78. H.Zou, X.Q.Zhu, Y.F.Hu, Y.X.Sui, Y.M.Sun, J.H.Zhang, L.Zheng, Z.T.Song. *J. Appl. Phys.*, **120**, 245303 (2016)
79. Z.H.Zheng, P.Fan, J.T.Luo, G.X.Liang. *J. Phys. Chem. Solids*, **103**, 82 (2017)
80. Y.F.Hu, H.Zou, L.Yuan, Z.J.Xue, Y.X.Sui, W.H.Wu, J.H.Zhang, X.Q.Zhu, S.N.Song, Z.T.Song. *Scr. Mater.*, **115**, 19 (2016)
81. H.Zou, Y.F.Hu, X.Q.Zhu, Y.M.Sun, L.Zheng, Y.X.Sui, S.C.Wu, Z.T.Song. *J. Mater. Sci.*, **52**, 5216 (2017)
82. C.C.Coffin, S.Johnson. *Proc. R. Soc., Ser. A*, **146**, 564 (1934)
83. C.E.Wickersham, G.Bajor, J.E.Greene. *J. Vac. Sci. Technol. A*, **1**, 1857 (1983)
84. B.Gholipour, C.C.Huang, D.W.Hewak. *J. Mater. Sci.: Mater Electron*, **26**, 4763 (2015)
85. M.A.Hughes, Y.Fedorenko, R.M.Gwilliam, K.P.Homewood, S.Hinder, B.Gholipour, D.W.Hewak, T.-H.Lee, S.R.Elliott, R.J.Curry. *Appl. Phys. Lett.*, **105**, 083506 (2014)
86. R.E.Simpson. PhD Thesis. University of Southamptom, England, 2008
87. *Phase Change Memory Market To Reach USD 46.52 Billion By 2026 | Reports and Data*; https://www.globenewswire.com/news-release/2019/11/13/1946534/0/en/Phase-Change-Memory-Market-To-Reach-USD-46-52-Billion-By-2026-Reports-And-Data.html (Last access 31.08.2022)
88. D.T.Castro, L.Goux, G.A.M.Hurkx, K.Attenborough, R.Delhougne, J.Lisoni, F.J. Jedema, M.A.A.t.Zandt, R.A.M.Wolters, D.J.Gravesteijn, M.A.Verheijen, M.Kaiser, R.G.R.Weemaes, D.J.Wouters. In *IEEE Int. Electron Devices Meeting*. (Washington: IEEE, 2007). P. 315
89. D.S.Suh, C.Kim, K.H.Kim, Y.Khang, T.Y.Lee, Y.S.Kang, T.S.Park, Y.G.Yoon, J.Im, J.Ihm. *Appl. Phys. Lett.*, **96**, 123115 (2010)
90. M.Stegmaier, C.Rios, H.Bhaskaran, W.H.P.Pernice. *ACS Photon.*, **3**, 828 (2016)
91. B.-S.Lee, R.M.Shelby, S.Raoux, Ch. T.Retter, G.W.Burr, St.N.Bogle, K.Darmawikarta, St.G.Bishop, J.R.Abelson. *J. Appl. Phys.*, **115**, 063506 (2014)
92. M.Salinga, E.Carria, A.Kaldenbach, M.Bornhofft, J.Benke, J.Mayer, M.Wuttig. *Nat. Commun.*, **4**, 2371 (2013)
93. J. Orava, D.W.Hewak, A.L.Greer. *Adv. Funct. Mater.*, **25**, 4851 (2015)
94. J. Pries, S.Wei, M.Wuttig, P.Lucas. *Adv. Mater.*, **31**, 1900784 (2019)
95. I.V.Karpov, M.Mitra, D.Kau, G.Spadini, Y.A.Kryukov, V.G.Karpov. *Appl. Phys. Lett.*, **92**, 173501 (2008)
96. V.G.Karpov, Y.A.Kryukov, M.Mitra, I.V.Karpov. *J. Appl. Phys.*, **104**, 054507 (2008)
97. V.G.Karpov. *Appl. Phys. Lett.*, **97**, 033505 (2010)
98. D.Krebs, T.Bachmann, P.Jonnalagadda, L.Dellmann, S.Raoux. *New J. Phys.*, **16**, 043015 (2014)
99. J.L.M.Oosthoek, D.Krebs, M.Salinga, D.J.Gravesteijn, G.A.M.Hurkx, B J.Kooi. *J. Appl. Phys.*, **112**, 084506 (2012)
100. C.Longeaud, J.Luckas, D.Krebs, R.Carius, J.Klomfass, M.Wuttig. *J. Appl. Phys.*, **112**, 113714 (2012)
101. P.I.Lazarenko, A.A.Sherchenkov, S.A.Kozyukhin, A.V.Babich, S.P.Timoshenkov, D.G.Gromov, A.S.Shuliatyev, E.N.Redichev. *AIP Conf. Proc.*, **1727**, 020013 (2016)
102. K.Tsendin. *Phys. Status Solidi B*, **246**, 1831 (2009)
103. M.Le Gallo, A.Athmanathan, D.Krebs, A.Sebastian. *J. Appl. Phys.*, **119**, 025704 (2016)
104. D.Ielmini. *Phys. Rev. B*, **78**, 035308 (2008)
105. V.G.Karpov, Y.A.Kryukov, S.D.Savransky, I.V.Karpov. *Appl. Phys. Lett.*, **90**, 123504 (2007)
106. J.Liu. *IEEE Trans. Electron Devices*, **64**, 2207 (2017)
107. D.Ielmini, Y.Zhang. *J. Appl. Phys.*, **102**, 054517 (2007)
108. J.Luckas, S.Kremers, D.Krebs, M.Salinga, M.Wuttig, C.Longeaud. *J. Appl. Phys.*, **110**, 013719 (2011)

109. M.Rutten, M.Kaes, A.Albert, M.Wuttig, M.Salinga. *Sci. Rep.*, **5**, 1 (2015)
110. M.Le Gallo, D.Krebs, F.Zipoli, M.Salinga, A.Sebastian. *Adv. Electron. Mater.*, **4**, 1700627 (2018)
111. M.Rizzi, A.Spessot, P.Fantini, D.Ielmini. *Appl. Phys. Lett.*, **99**, 223513 (2011)
112. J.Y.Raty, W.Zhang, J.Luckas, C.Chen, R.Mazzarello, C.Bichara, M.Wuttig. *Nat. Commun.*, **6**, 1 (2015)
113. J.C.Martinez, L.Lu, J.Ning, W.Dong, T.Cao, R.E.Simpson. *Phys. Status Solidi B*, **257**, 1900289 (2020)
114. Q.Li, K.Xu, X.Wang, H.Huang, L.Ma, C.Bi, Z.Yang, Y.Li, Y.Zhao, S.Fan, J.Liu, C.Hu. *J. Mater. Chem. C*, **7**, 4132 (2019)
115. J.Akola, R.O.Jones. *Phys. Rev. B*, **76**, 235201 (2007)
116. M.E.Fedyanina, P.I.Lazarenko, Yu.V.Vorobyov, S.A.Kozyukhin, A.A.Dedkova, A.O.Yakubov, V.S.Levitskii, I.V.Sagunova, A.A.Sherchenkov. *Semiconductors*, **54**, 1775 (2020)
117. J-W.Park, S.H.Eom, H.L.Juarez, L.L.F.Da Silva, Y.-S.Kang, T.-Y.Lee, Y.H.Khang. *Phys. Rev. B*, **80**, 115209 (2009)
118. J.-W.Park, S.H.Baek, T.D.Kang, H.Lee, Y.-S.Kang, T.-Y.Lee, D.-S.Suk, K.J. Kim, C.K.Kim, Y.H.Khang, J.L.F.Da Silva, S.-H.Wei. *Appl. Phys. Lett.*, **93**, 021914 (2008)
119. A.Pirovano, A.L.Lacaita, A.Benvenuti, F.Pellizzer, R.Bez. *IEEE Trans. Electron Devices*, **51**, 452 (2004)
120. G.E.Jellison Jr., F.A.Modine. *Appl. Phys. Lett.*, **69**, 371 (1996)
121. A.S.Ferlauto, G.M.Ferreira, J.M.Pearce, C.R.Wronski, R.W.Collins, X.Deng, G.Ganguly. *J. Appl. Phys.*, **92**, 2424 (2002)
122. A.V.Kolobov, J.Tominaga, P.Fons. In *Phase-Change Memory Materials. Springer Handbook of Electronic and Photonic Materials*. (Washington, DC: Springer; IEEE, 2007). P. 1149
123. N.Miyagawa. *Front. Optoelectron.*, **7**, 409 (2014)
124. E.E.-T.Hwu, A.Boisen. *ACS Sens.*, **3**, 1222 (2018)
125. S.B.Eryilmaz, D.Kuzum, R.Jeyasingh, S.B.Kim, M.Bright-Sky, C.Lam, H.-S.Ph. Wong. *Front. Neurosci.*, **8**, 205 (2014)
126. G.W.Burr, M.J.Breitwisch, M.Franceschini, D.Garetto, K.Gopalakrishnan, B.Jackson, B.Kurdi, C.Lam, L.A.Lastras, A.Padilla, B.Rajendran, S.Raoux, R.S.Shenoy. *J. Vacuum Sci. Technol. B*, **28**, 223 (2010)
127. G.Navarro. In *Reliability Analysis of Embedded Phase-Change Memories Based on Innovative Materials*. (Grenoble: Université de Grenoble, 2013). P. 183
128. M.J.Kang, T.J.Park, Y.W.Kwon, D.H.Ahn, Y.S.Kang, H.Jeong, S.J.Ahn, Y.J.Song, B.C.Kim, S.W.Nam, H.K.Kang, G.T.Jeong, C.H.Chung. In *2011 International Electron Devices Meeting*. (Washington: IEEE, 2011). P. 39
129. I.S.Kim, S.L.Cho, D.H.Im, E.H.Cho, D.H.Kim, G.H.Oh, D.H.Ahn, S.O.Park, S.W.Nam, J.T.Moon, C.H.Chung. In *2010 Symposium on VLSI Technology*. (Honolulu, 2010). P. 203; https://ieeexplore.ieee.org/abstract/document/5556228 (Last access 31.08.2022)
130. H.M.Cheng, F.Carta, W.-C.Chien, H.-L.Lung, M.J.Bright-Sky. *J. Phys. D*, **52**, 473002 (2019)
131. P.Hosseini, C.D.Wright, H.Bhaskaran. *Nature (London)*, **511**, 206 (2014)
132. A.V.Pogrebnyakov, J.A.Bossard, J.P.Turpin, J.D.Musgraves, H.J.Shin, C.Rivero-Baleine, N.Podraza, K.A.Richardson, D.H.Werner, T.S.Mayer. *Opt. Mater. Express*, **8**, 2264 (2018)
133. Y.Qu, Q.Li, L.Cai, M.Pan, P.Ghosh, K.Du, M.Qiu. *Light: Sci. Appl.*, **7** (1), 1 (2018)
134. M.Rude, J.Pello, R.E.Simpson, J.Osmond, G.Roelkens, J.J.van der Tol, V.Pruneri. *Appl. Phys. Lett.*, **103**, 141119 (2013)
135. P.I.Trofimov, I.G.Bessonova, P.I.Lazarenko, D.A.Kirilenko, N.A.Bert, S.A.Kozyukhin, I.S.Sinev. *ACS Appl. Mater. Interfaces*, **13**, 32031 (2021)
136. P.Xu, J. Zheng, J.K.Doylend, A.Majumdar. *ACS Photon.*, **6**, 553 (2019)
137. Y.G.Chen, T.S.Kao, B.Ng, X.Li, X.G.Luo, B.Lukyanchuk, S.A.Maier, M.H.Hong. *Opt. Express*, **21**, 13691 (2013)
138. N.Farmakidis, N.Youngblood, X.Li, J.Tan, J.L.Swett, Z.Cheng, C.D.Wright, W.H.P.Pernice, H.Bhaskaran. *Sci. Adv.*, **5**, 2687 (2019)
139. Y.Lu, M.Stegmaier, P.Nukala, M.A.Giambra, S.Ferrari, A.Busacca, W.H.P.Pernice, R.Agarwal. *Nano Lett.*, **17**, 150 (2017)
140. K.Chaudhary, M.Tamagnone, X.Yin, C.M.Spagele, S.L.Oscurato, J. Li, C.Persch, R.Li, N.A.Rubin, L.A.Jauregui, K.Watanabe, T.Taniguchi, P.Kim, M.Wuttig, J.H.Edgar, A.Ambrosio, F.Capasso. *Nat. Commun.*, **10**, 1 (2019)
141. A.Sebastian, M.Le Gallo, E.Eleftheriou. *J. Phys. D*, **52**, 443002 (2019)
142. S.Wen, Y.Meng, M.Jiang, Y.Wang. *Sci Rep.*, **8**, 4979 (2018)
143. X.Li, N.Youngblood, C.Rios, Z.Cheng, C.D.Wright, W.H.Pernice, H.Bhaskaran. *Optica*, **6**, 1 (2019)
144. Z.Cheng,C.Ríos, W.H.P.Pernice, D.Wright, H.Bhaskaran. *Sci. Adv.*, **3**, e1700160 (2017)
145. J.Feldmann, N.Youngblood, C.D.Wright, H.Bhaskaran, W.H.P.Pernice. *Nature (London)*, **569**, 208 (2019)
146. I.Chakraborty, G.Saha, K.Roy. *Phys. Rev. Appl.*, **11**, 014063 (2019)
147. C.R.de Galarreta, I.Sinev, A.M.Alexeev, P.Trofimov, K.Ladutenko, S.G.-C.Carrillo, E.Gemo, A.Baldycheva, J.Bertolotti, C.D.Wright. *Optica*, **7**, 476 (2020)
148. C.R.de Galarreta, A.M.Alexeev, Y.-Y.Au, M.Lopez-Garcia, M.Klemm, M.Cryan, J.Bertolotti, D.Wright. *Adv. Funct. Mater.*, **28** 1704993 (2018)
149. W.Zhu, R.Yang, Y.Fan, Q.Fu, H.Wu, P.Zhang, N.-H.Shen, F.Zhang. *Nanoscale*. **10**, 12054 (2018)
150. C.-Y.Hwang, G.H.Kim, J.-H.Yang, C.-S.Hwang, S.M.Cho, W.-J. Lee, J.-E.Pi, J.H.Choi, K.Choi, H.-O.Kim, S.-Y.Lee, Y.-H.Kim. *Nanoscale*, **10**, 22635 (2018)
151. S.Abdollahramezani, O.Hemmatyar, M.Taghinejad, H.Taghinejad, A.Krasnok, A.A.Eftekhar, C.Teichrib, S.Deshmukh, M.El-Sayed, E.Pop, M.Wuttig, A.Alu, W.Cai, A.Adibi. *Nat. Commun.*, **13**, 1696 (2022)
152. H.Iwasaki, M.Harigaya, O.Nonoyama, Y.Kageyama, M.Takahashi, K.Yamada, H.Deguchi, Y.Ide. *Jpn. J. Appl. Phys.*, **32** (11S), 5241 (1993)
153. K.Nakayama, K.Kojima, Y.Imai, T.Kasai, S.Fukushima, A.Kitagawa, M.Kumeda, Y.Kakimoto, M.Suzuki. *Jpn. J. Appl. Phys.*, **42** (2A), 404 (2003)
154. K.Singh, S.Kumari, H.Singh, N.Bala, P.Singh, A.Kumar, A.Thakur. *Appl. Nanosci.*, 1 (2021); https://link.springer.com/article/10.1007/s13204-021-01911-7#article-info
155. M.Bouška, S.Pechev, Q.Simon, R.Boidin, V.Nazabal, J.Gutwirth, E.Baudet, P.Němec. *Sci. Rep.*, **6**, 26552 (2016)
156. S.Buller, Ch.Koch, W.Bensch, P.Zalden, R.Sittner, St.Kremers, M.Wuttig, U.Schurmann, L.Kienle, Th.Leichtwei, Ju.Janek, B.Schonborn. *Chem. Mater.*, **24**, 3582 (2012)
157. A.Lotnyk, I.Hilmi, U.Ross, B.Rauschenbach. *Nano Res.*, **11**, 1676 (2018)
158. S.R.Ovshinsky. In *Proceedings 7th International Conference on Amorphous Liquid and Semiconductors*. Centre for Industrial Consultancy and Liaison; University of Edinburgh, Edinburgh, 1977. P. 519
159. R.Flasck, M.Izu, K.Sapru, T.Anderson, S.R.Ovshinsky, H.Fritzsche. In *Proceedings 7th International Conference on Amorphous Liquid and Semiconductors*. Centre for Industrial Consultancy and Liaison; University of Edinburgh, Edinburgh, 1977. P. 524
160. T.Tsvetkov, B.Amov, E.Vateva,V.Averyanov. *Phys. Status Solidi A*, **119**, 107 (1990)
161. M.A.Hughes, Y.Fedorenko, B.Gholipour, J.Yao, T-H.Lee, R.M.Gwilliam, K.P.Homewood, S.Hinder, D.W.Hewak, S.R.Elliott, R.J.Curry. *Nat. Commun.*, **5**, 1 (2014)

162. S.A.Kozyukhin, A.A.Sherchenkov, V.M.Novotortsev, S.P.Timoshenkov. *Ross. Nanotechnol.,* **6** (3 – 4), 50 (2011)
163. S.Kozyukhin, M.Veres, H.P.Nguyen, A.Ingram, V.Kudoyarova. *Phys. Proc*., **44**, 82 (2013)
164. S.Kozyukhin, A.Sherchenkov, A.Babich, P.Lazarenko, H.P.Nguyen, O.Prikhodko. *Can. J. Phys*., **92**, 684 (2014)
165. S.A.Dembrovskii, E.A.Chechetkina. In *Stekloobrazovanie* (Glass Formation). (Moscow; Nauka, 1990). P. 279
166. V.S.Urusov. In *Teoriya Izomorfnoi Smesimosti (Theory of Isomorphic Miscibility)*. (Moscow: Nauka, 1977). P. 251
167. X.Zhou, M.Xia, F.Rao, L.Wu, X.Li, Z.Song, S.Feng, H.Sun. *ACS Appl. Mater. Interfaces*, **6**, 14207 (2014)
168. T.Li, L.Wu, X.Ji, Y.Zheng, G.Liu, Z.Song, J.Shi, M.Zhu, S.Song, S.Feng. *AIP Adv*., **8**, 025201 (2018)
169. P.Guo, J.A.Burrow, G.A.Sevison, A.Sood, M.Asheghi, J.R.Hendrickson, K.E.Goodson, I.Agha, A.Sarangan. *Appl. Phys. Lett*., **113**, 171903 (2018)
170. H.You, Y.Hu, X.Zhu, H.Zou. *J. Mater. Sci: Mater. Electron*., **28**, 5562 (2017)
171. P.Singh, A.Thakur. *Acta Crystallogr., Sect. A*, **73**, 1378 (2017)
172. P.I.Lazarenko, A.A.Sherchenkov, S.A.Kozyukhin, A.V.Babich, H.P.Nguen, S.P.Timoshenkov, D.G.Gromov, A.O.Yakubov, D.Y.Terekhov. *J. Phys. Conf. Ser*., **690**, 012006 (2016)
173. M.Agati, F.Renaud, D.Benoit, A.Claverie. *MRS Commun*., **8**, 1145 (2018)
174. R.Roy, A.Louiset, M.Benoit, L.Calmels. *Phys. Rev*., **99**, 245124 (2019)
175. K.Ding, K.Ren, F.Rao, Zh.Song, L.Wu, B.Liu, S.Feng. *Mater. Lett*., **125**, 143 (2014)
176. M.Choi, H.Choi, J.Ahn, Y.T.Kim. *Scr. Mater*., **170**, 16 (2019)
177. V.Madhavan, M.Carignano, A.Kachmar, K.Sangunni. *Sci. Rep*., **9**, 12985 (2019)
178. Q.Yin, L.Chen. *J. Alloys Compd*., **770**, 692 (2019)
179. S.Kumar, P.Sharma, V.Sharma. *Res. Phys*., **13**, 102276 (2019)
180. R.Svoboda, V.Karabyn, J.Malek, M.Frumar, L.Benes, M.Vlcek. *J. Alloys Compd*., **674**, 63 (2016)
181. J.Fu, X.Shen, Q.Nie, G.Wang, L.Wu, S.Dai, T.Xu, R.P.Wang. *Appl. Surf. Sci*., **264**, 269 (2013)
182. J.Feng, Y.Zhang, B.W.Qiao, Y.F.Lai, Y.Y.Lin, B.C.Cai, T.A.Tang, B.Chen. *Appl. Phys. A*, **87**, 57 (2007)
183. Y.Wang, Y.Zheng, G.Liu, T.Li, T.Guo, Y.Cheng, S.Lv, S.Song, K.Ren, Z.Song. *Appl. Phys. Lett*., **112**, 133104 (2018)
184. T.Zhang, B.Zhang, R.Shao, K.Zheng. *Mater. Lett*., **128**, 329 (2014)
185. Q.Wang, B.Liu, Y.Xia, Y.Zheng, R.Huo, Q.Zhang, S.Song, Y.Cheng, Z.Song, S.Feng. *Appl. Phys. Lett*., **107**, 222101 (2015)
186. Y.J. Huang, Y.C.Chen, T.E.Hsieh. *J. Appl. Phys*., **106**, 034916 (2009)
187. J.H.Seo, K.H.Song, H.Y.Lee. *J. Appl. Phys*., **108**, 064515 (2010)
188. A.Kelly, G.W.Groves. In *Crystallography and Crystal Defects*. Addison-Wesley, Reading, 1970. P. 163
189. P.Singh, P.Sharma, V.Sharma, A.Thakur. *Semicond. Sci. Technol*., **32**, 045015 (2017)
190. J.A.Dean. In *Lange's Handbook of Chemistry*. (5th End). (New York: McGraw-Hill Inc. 1999). P. 1291
191. K.J.Rao, R.Mohan. *Solid State Commun*., **39**, 1065 (1981)
192. S.Pizzini. In *Physical Chemistry of Semiconductor Materials and Processes*. (Hoboken: Wiley, 2015). P. 413
193. J.A.Dean. In *Lange's Handbook of Chemistry*. (New York: McGraw-Hill, 2004). P. 1291
194. G.Singh, A.Kaura, M.Mukul, S.Tripathi. *J. Mater. Sci*., **48**, 299 (2013)
195. P.Lazarenko, V.Kovalyuk, P.An, S.Kozyukhin, V.Takáts, A.Golikov, V.Glukhenkaya, Y.Vorobyov, T.Kulevoy, A.Sherchenkov, G.Goltsman. *Acta Mater*., **234**, 117994 (2022)
196. T.Park, S.Choi, M.Kang. *Thin Solid Films*, **515**, 5049 (2007)
197. M.Lee, K.Yong, Ch.Gan, L.Ting, S.Daud, L.Shi. *J. Phys. D*, **41**, 215402 (2008)
198. S.Gu, L.Hou, Q.Zhao, R.Huang. *Chin. Opt. Lett*., **1**, 716 (2003)
199. W.Song, L.Shi, X.Miao, T.Chong. *Appl. Phys. Lett*., **90**, 091904 (2007)
200. K.Wang, C.Steimer, D.Wamwangi, S.Ziegler, M.Wuttig, J.Tomforde, W.Bensch. *Microsyst. Technol*., **13**, 203 (2007)
201. P.Zalden, C.Koch, M.Paulsen, M.Esters, D.C.Johnson, M.Wuttig, A.M.Lindenberg, W.Bensch. *Adv. Funct. Mater*., **31**, 2004803 (2021)
202. W.Li, F.Liu, Y.Zhang, G.Han, W.Han, F.Liu, N.Sun. *J. Non-Cryst. Solids*, **516**, 99 (2019)
203. Q.X.Yin, L.Chen. *Mater. Res. Express*, **4**, 016407 (2017)
204. S.Dyussembayev, O.Prikhodko, K.Tsendin, S.Timoshenkov, N.Korobova. In *Photonic Fiber and Crystal Devices: Advances in Materials and Innovations in Device Applications VIII*. Vol. 9200. (San Diego, CA: SPIE Press, 2014). P. 920014
205. J.M.Skelton, A.R.Pallipurath, T.-H.Lee, S.R.Elliott. *Adv. Funct. Mater*., **24**, 7291 (2014)
206. D.R.Lide. In *Handbook of Chemistry and Physics*. (78th Edn). (Boca Raton, FL: CRC, 1997). P.9
207. S.A.Kozyukhin, H.P.Nguen. M.Beresh, V.Kh.Khudoyarova, I.V.Razumovskaya. *Vestn. RGRTU*, **42** (44), 74 (2012)
208. P.Lazarenko, S.Kozyukhin, A.Sherchenkov, A.Yakubov, Y.Zaytseva, D.Dronova, O.Boytsova, Yu.Chigirinsky, A.Zabolotskaya, V.Kozik. *J. Phys.: Conf. Ser*., **1611** (1), 012044 (2020)
209. J.C.Schottmiller, D.L.Bowman, C.Wood. *J. Appl. Phys*., **39**, 1663 (1967)
210. S.R.Elliott, A.T.Steel. *J. Phys. C*., **20**, 4335 (1987)
211. N.Tohge, Y.Yamamoto, T.Minami, M.Tanaka. *Appl. Phys. Lett*., **34**, 640 (1979)
212. P.Nagels, M.Rotti, S.Vikhrov. *J. Phys. Colloques*, **42** (C4), 907 (1981)
213. K.L.Bhatia, G.Parthasarathy, A.Sharma, E.S.R.Gopal. *Phys. Rev. B*, **38**, 6342 (1988)
214. E.-R.Sittner, K.S.Siegert, P.Jost, C.Schlockermann, F.R.L.Lange, M.Wuttig. *Phys. Status Solidi A*, **210**, 147 (2012)
215. R.E.Simpson, P.J. Fons, A.Kolobov, M.Kuwahara, J.Tominaga. *Jpn. J. Appl. Phys*., **48**, 03A062 (2009)
216. K.Ren, Y.Wang, S.Lv, S.Zhu, T.Xin, Z.Song. *J. Mater. Chem. C*, **7**, 11813 (2019)
217. M.-C.Jung, Y.M.Lee, H.-D.Kim, M.G.Kim, H.J. Shin, K.H.Kim, S.A.Song, H.S.Jeong, C.H.Ko, M.Han. *Appl. Phys. Lett*., **91**, 083514 (2007)
218. S.Tripathi, P.Kotula, M.K.Singh, C.Ghosh, G.Bakan, H.Silva, C.B.Carter. *ECS J. Solid State Sci. Technol*., **9**, 054007 (2020)
219. Y.-H.Perng, Y.-T.Hsu, L.-H.Chou. *MRS Proc*., **1072** (2008)
220. T.H.Jeong, H.Seo, K.L.Lee, S.M.Choi, S.J. Kim, S.Y.Kim. *Jpn. J. Appl. Phys*., **40**, 1609 (2001)
221. S.Privitera, E.Rimini, R.Zonca. *Appl. Phys. Lett*., **85**, 3044 (2004)
222. B.Liu, Z.Song, T.Zhang, S.Feng, B.Chen. *Appl. Surf. Sci*., **242** (1 – 2), 62 (2005)
223. B.Liu, Z.Song, T.Zhang, S.Feng, B.Chen. In *Fifth International Conference on Thin Film Physics and Applications*. Vol. 5774. (Bellingham: SPIE Press, 2004). P. 287
224. E.Gourvest, B.Pelissier, C.Vallee, A.Roule, S.Lhostis, S.Maitrejean. *J. Electrochem. Soc*., **159** (4), 373 (2012)
225. R.Golovchak, Y.G.Choi, S.Kozyukhin, Yu.Chigirinsky, A.Kovalskiy, P.Xiong-Skiba, J.Trimble, R.Pafchek, H.Jain. *Appl. Surf. Sci*., **332**, 533 (2015)
226. M.Agati, C.Gay, D.Benoit, A.Claverie. *Appl. Surf. Sci*., **518**, 146227 (2020)
227. P.Noe, C.Sabbione, N.Bernier, N.Castellani, F.Fillot, F.Hippert. *Acta Mater*., **110**, 142 (2016)

228. L.V.Yashina, R.Puttner, V.S.Neudachina, T.S.Zyubina, V.I.Shtanov, M.V.Poygin. *J. Appl. Phys.*, **103**, 094909 (2008)
229. R.E.Simpson, M.Krbal, P.Fons, A.V.Kolobov, J.Tominaga, T.Uruga, H.Tanida. *Nano Lett.*, **10**, 414 (2010)
230. Q.Yin, L.Chen. *J. Mater. Sci.: Mater. Electron.*, **29**, 16523 (2018)
231. C.Koch, A.L.Hansen, T.Dankwort, G.Schienke, M.Paulsen, D.Meyer, M.Wimmer, M.Wuttig, L.Kienle, W.Bensch. *RSC Adv.*, **7**, 17164 (2017)
232. P.Guo, G.A.Sevison, J.A.Burrow, I.Agha, A.Sarangan. In *Nanoengineering: Fabrication, Properties, Optics, and Devices XV*. Vol. 10730. (San Diego, CA: SPIE Press, 2018). P. 107300L
233. L.Cao, X.Ji, W.Zhu, Q.She, Y.Chen, Z.Hu, S.Guo, Z.Song, F.Rao, B.Qian, L.Wu. *ECS Solid State Lett.*, **4** (12), 102 (2015)
234. Y.Hu, R.Zhang, T.Lai, X.Zhu, H.Zou, Z.Song. *ECS J. Solid State Sci. Technol.*, **6**, 866 (2017)
235. J.Tominaga, T.Nakano, N.Atoda. *Jpn. J. Appl. Phys.*, **37** (4A), 1852 (1998)
236. T.H.Jeong, M.R.Kim, H.Seo, S.J.Kim, S.Y.Kim. *J. Appl. Phys.*, **86**, 774 (1999)
237. J.A.Kalb, C.Y.Wen, F.Spaepen, H.Dieker, M.Wuttig. *J. Appl. Phys.*, **98** (5), (2005)
238. P.La Fata, F.Torrisi, S.Lombardo, G.Nicotra, R.Puglisi, E.Rimini. *J. Appl. Phys.*, **105**, 083546 (2009)
239. X.Y.Liu. *J. Chem. Phys.*, **112**, 9949 (2000)
240. S.A.Kozyukhin, I.I.Nikolaev, P.I.Lazarenko, G.A.Valkovskiy, O.Konovalov, A.V.Kolobov, N.A.Grigoryeva. *J. Mater. Sci.: Mater. Electron.*, **31**, 10196 (2020)
241. S.Raoux, J.L.Jordan-Sweet, A.J. Kellock. *J. Appl. Phys.*, **103**, 114310 (2008)
242. N.Ohshima. *J Appl. Phys.*, **79**, 8357 (1996)
243. A.Babich, A.Sherchenkov, S.Kozyukhin, P.Lazarenko, O.Boytsova, A.Shuliatyev. *J. Therm. Anal. Calorim.*, **127**, 283 (2016)
244. N.Kraft, G.Wang, H.Bryja, A.Prager, J. Griebel, A.Lotnyk. *Mater. Design*, **199**, 109392 (2021)
245. P.Yeoh, Y.Ma, D.A.Cullen, J.A.Bain, M.Skowronski. *Appl. Phys. Lett.*, **114**, 163507 (2019)
246. S.H.Oh, K.Baek, S.K.Son, K.Song, J.W.Oh, S.-J.Jeon, W.Kim, J.H.Yoo, K.J.Lee. *Nanoscale Adv.*, **2**, 3841 (2020)
247. H.Seo, T.H.Jeong, J.W.Park, C.Yeon, S.J.Kim, S.Y.Kim. *Jpn. J. Appl. Phys.*, **39**, 745 (2000)
248. H.Kolpin, D.Music, G.Laptyeva, R.Ghadimi, F.Merget, S.Richter, R.Mykhaylonka, J.Mayer, J.M.Schneider. *J. Phys. Condens. Mater*, **21**, 435501 (2009)
249. K.Do, D.Lee, D.H.Ko, H.Sohn, M.H.Cho. *J. Electrochem. Soc.*, **158**, H390 (2011)
250. K.Do, H.Sohn, D.H.Ko. *J. Electrochem. Soc.*, **154**, H867 (2007)
251. T.H.Lee, D.Loke, S.R.Elliott. *Adv. Mater.*, **27**, 5477 (2015)
252. R.Kojima, S.Okabayashi, T.Kashihara, K.Horai, T.Matsunaga, E.Ohno, N.Yamada, T.Ohta. *Jpn. J. Appl. Phys.*, **37**, 2098 (1998)
253. T.H.Jeong, M.R.Kim, H.Seo, J.W.Park, C.Yeon. *Jpn. J. Appl. Phys.*, **39**, 2775 (2000)
254. K.H.Kim, J.C.Park, J.H.Lee, J.G.Chung, S.Heo, S.J.Choi. *Jpn. J. Appl. Phys.*, **49**, 101201 (2010)
255. L.Cheng, L.Wu, Z.Song, F.Rao, C.Peng, D.Yao, B.Liu, L.Xu. A*ppl. Phys. Lett.*, **113**, 044514 (2013)
256. F.Fillot, C.Sabbione, F.Pierre, F.Hippert, P.Noe. *J. Appl. Crystallogr.*, **51**, 1691 (2018)
257. M.A.Luong, D.Wen, E.Rahier, N.R.Ramond, B.Pecassou, Y.Le Friec, D.Benoit, A.Claverie. *Phys. Status Solidi, Rapid Res. Lett.*, **15**, 2000443 (2021)
258. J.Y.Cho, D.Kim, Y.J. Park, T.Y.Yang, Y.Y.Lee, Y.C.Joo. *Acta Mater.*, **94**, 143 (2015)
259. H.Y.Cheng, W.C.Chien, M.BrightSky, Y.H.Ho, Y.Zhu, A.Ray, R.Bruce, W.Kim, C.W.Yeh, H.L.Lung, C.Lam. In *IEEE International Electron Devices Meeting (IEDM)*. (Washington, DC; IEEE, 2015). P. 3
260. S.Kang, W.Y.Cho, B.H.Cho, K.J.Lee, C.S.Lee, H.R.Oh, B.G.Choi, Q.Wang, H.J.Kim, M.H.Park, Y.H.Ro, S.Kim, C.G.Ha, K.S.Kim, Y.R.Kim, D.E.Kim, C.K.Kwak, H.G.Byun, G.Jeong, H.Jeong, K.Kim, Y.S.Shin. *IEEE J. Solid-State Circuits – Front Cover.*, **42**, 210 (2007)
261. H.Li, Y.Chen. In *Nonvolatile Memory Design Magnetic, Resistive, and Phase Change*. (Boca Raton, FL: CRC Press, 2012). P. 203
262. B.T. Ahn. *Solid State Phenom.*, **124 – 126**, 21 (2007)
263. H.Y.Cheng, J.Y.Wu, R.Cheek, S.Raoux, M.BrightSky, D.Garbin, S.Kim, T.H.Hsu, Y.Zhu, E.K.Lai, E.Joseph, A.Schrott, S.C.Lai, A.Ray, H.L.Lung, C.Lam. In *International Electron Devices Meeting*. (San Francisco, CA: IEEE, 2012). P. 31.1
264. G.Navarro, V.Sousa, P.Noe. N.Castellani, M.Coue, J. Kluge, A.Kiouseloglou, C.Sabbione, A.Persico, A.Roule, O.Cueto, S.Blonkowski, F.Fillot, N.Bernier, R.Annunziata, M.Borghi, E.Palumbo, P.Zuliani, L.Perniola. In *IEEE 8th International Memory Workshop*. (Paris: IEEE, 2016). P. 1
265. A.Bourgine, J.Grisolia, M.Vallet, D.Benoit, Y.Le Friec, V.Caubet-Hilloutou, A.Claverie. *Solid State Electron.*, **172**, 107871 (2020)
266. D.Yao, X.Zhou, L.Wu, Z.Song, L.Cheng, F.Rao, B.Liu, S.Feng. *Solid State Electron.*, **79**, 138 (2013)
267. W.Zhou, L.Wu, X.Zhou, F.Rao, Z.Song, D.Yao, W.Yin, S.Song, B.Liu, B.Qian, S.Feng. *Appl. Phys. Lett.*, **105**, 243113 (2014)
268. W.K.Njoroge, H.W.Woltgens, M.Wuttig. *J. Vac. Sci. Technol. A*, **20**, 230 (2002)
269. V.Bragaglia, B.Jenichen, A.Giussani, K.Perumal, H.Riechert, R.Calarco. *J. Appl. Phys.*, **116**, 054913 (2014)
270. T.P.L.Pedersen, J.Kalb, W.K.Njoroge, D.Wamwangi, M.Wuttig, F.Spaepen. *Appl. Phys. Lett.*, **79**, 3597 (2001)
271. I.M.Park, J.K.Jung, S.O.Ryu, K.-J.Choi, B.-G.Yu, Y.-B.Park, S.M.Han, Y.-C.Joo. *Thin Solid Films*, **517**, 848 (2008)
272. C.F.Chen, A.Schrott, M.H.Lee, S.Raoux, Y.H.Shih, M.Breitwisch, F.H.Baumann, E.K.Lai, T.M.Shaw, P.Flaitz, R.Cheek, E.A.Joseph, S.H.Chen, B.Rajendran, H.L.Lung C.Lam. In *IEEE International Memory Workshop*. (Dresden: IEEE, 2009). P. 1
273. H.-B.Kang, T.-Y.Kim, Y.-H.Kim, S.-M.Cho, S.Cheon, C.-Y.Hwang, C.-S.Hwang, S.-Y.Lee, S.-M.Yoon. *J. Nanosci. Nanotechnol.*, **18**, 6033 (2018)
274. L.Lu, W.Dong, J.K.Behera, L.Chew, R.E.Simpson. *J. Mater. Sci.*, **54**, 2814 (2019)
275. L.Lu, R.E.Simpson, S.K.Valiyaveedu. *J. Opt. UK*, **20**, 103001 (2018)
276. S.I.Oh, I.H.Im, C.Yoo, S.Y.Ryu, Y.Kim, S.Choi, T.Eom, C.S.Hwang, B.J. Choi. *Micromachines*, **10** (5), 281 (2019)
277. K.Aryana, J.T.Gaskins, J.Nag, D.A.Stewart, Z.Bai, S.Mukhopadhyay, J.C.Read, D.H.Olson, E.R.Hoglund, J.M.Howe, A.Giri, M.K.Grobis, P.E.Hopkins. *Nat. Commun.*, **12**, 774 (2021)
278. L.Li, S.Song, Y.Xue, X.Chen, J.Zhao, J.Shen, Z.Song. *J. Mater. Sci. Mater. El.*, **31**, 10912 (2020)
279. S.Guo, Z.Hu, X.Ji, T.Huang, X.Zhang, L.Wu, Z.Song, J.Chua. *RSC Adv.*, **4**, 57218 (2014)
280. P.Guo, J.A.Burrow, G.A.Sevison, H.Kwon, C.Perez, J.R.Hendrickso, E.M.Smith, M.Asheghi, K.E.Goodson, I.Agha, A.M.Sarangan. *Appl. Phys. Lett.*, **116**, 131901 (2020)
281. X.Cheng, F.Mao, Z.Song, C.Peng, Y.Gong. *Jpn. J. Appl. Phys.*, **53**, 050304 (2014)

282. *ISO 16750-4 : 2010. Road Vehicles – Environmental Conditions and Testing for Electrical and Electronic Equipment – Part 4: Climatic Loads*; https://www.iso.org/ru/standard/46043.html (Last access 03.09.2022)
283. *AEC-Q100-Rev-H: Failure Mechanism Based Stress Test Qualification for Integrated Circuits*; http://www.aecouncil.com/AECDocuments.html (Last access 03.09.2022)
284. A.I.Popov, N.I.Michalev, V.R.Shemetova. *Philos. Mag. B*, **47**, 73 (1983)
285. A.Popov. In *Disordered Semiconductors: Physics and Application*. (2nd Edn). (New York: Jenny Stanford Publishing, 2018). P. 328
286. A.I.Popov, V.A.Vorontsov, I.A.Popov. *Fiz. Tekh. Poluprovod.*, **35**, 665 (2001)
287. D.S.Sanditov, G.M.Bartenev. In *Fizicheskie Svoistva Neuporyadochennykh Struktur. (Physical Properties of Disordered Structures)*. (Novosibirsk: Nauka, 1982). P. 259
288. F.F.Khokhlov, A.I.Mashin, D.A.Khokhlov. *Pis'ma ZhETF,* **67**, 646 (1998)
289. A.M.Mashin, A.F.Khokhlov. *Fiz. Tekh. Poluprovod.*, **33**, 1001 (1999)
290. A.F.Khokhlov, A.M.Mashin. In *Allotropiya Kremniya* (Allotropy of Silicon). (Nizhnii Novgorod: NNGU, 2001). P. 163
291. A.I.Andrievskii, I.D.Nabitovich. *Dokl. Akad. Nauk SSSR*, **124**, 321 (1959)
292. I.D.Nabitovich, A.I.Andrievskii. *Kristallografiya*, **5**, 465 (1960)
293. Yu.G.Poltavtsev. In *Struktura Poluprovodnikovykh Rasplavov. (Structure of Semiconductor Melts)*. (Moscow: Metallurgiya, 1984). P. 176
294. K.Miyauchi, J.Qui, M.Shojiya, N.Kawamura. *J. Non-Cryst. Solids*, **279**, 186 (2001)
295. Sh.Sh.Sarsembinov, O.Yu.Prikhodko, A.P.Ryaguzov, S.Ya.Maksimova. *Semicond. Sci. Technol.*, **16**, 44 (2001)
296. Sh.Sh.Sarsembinov, O.Yu.Prikhodko, A.P.Ryaguzov, S.Ya.Maksimova. *Semicond. Sci. Technol.*, **16**, 872 (2001)
297. J.C.Philips. *J. Non-Cryst. Solids*, **34**, 153 (1979)
298. J.C.Phillips. *Phys. Status Solidi B*, **101**, 473 (1980)
299. S.S.Yun, R.L.Cappelletti, R.N.Enzweiler, P.Boolchand. *Phys. Rew. B*, **39**, 8702 (1989)
300. B.G.Aitken. In *Proceedings of the International Congress on Glass Invited Papers*. (Edinburgh: Society of Glass Technology, 2001). P. 135
301. A.I.Popov. *Fiz. Khim. Stekla*, **20**, 803 (1994)
302. A.Feltz. Amorphe und glasartige anorganische Festkörper. (Berlin: Akademie-Verlag, 1983)
303. R.Ya.Golovchak, S.A.Kozyukhin, A.Kozdras, O.I.Shpotyuk., V.M.Novotortsev. *Inorg. Mater.*, **46**, 911 (2010); https://doi.org/10.1134/S0020168510080200
304. R.Golovchak, A.Kozdras, S.Kozyukhin, O.Shpotyuk. *Nucl. Instrum. Methods Phys. Res., Sect. B*, **26**, 2958 (2009)
305. P.Lucas, E.A.King, A.Doraiswami, P.Jivaganont. *Phys. Rev. B*, **71**, 104207 (2005)
306. R.Golovchak, A.Kozdras, O.Shpotyuk. *Solid State Commun.*, **145**, 423 (2008)
307. J.S.Knights, R.A.Lujan. *Appl. Phys. Lett.*, **35**, 214 (1979)
308. A.I.Popov. *J. Optoelectron. Adv. Mater.*, **4**, 481 (2002)
309. O.A.Golikova. *Fiz. Tekh. Poluprov.*, **25**, 1517 (1991)
310. I.A.Popov. *Fiz. Tekh. Poluprov*, **30**, 466 (1996)
311. I.A.Popov, G.Van Doorselaer, A.Van Calster, H.De Smet, E.Boesman, F.Callens. In *Proceedings of the International Congress on Imaging Science*. (Antwerpen, Belgium: University of Antwerpen, 1998). P. 315
312. S.A.Dembovskii, E.A.Chechetkina, S.A.Kozuyukhin.. *Pis'ma ZhETF*, **4**, 74 (1985)
313. S.A.Dembovskii, A.S.Zyubin, F.V.Grigor'ev. *Semiconductors*, **32**, 843 (1998)
314. J.Tominaga, T.Shima, P.Fons, R.Simpson, M.Kuwahara, A.Kolobov. *Jpn. J. Appl. Phys.*, **48**, 03A053 (2009)
315. V.Weidenhof, I.Friedrich, S.Ziegler, M.Wuttig. *J. Appl. Phys.*, **89** (6), 15 (2001)
316. E.Garcıa-Garcıa, A.Mendoza-Galvan, Y.Vorobiev, E.Morales-Sanchez, J.Gonzalez-Hernandez, G.Martınez, B.S.Chao. *J. Vac. Sci. Technol. A*, **17**, 1805 (1999)
317. P.K.Khulbe, X.Xun, M.Mansuripur. *Proc. SPIE*, **3864**, 38641V (1999)
318. Q.F.Wang, L.P.Shi, Z.B.Wang, B.Lan, K.J.Yi, M.H.Hong, T.C.Chong. *Proc. SPIE*, **5069**, 165 (2003)
319. X.Sun, M.Ehrhardt, A.Lotnyk, P.Lorenz, E.Thelander, J.W.Gerlach, T.Smausz, U.Decker, B.Rauschenbach. *Sci. Rep.*, **6**, 1 (2016)
320. G.Zhang, D.Gu, X.Jiang, Q.Chen, F.Gan. *Solid State Commun.*, **133**, 209 (2005)
321. J.Siegel, W.Gawelda, D.Puerto, C.Dorronsoro, J.Solis, C.N.Afonso, J.C.G.de Sande, R.Bez, A.Pirovano, C.Wiemer. *J. Appl. Phys.*, **103**, 023516 (2008)
322. T.Kunkel, Y.Vorobyov, M.Smayev. *J. Alloys Compd.*, **851**, 156924 (2021)
323. T.Kunkel, Y.Vorobyov, M.Smayev, P.Lazarenko, A.Romashkin, S.Kozyukhin. *Mater. Sci. Semicond. Proc.*, **139**, 106350 (2022)
324. H.Santoh, Y.Hongo, K.Tajima, M.Konishi, T.Saiki. In *Proceedings of the 2009 EPCOS Meeting*. American Society of Mechanical Engineers, (Aachen, Germany, 2009). P. 4.
325. K.Makino, J. Tominaga, M.Hase. *Opt. Express*, **19**, 1260 (2011)
326. J. Hernandez-Rueda, A.Savoia, W.Gawelda, J.Solis, B.Mansart, D.Boschetto, J.Siegel. *Appl. Phys. Lett.*, **98**, 251906 (2011)
327. S.C.Tiwari, R.K.Kalia, A.Nakano, F.Shimojo, P.Vashishta, P.S.Branicio. *J. Phys. Chem. Lett.*, **11**, 10242 (2020)
328. L.X.Benedict. *Phys. Rev. B*, **63**, 075202 (2001)
329. P.Stampfli, K.H.Bennemann. *Appl. Phys. A*, **60**, 191 (1995)
330. Y.-H.Cheng, S.Teitelbaum, F.Gao, K.Nelson. *EPJ Web Conf.*, **205**, 04011 (2019)
331. A.V.Kolobov, A.S.Mishchenko, P.Fons, S.M.Yakubenya, J.Tominaga. *J. Phys.: Condens. Matter*, **19**, 455209 (2007)
332. A.V.Kolobov, M.Krbal, P.Fons, J.Tominaga, T.Uruga. *Nat. Chem.*, **3**, 311 (2011)
333. G.Lucovsky, R.White. *Phys. Rev. B*, **8**, 660 (1973)
334. J.Robertson, K.Xiong, P.W.Peacock. *Thin Solid Films*, **515**, 7538 (2007)
335. W.Welnic, A.Pamungkas, R.C.Steimer, S.Blugel, M.Wuttig. *Detemple Nat. Mater.*, **5**, 56 (2005)
336. I.Gnilitskyi, T.J.-Y.Derrien, Y.Levy, N.M.Bulgakova, T.Mocek, L.Orazi. *Sci. Rep.*, **7**, 8485 (2017)
337. M.Sanz, E.Rebollar, R.A.Ganeev, M.Castillejo. *Appl. Surf. Sci.*, **278**, 325 (2013)
338. M.Martinez-Calderon, J.Azkona, N.Casquero, A.Rodríguez, M.Domke, M.Gomez-Aranzadi, S.M.Olaizola, E.Granados. *Sci. Rep.*, **8**, 1 (2018)
339. M.K.Kuntumalla, K.Rajamudili, N.N.Rao, S.S.Srikanth. *Appl. Phys. Lett.*, **104**, 161607 (2014)
340. R.Kuladeep, C.Sahoo, N.N.Rao. *Appl. Phys. Lett.*, **104**, 222103 (2014)
341. G.Miyaji, K.Miyazaki. *Appl. Phys. Lett.*, **103**, 071910 (2013)
342. M.Rohloff, S.K.Das, S.Hohm, R.Grunwald, A.Rosenfeld, J.Kruger, J.Bonse. *J. Appl. Phys.*, **110**, 014910 (2011)
343. R.Drevinskas, P.G.Kazansky. *APL Photon.*, **2**, 066104 (2017)
344. J. Bonse, S.Graf. *Laser Photon. Rev.*, **14**, 2000215 (2020)
345. S.Graf, F.A.Muller. *Appl. Surf. Sci.*, **331**, 150 (2015)
346. J.Bonse, J.Kruger, S.Hohm, A.Rosenfeld. *J. Laser Appl.*, **24**, 042006 (2012)
347. Y.Katsumata, T.Morita, Y.Morimoto, T.Shintani, T.Saiki. *Appl. Phys. Lett.*, **105**, 031907 (2014)
348. Y.Li, V.A.Stoica, L.Endicott, G.Wang, H.Sun, K.P.Pipe, C.Uher, R.Clarke. *Appl. Phys. Lett.*, **99**, 121903 (2011)

349. S.A.Yakovlev, A.V.Ankudinov, Yu.V.Voroboev, M.M.Voronov, S.A.Kozyukhin, B.T.Melekh, A.P.Pevtsov. *Semiconductors*, **52**, 809 (2018)
350. S.Kozyukhin, P.Lazarenko, Y.Vorobyov, A.Baranchikov, V.Glukhenkaya, M.Smayev, A.Sherchenkov, Y.Sybina, A.Polohin, V.Sigaev. *Opt. Laser Technol.*, **113**, 87 (2019)
351. S.Kozyukhin, M.Smayev, V.Sigaev, Y.Vorobyov, Y.Zaytseva, A.Sherchenkov, P.Lazarenko. *Phys. Status Solidi B*, **257**, 1900617 (2020)
352. J.E.Sipe, J.F.Young, J.S.Preston, H.M.van Driel. *Phys. Rev. B*, **27**, 1141 (1983)
353. S.Zabotnov, A.Kolchin, D.Shuleiko, D.Presnov, T.Kaminskaya, P.Lazarenko, V.Glukhenkaya, T.Kunkel, S.Kozyukhin, P.Kashkarov. *Micro*, **2** (1), 88 (2022)
354. T.T.Nang, M.Okuda, T.Mastushita. *Phys. Rev. B*, **19**, 947 (1979)
355. T.T.Nang, M.Okuda, T.Matsushita. *J. Non-Cryst. Solids*, **33**, 311 (1979)
356. K.Tanaka. *J. Non-Cryst. Solids*, **59** – **60**, 925 (1983)
357. K.Tanaka. *Appl. Phys. Lett.*, **26**, 243 (1975)
358. A.V.Kolobov, J.Tominaga. *Springer Ser. Mater. Sci.*, **164**, 276 (2012)
359. V.I.Mikla, V.V.Mikla. In *Metastable States in Amorphous Chalcogenide Semiconductors. Springer Series in Materials Science*. (Eds R.Hull, R.M.Osgood Jr., J. Parisi, H.Warlimont). (New York; Springer, 2010). P. 130
360. A.Zakery, S.R.Elliott. In *Optical Nonlinearities in Chalcogenide Glasses and their Applications. Springer Series in Optical Sciences*. (Heidelberg: Springer-Verlag, 2007). P. 200
361. S.R.Ovshinsky, P.H.Klose. *J. Non-Cryst. Solids*, **8** – **10**, 892 (1972)
362. A.Suzuki, T.Matsushita, M.Okuda, T.T.Nang. *Jpn. J. Appl. Phys.*, **18**, 47 (1979)
363. A.H.Zewail. *J. Phys. Chem. A*, **104**, 5660 (2000)
364. T.Wei, J. Wei, K.Zhang, H.Zhao, L.Zhang. *Sci. Rep.*, **7**, 42712 (2017)
365. J. Shanmugam, K.B.Borisenko, A.Luers, P.Ewart, P.Shah, B.A.O.Williams, C.Craig, D.W.Hewak, R.Hussain, T.Javorfi, G.Siligardi, M.Bosman, A.I.Kirkland. *Phys. Status Solidi RRL*, **13**, 1900449 (2019)
366. K.B.Borisenko, J. Shanmugam, B.A.O.Williams, P.Ewart, dB.Gholipour, D.W.Hewak, R.Hussain, T.Javorfi, G.Siligardi, A.I.Kirkland. *Sci. Rep.*, **5**, 1 (2015)